UNIVERSITY OF PADOVA
SCHOOL OF ENGINEERING
DEPARTMENT OF INFORMATION ENGINEERING

Thesis to obtain the Master of Science degree in
Telecommunication Engineering

OPTIMIZATION OF THE DEGRADATION INTRODUCED BY THE COMBINED NONLINEARITY OF SIEBEN'S ARCHITECTURE AND PIN PHOTODIODE IN SSB MB-OFDM OPTICAL METROPOLITAN NETWORKS

Author:
Callegher Luca

Supervisors:
Prof. Dr. Adolfo da Visitação Tregeira Cartaxo[1]
Dr. Tiago Manuel Ferreira Alves[1]
Prof. Luca Palmieri[2]

ACADEMIC YEAR 2014/2015

[1]Optical Communications and Photonics Group, Department of Electrical and Computer Engineering, Instituto Superior Técnico, Universidade de Lisboa, Lisbon (Portugal)
[2]Photonics and Electromagnetics Group, Department of Information Engineering, University of Padova, Padova (Italy)

This dissertation was performed under the project "Metro networks based on multi-band orthogonal frequency-division multiplexing signals"
(MORFEUS-PTDC/EEI-TEL/2573/2012) funded by Fundação para a Ciência e Tecnologia from Portugal, under the supervision of
Prof. Dr. Adolfo da Visitação Tregeira Cartaxo
and Dr. Tiago Manuel Ferreira Alves
from Instituto Superior Técnico, Lisbon (Portugal).

This dissertation was reviewed by Prof. Luca Palmieri from University of Padova.

Acknowledgements

First of all, I would like to express my gratitude to Professor Adolfo Cartaxo and Dr. Tiago Alves for all the support provided during the development of this dissertation, for having always had time to answer my questions and for the accurate and rigorous review of this work.
I would like to express my gratitude to Professor Luca Palmieri for having always been available when I needed his help and for the accurate review this work.
I would like to thank Ph.D student Eng. Pedro Cruz, MSc. João Rosário and MSc. student Artur Duarte for always answering my questions and for all the precious advice during my stay at Instituto Superior Técnico, Lisbon.
Last but not least, I am extremely grateful to my family for the support and encouragement throughout my whole education career. This dissertation would not have been possible without their support.

Abstract

Multi-band (MB) orthogonal frequency division multiplexing (OFDM) has been recently proposed to provide allocation flexibility and granularity in high capacity optical metropolitan networks. OFDM provides high spectral efficiency and robustness to fibre dispersion. Transmission of single-sideband (SSB) signals has been appointed as a solution to deal with chromatic dispersion induced power fading (CDPF).

An optical modulator, called Sieben's architecture, is considered in this work to generate the optical SSB MB-OFDM signal. A condition to obtain SSB signals, at the Sieben's architecture output, for every bias voltage, is identified. A detailed analysis of second-order distortion introduced by the SSB modulator under consideration, when the modulator input is an MB-OFDM signal comprising virtual carriers, is provided. Different kinds of second-order distortion terms are analytically identified, together with their frequency location and bandwidth.

At the receiver, the optical signal detection process is accomplished using a positive-intrinsic-negative (PIN) photodetector. The effect of Sieben's architecture and PIN combined non-linearities is analysed.

Performances of a 112 Gbit/s 12-bands MB-OFDM system are assessed through numerical simulations and through the development of an analytical model. Good agreement between numerical and analytical results is shown. The optical signal-to-noise ratio (OSNR) to achieve a bit error rate (BER) of 10^{-3} is used as figure of merit.

Table of Contents

List of Figures

List of Tables

List of Acronyms

Acronym	Description
A/D	Analogue-to-Digital
ADM	Add-Drop Multiplexer
AM	Analytical Method
ASE	Amplified Spontaneous Emission
BER	Bit Error Ratio
BG	Band Gap
BPF	Band Pass Filter
BS	Band Selector
CD	Chromatic Dispersion
CDPF	Chromatic Dispersion induced Power Fading
CP	Cyclic Prefix
D/A	Digital-to-Analogue
DC	Direct Current
DD	Direct Detection
DEC	Direct Error Counting
DFT	Discrete Fourier Transform

DSP	Digital Signal Processing
E/O	Electrical-to-Optical
EDFA	Erbium Doped Fibre Amplifier
EGA	Exhaustive Gaussian Approach
ESNR	Electrical Signal-to-Noise Ratio
EV	Error Vector
EVM	Error Vector Magnitude
FEC	Forward Error Correction
FFT	Fast Fourier Transform
HC	Hybrid Coupler
ICI	Inter-Channel Interference
IDFT	Inverse Discrete Fourier Transform
IFFT	Inverse Fast Fourier Transform
ISI	Inter-Symbol Interference
LPF	Low Pass Filter
LM	Linearised Model
MB	Multi Band
MB-OFDM	Multiband - Orthogonal Frequency Division Multiplexing
MBP	Minimum Bias Point
MCM	Multi Carrier Modulation

MMF	Multi-Mode Fibre
MZM	Mach-Zehnder Modulator
NS	Numerical Simulation
OADM	Optical Add-Drop Multiplexer
OBPR	Optical carrier-to-Band Power Ratio
ODU4	Optical channel Data Unit 4
O/E	Optical-to-Electrical
O-E-O	Optical-to-Electrical and Electrical-to-Optical
OFDM	Orthogonal Frequency Division Multiplexing
OSNR	Optical Signal-to-Noise Ratio
OTU4	Optical channel Transport Unit 4
PIN	Positive-Intrinsic-Negative
PMD	Polarization Mode Dispersion
P\S	Parallel-to-Serial
QAM	Quadrature Amplitude Modulation
QBP	Quadrature Bias Point
RM	Real Model
RMS	Root Mean Square
ROADM	Reconfigurable Optical Add-Drop Multiplexer
SNR	Signal-to-Noise Ratio

S\P	Serial-to-Parallel
SSB	Single Sideband
SSBI	Signal-to-Signal Beat Interference
SSMF	Standard Single-Mode Fibre
VBG	Virtual Carrier-to-Band Gap
VBPR	Virtual Carrier-to-Band Power Ratio
WDM	Wavelength Division Multiplexing

List of Symbols

Symbol	Designation
B_w	OFDM signal bandwidth
$B_{MB-OFDM}$	MB-OFDM signal bandwidth
c	light speed
D_λ	chromatic dispersion per unit length at wavelength λ
$\Delta\lambda_S$	optical signal spectral width
$f_{c,n}$	central frequency of the nth MB-OFDM signal band
$f_{n,e}$	electrical amplifier noise figure
$f_{n,EDFA}$	EDFA noise figure
g_e	electrical amplifier gain
g_{EDFA}	EDFA gain
h	Planck constant
$H_H(f)$	HT transfer function

$i_{pin}(t)$	current at the PIN output
k_B	Boltzmann constant
L_f	fibre length
λ_0	optical carrier wavelength
M	QAM modulation order
N_b	Number of bands of an MB-OFDM signal
N_{sc}	Number of subcarriers within one OFDM symbol
R_b	OFDM signal bit rate
$R_{MB-OFDM}$	MB-OFDM signal bit rate
R_L	PIN bias resistance
R_λ	PIN responsivity
S_w	frequency slot width
S_{th}	two sided PSD of the thermal noise at the electrical amplifier output
t_s	OFDM symbol duration without cyclic prefix
T_s	OFDM symbol duration including cyclic prefix
T_g	cyclic prefix duration
T_r	room temperature
t_d	chromatic dispersion-induced time spreading

V_b	MZM bias voltage
V_x	MZM switching voltage

Chapter 1

Introduction

1.1 Scope of the work

This thesis fits in the area of optical fibre telecommunication systems. More precisely, the transmission of multi-band (MB) orthogonal frequency division multiplexing (OFDM) signals along direct-detection (DD) optical metropolitan (metro) networks is considered. To deal with the chromatic dispersion induced power fading (CDPF), single-sideband (SSB) signals are considered. The generation of SSB signals is achieved through the architecture described in [1], also referred as Sieben's architecture. A positive-intrinsic-negative (PIN) photodetector is employed in the optical signal detection process. The aim of this work is to evaluate and minimize the degradation induced by the Sieben's architecture and PIN nonlinearities on MB-OFDM signals transmitted in DD metro networks.

An introduction to the main concepts related to this dissertation is provided in the following subsections. The fundamental characteristics of a metro network are described and brief history of the OFDM technology is presented. The two main approaches for optical OFDM detection are introduced, along with the MB-OFDM concept.

1.1.1 Optical metropolitan networks

Among telecommunication networks, it is usually possible to distinguish between long-haul core networks, regional networks, metropolitan networks and access networks. Long-haul core networks are high data rates networks which cover long distances. Access networks are used to provide direct connectivity between end users and their service providers. They extend for short distances. Metro networks represent the interface between core networks and access networks [2]. The extension of a metro network, as well as the distance between two consecutive network nodes (span), may considerably vary, depending on the geographical characteristics of the region in which the network itself is installed [3]. However, the extension of a metro network typically ranges between 150 km to 300 km [2][4], and span distances can range between 5 km to 100 km [3]. The ring topology is commonly used among

metro networks [2][4][5], due to its intrinsic reliability.

A metro network has to aggregate traffic from the access networks, to transfer traffic between different access networks and, if required, to deliver traffic to the core network. A metro network is thus characterized by rapidly changing traffic patterns. Therefore, the ability for network scalability, modularity, reconfiguration, and bandwidth provisioning with various levels of granularity is highly desirable in metro networks.
At the same time, metro networks are much more cost-sensitive than long-haul networks, since the infrastructure cost is divided among a smaller number of customers [4][5]. Hence, to provide the aforementioned desired characteristics, it is important to find cost-effective solutions.

The wavelength-division multiplexing (WDM) technique is widely used in optical networks [6]. In a WDM system, the optical transmission spectrum is divided into a number of non-overlapping optical channels (also referred as wavelengths). Independent data streams can be transmitted in parallel along different optical channels, within the same optical fibre [7], thus enhancing the system capacity.
When used together with optical switching technologies and reconfigurable optical add–drop multiplexers (ROADMs), WDM systems offer the capability for wavelength routing [4], i.e., routing capabilities without the need for optical-to-electrical and electrical-to-optical (O-E-O) conversion (a characteristic sometimes referred as transparency). Therefore, the WDM technique already provides a certain degree of flexibility, reconfigurability, and bandwidth provisioning.
However, the use of an electrical aggregation layer remains mandatory to achieve a finer granularity than the one provided by optical channels [8]. Thus, new techniques enabling routing with granularity at the sub-wavelength level are highly desired for future transparent metro networks [3].

1.1.2 History of OFDM

OFDM is a modulation and multiplexing technique in which information symbols are transmitted on a number of different subcarriers. Distinguishing features of OFDM are high spectral efficiency and robustness against inter-symbol interference (ISI), in dispersive channels. Nowadays, OFDM is widely used in both wired and wireless communication systems. In this subsection, the history of OFDM is briefly presented.

In 1966 Robert W. Chang of Bell Labs described for the first time the possibility of exploiting orthogonal frequencies for data transmission [9]. 1969 was a key year for OFDM, as it was recognized that the discrete Fourier transform (DFT) algorithm can be used to generate the OFDM signal. Other milestone concepts, such as the introduction of the cyclic

prefix and the importance of combining forward error correction (FEC) with OFDM, were proposed in 1980 and 1987 respectively.

In the mid-1980s, almost twenty years after the formulation of the fundamental concept, when the integrated CMOS technology became sufficiently mature, OFDM began to be considered for practical wired and wireless applications. OFDM has since been adopted in a large number of widely used standards. Among these standards there are [6]:

- asymmetric digital subscriber line (ADSL, ITU G.992.1)
- european digital video broadcasting (DVB)
- wireless local area networks (WiFi, IEEE 802.11a/g)
- wireless metropolitan area networks (WiMAX, 802.16e)
- fourth generation mobile communication technology, long-term evolution (LTE)

It is only recently that OFDM has been considered for optical communications, despite the number of advantages that it can bring to this field. The first paper on optical OFDM in the open literature was reported in 1996 [10]. However, the possibility of using OFDM to cope with optical channel dispersion was recognized only later. For instance, the use of OFDM to combat modal-dispersion in multi-mode fibre (MMF) was proposed in 2001. Nowadays optical OFDM has attracted the attention of the optical communication community. An increasing number of works, in which optical OFDM is analysed from both a theoretical and a practical point of view, have been presented [10].

1.1.3 Main approaches for optical OFDM detection

In an optical system, the detection process, i.e., the optical-to-electrical (O/E) conversion of the received optical signal, plays a fundamental role. With reference to the detection process, it is possible to distinguish between two main types of optical OFDM: coherent optical OFDM (CO-OFDM) and direct detection optical OFDM (DD-OFDM). CO-OFDM exhibits better performance, when compared to DD-OFDM [11]. However, DD-OFDM is a much more cost-effective solution and therefore still convenient to be implemented [12]. In our work, since we are dealing with cost-sensitive metro networks, DD-OFDM is the considered solution.

Coherent optical OFDM

CO-OFDM represents the ultimate performance in receiver sensitivity, spectral efficiency, and robustness against chromatic dispersion (CD) and polarization mode dispersion (PMD), however, it requires the highest complexity in transceiver design [6]. Figure 1.1 shows a possible scheme for the O/E conversion block of a CO-OFDM receiver. In Figure 1.1, E_O

is (the baseband representation of) the incoming optical OFDM signal (to be detected), E_{LL} is the electrical field at the output of a local oscillator (laser) and I_O is the complex photocurrent at the O/E block output. Without going into the detection details, notice that I_O is a replica of the incoming OFDM signal, multiplied by the complex conjugate of the local oscillator electrical field (E^*_{LL}). Figure 1.1 shows that CO-OFDM requires a local oscillator, a 90° optical hybrid and a number of balanced PIN photodiodes. The resulting architecture is quite complex, especially considering that, on the other and, DD-OFDM requires only one photodiode.

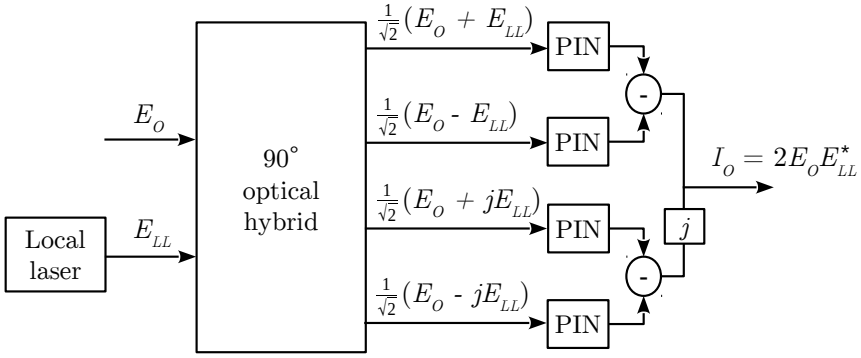

Figure 1.1: Conceptual scheme of a possible O/E converter of a CO-OFDM receiver. Adapted from [6].

Moreover, due to its sensitivity to frequency offsets [13] and phase noise [14], CO-OFDM requires very narrow-linewidth lasers sources at both the transmitter and the receiver [15], and extra signal processing accounting for the phase and frequency offsets estimation [11]. Better performances of CO-OFDM, when compared to DD-OFDM, are obtained at the price of higher cost and complexity.
A detailed description of a CO-OFDM system is beyond the scope of this work. Further information can be found in [6].

Direct detection optical OFDM

The key advantage of DD-OFDM is that it requires only one photodiode at the receive [15]. Moreover, when dealing with DD-OFDM, there is no need to estimate the phase and frequency offsets and, at the transmitter, low-cost lasers with megahertz-level linewidth can be used [12]. When DD-OFDM is considered, an optical carrier is transmitted together with the optical OFDM signal, along the optical channel. At the photodiode output, from the beat between the OFDM band and the optical carrier, a frequency-shifted replica of the information bearing signal originates. In turn, from this replica, data can be recovered. However, due to the square-law characteristic of the photodiode, some unwanted mixed products appear in the photodetected signal. Among these unwanted products, we can identify a signal-to-signal product, also known as signal-to-signal beat interference (SSBI) and a direct current (DC) component. Additional mixed products can originate in the

presence of noise. The SSBI was already identified as one of the main impairments in DD-OFDM [11] and a number of different techniques to mitigate its effect were proposed [12][15][16][17]. If a sufficiently wide frequency gap is placed between the optical OFDM signal and the optical carrier, it can be shown that, at the photodiode output, the spectrum of the SSBI term does not overlap the spectrum of the useful signal [15]. The SSBI can thus be removed with simple filtering techniques. To completely accommodate the SSBI, a frequency gap with size comparable to the OFDM signal bandwidth should be used, thus greatly reducing the spectral efficiency. Alternative techniques, such as the one proposed in [12], allow to iterative estimate the SSBI, in the digital domain, and to subtract it from the received signal, avoiding the use of the frequency gap and increasing the spectral efficiency.

1.1.4 Optical multiband-OFDM concept

An MB-OFDM signal is composed of a number of independent OFDM signals, also referred as OFDM bands. Figure 1.2 illustrates the spectrum of an optical MB-OFDM signal, composed of four bands, that fits into the ith channel of a WDM system. Each OFDM band does not overlap in frequency with the others and, as highlighted in Figure 1.2, adjacent bands are separated by a frequency gap (or band gap - BG). In general, BGs are required due to the finite selectivity of optical devices, such as optical filters or ROADMs, employed along the MB-OFDM system.

Although the presence of BGs may lead to a spectral efficiency reduction, the use of an MB-OFDM signal, instead of a single OFDM signal of equivalent bandwidth, brings some advantages. The main challenge in OFDM is probably the realization of digital-to-analogue (D/A) and analogue-to-digital (A/D) converters, that are required at the transmitter and receiver, respectively [18]. Since an MB-OFDM signal can be generated and detected in a "band-by-band" manner, a significant reduction of the required D/A and A/D converters bandwidth can be achieved [18]. Moreover, the use of optical MB-OFDM signals allows optical routing at a sub-wavelength level [8], as highly desired in future transparent optical networks [3].

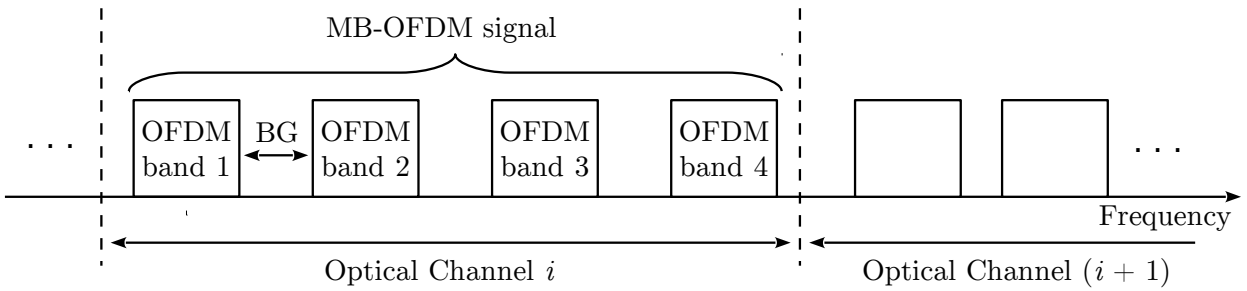

Figure 1.2: Illustration of the spectrum of an optical MB-OFDM signal that fits into an optical channel of a WDM system.

MB-OFDM routing concept

MB-OFDM optical routing is based on the insertion (add function) and/or the extraction (drop function) an OFDM band or a group of bands from an MB-OFDM signal, at a certain network node. ROADMs can be employed to realize the add/drop functions. Since an extracted band can be delivered to another network node, with no need of O-E-O conversion, routing at a granularity level finer than the one provided by the WDM technique is achieved, while preserving the network transparency.
An example of band extraction and insertion is provided in Figure 1.3. In Figure 1.3, an MB-OFDM signal composed of four OFDM bands is delivered to a network node. The node drops bands 1 and 3, while adding a new band ($3'$) to the MB-OFDM signal.

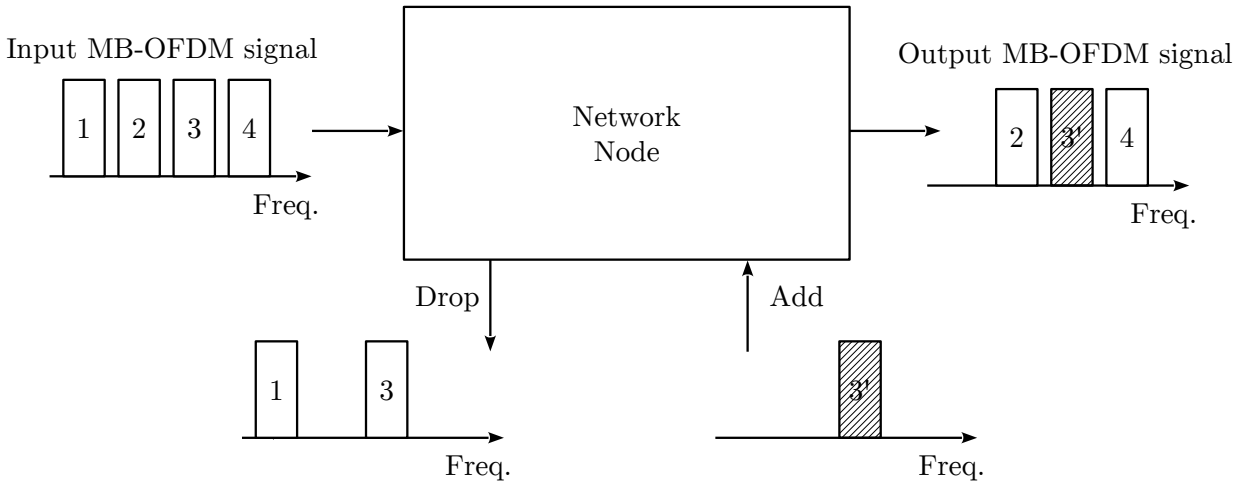

Figure 1.3: Illustration of the add/drop functions of a network node.

The add/drop function of OFDM bands has already been demonstrated in the literature. For instance, in [19], a variable bit rate add/drop function, considering a 30×26 Gbps MB-OFDM signal and using commercially available configurable optical filters, is experimentally demonstrated.

DD MB-OFDM channels

Let us define a DD MB-OFDM channel as an MB-OFDM signal comprising one or more optical carriers to assist photodetection. A number of DD MB-OFDM channels have been proposed in the literature. The DD MB-OFDM channel proposed in [20] consist of an MB-OFDM signal at the center and two optical carriers, inserted at both sides of the MB-OFDM signal, to assist photodetection. In [20], the following results are experimentally achieved: (i) 214 Gbit/s per wavelength at a distance of 720 km along standard single-mode fibre (SSMF) and (ii) 117 Gbit/s at a distance of 1200 km along SSMF, with sensitivity of 21.2 dB.
The DD MB-OFDM channel proposed in [21] is a variant of the channel proposed in [20]. In [21] a 432 Gbit/s transmission along 3040 km of SSMF is experimentally demonstrated.

The solutions proposed in [20] and in [21] are both designed for long-haul transmission systems. These solutions require dual-band optical filters before photodetection and receivers with considerable bandwidth, which may lead to a significant implementation cost.
An alternative solution, targeting cost-sensitive metro networks and data rates of 40 Gbps and 100 Gbps, is described in [3]. In [3], to assist photodetection, an electrically-generated carrier is associated to each OFDM band (see the virtual carrier concept in subsection 2.4.2). This solution allows to relax the bandwidth requirements for the receiver and to avoid the use of a dual-band optical filter. In this work, the solution proposed in [3] is considered.

1.2 Objectives and structure of the dissertation

The aim of this work is to evaluate and optimize the degradation induced by the Sieben's architecture and PIN nonlinearities on MB-OFDM signals transmitted in DD metro networks. The dissertation is organised in five chapters and one appendix.

Chapter 2 provides a review of basic OFDM and optical MB-OFDM concepts. The mathematical formulation of an OFDM symbol is presented and key aspects, such as efficient implementation, cyclic prefix and spectral efficiency, are discussed. The most important parameters of an MB-OFDM system are identified and described. A basic scheme of an MB-OFDM system, highlighting the functional blocks required to generate and detect an OFDM signal, is proposed. The carrier-assisted photodetection process is discussed and the two types of noise considered in this work are presented.

Chapter 3 deals with the analysis of Sieben's architecture and PIN nonlinearities. A condition to obtain SSB signals, at the Sieben's architecture output, for every bias voltage, is identified. Through the use of the Taylor expansion, second-order nonlinear products introduced by the Sieben's architecture are identified, and their frequency location and bandwidth is determined. The PIN output in two different scenarios, namely with and without a band-selector (BS) before photodetection, is mathematically described.

In Chapter 4, the performance of a 112 Gbit/s MB-OFDM system comprising 12 OFDM bands is assessed. Some performance evaluation methods are introduced. A SSBI mitigation method is presented. Considering back-to-back transmission, a qualitative and quantitative evaluation of distortion and noise effects on system performance is provided.

Chapter 5 presents the final conclusion of this dissertation and proposes future work on this subject.

Appendix A provides support to the analytical work done in Chapter 3. Some useful theorems and mathematical results are reported in this appendix.

1.3 Main original contributions

In this dissertation, a direct-detection virtual carrier-assisted SSB MB-OFDM system, employing the Sieben's architecture as optical modulator, is considered. With reference to this system, the most important contributions of this work are:

- Identification of a condition to obtain a SSB signal, at the Sieben's architecture output, for every bias voltage.
- Analysis of second-order distortion introduced by the Sieben's architecture and PIN photodiode, highlighting frequency location and bandwidth of distortion terms.
- Identification of the main system impairments using both numerical simulations and an *ad hoc* theoretical model.
- Evaluation of the OSNR required to achieve a BER of 10^{-3} in a 12-bands 112 Gbit/s system.

Chapter 2

OFDM and optical MB-OFDM systems description

2.1 OFDM theoretical basis

OFDM is a modulation and multiplexing technique that belongs to the class of multi-carrier modulation (MCM) schemes [9]. In a MCM system, information symbols are transmitted in parallel on a number of different narrowband subcarriers. As a result, if compared with a serial system with the same total data rate, each symbol has longer duration and is less vulnerable to channel dispersion. In a classical MCM system, there are frequency guard bands between subcarriers, thus allowing the receiver to recover individual subcarriers using analogue filtering techniques, but greatly reducing the spectral efficiency. In an OFDM system, high spectral efficiency is achieved using orthogonal subcarriers. Different subcarriers can partially overlap in frequency without interfering during the demodulation process.

2.1.1 Orthogonality property

Let $s_k(t)$ be the waveform of the kth OFDM subcarrier. By definition, all the carrier waveforms are orthogonal to each other, in the sense that [6]

$$< s_k, s_l > \equiv \int_{-\infty}^{+\infty} s_k(t) s_l^*(t) dt = \begin{cases} 1, & k = l \\ 0, & \text{otherwise} \end{cases} \tag{2.1}$$

$$\text{for every } k, l = 0, 1, ..., N_{sc} - 1$$

where $< s_k, s_l >$ denotes the inner product between two subcarrier signals and N_{sc} is the number of subcarriers. A common choice for the subcarrier waveform is [6]

$$s_k(t) = \Pi(t) e^{j2\pi f_k t} \tag{2.2}$$

$$\Pi(t) = \begin{cases} 1, & 0 < t \leq t_s \\ 0, & \text{otherwise} \end{cases} \tag{2.3}$$

being $\Pi(t)$ the pulse shaping function, f_k the frequency of kth subcarrier, t_s the OFDM symbol duration without cyclic prefix (CP) and j is the imaginary unit. As each waveform is windowed, in an ideal channel, consecutive OFDM symbols do not interfere. Substituting equation (2.2) in equation (2.1) we obtain

$$< s_k, s_l >= \int_0^{t_s} e^{j2\pi(f_k - f_l)t} dt =$$

$$e^{j\pi(f_k - f_l)t_s} \frac{\sin(\pi(f_k - f_l)t_s)}{\pi(f_k - f_l)} = \begin{cases} t_s, & k = l \\ 0, & \text{otherwise} \end{cases} \tag{2.4}$$

where the last equality holds only if

$$f_k - f_l = \frac{m}{t_s} \qquad m \in \mathbb{Z}\backslash\{0\} \tag{2.5}$$

Equation (2.4), together with condition (2.5), shows that, except for a multiplicative constant (t_s), the orthogonality property is satisfied simply with a proper choice of the subcarrier frequencies. More specifically, if subcarriers have frequencies spaced by multiples of $1/t_s$, they can occupy the same frequency space without interfering, thus achieving high spectral efficiency.

2.1.2 Mathematical description of an OFDM symbol

Any OFDM symbol can be represented as [10]

$$s(t) = \sum_{k=0}^{N_{sc}-1} c_k s_k(t) \tag{2.6}$$

where c_k is the information symbol at the kth subcarrier. Let $r(t)$ be a received OFDM symbol. Exploiting the orthogonality property, the receiver can recover each information symbol using a filter that matches the subcarrier waveform

$$c'_k = \frac{1}{t_s} \int_0^{t_s} r(t) s_k^*(t) dt =$$

$$\frac{1}{t_s} \int_0^{t_s} r(t) e^{-j2\pi f_k t} dt \tag{2.7}$$

From equation (2.6), it can be seen that, at the transmitter, each subcarrier is modulated by the respective information symbol, thus requiring at least an oscillator and a filter for each subacarrier. Similarly, from equation (2.7), it follows that oscillators and filters are

needed for every subcarrier even at the receiver.

2.1.3 IDFT/DFT implementation

As noted in section 2.1.2, the direct implementation of the OFDM technique would require an array of N_{sc} synchronized filters and oscillators at both the transmitter and receiver sides. This leads to an extremely complex and rigid architecture. Fortunately, most of the multiplexing and modulation can be done digitally. Let s_m $(m = 0, 1, ..., N_{sc} - 1)$ be the discrete domain version of a single OFDM symbol (more specifically, substitute equation (2.2) in equation (2.6) and sample $s(t)$ at every time interval of duration t_s/N_s)

$$s_m = \sum_{k=0}^{N_{sc}-1} c_k e^{j2\pi f_k \frac{mt_s}{N_{sc}}} \qquad m = 0, 1, ..., N_{sc} - 1 \tag{2.8}$$

By rewriting the orthogonality condition (2.5) as $f_k = k/t_s$, and applying it to equation (2.8) we immediately obtain

$$s_m = \sum_{k=0}^{N_{sc}-1} c_k e^{j2\pi \frac{mk}{N_{sc}}} = F^{-1}\{c_k\} \qquad m = 0, 1, ..., N_{sc} - 1 \tag{2.9}$$

where $F^{-1}\{\cdot\}$ denotes the inverse discrete Fourier transform (IDFT) operation. Equation (2.9) mathematically proves that the discrete values of the transmitted OFDM symbol are a simple N-point IDFT of the information symbols, as was revealed for the first time in [22] in 1969. At the receiver, after analogue-to-digital conversion, discrete Fourier transform (DFT) can be used to perform demodulation and demultiplexing. As a result, in an OFDM system, the complexity of both transmitter and receiver can be transferred from the analogue to the digital domain, avoiding the use of large banks of synchronized oscillators an filters. Furthermore, the existence of the highly efficient inverse fast Fourier transform/fast Fourier transform (IFFT/FFT) algorithms pair ensures optimal performances.

2.1.4 Cyclic prefix

In a dispersive channel, each transmitted symbol is spread out in time, leading to interference between adjacent symbols. In most practical OFDM systems, to deal with dispersion, a cyclic prefix (CP) is added at the beginning of each OFDM symbol before transmission. CP insertion consist of appending a number of samples from the end of the symbol at the beginning of the same symbol. In other words, it is a form of guard interval in the time domain. The CP is the key feature for simple equalization in OFDM, as it ideally eliminates both inter-symbol interference (ISI) and inter-channel interference (ICI) from the received signal. The tradeoff is the overhead introduced by the CP itself. If t_s is the symbol duration without prefix and a CP with duration T_g is used, the symbol period becomes

$$T_s = t_s + T_g \tag{2.10}$$

and the overall data rate is reduced.

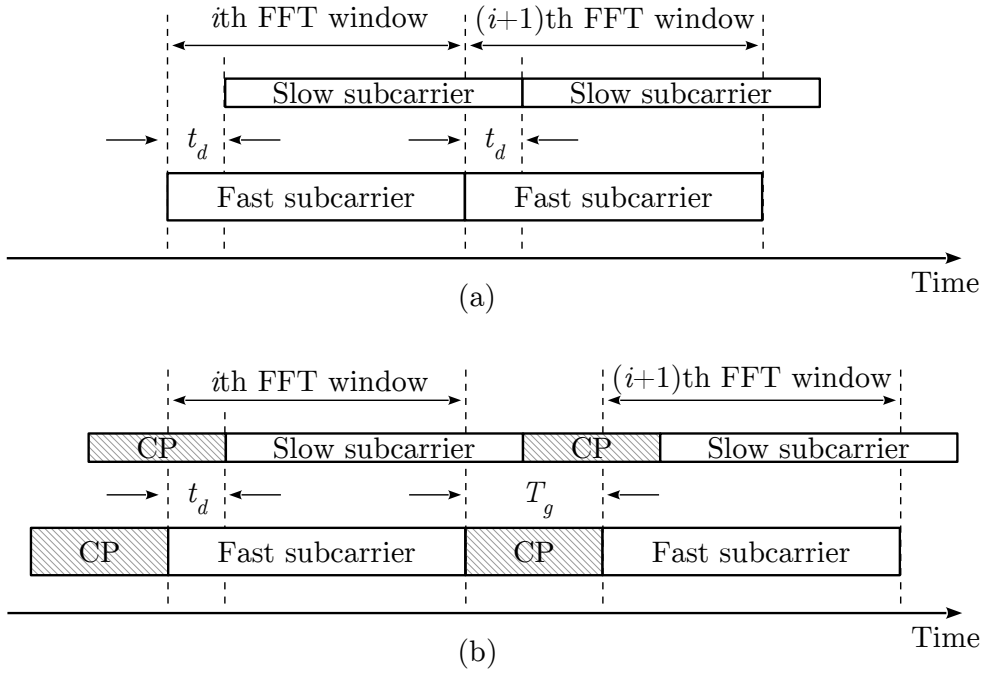

Figure 2.1: Received fast and slow subcarriers in presence of a dispersive channel (a) without cyclic prefix, (b) with cyclic prefix.

To understand how the CP works, let us consider two consecutive OFDM symbols. Assume, for simplicity, that each symbol has only two subcarriers. Upon transmission, the two subcarriers are aligned. In a dispersive channel (e.g. if signal undergoes chromatic dispersion (CD)), the two subcarriers have different group velocity. As a result, upon reception, one subcarrier is delayed against the other (let t_d be the delay spread). Suppose that the FFT window at the receiver is aligned with the 'fast subcarrier'. As shown in Figure 2.1(a), the 'slow subcarrier' has exceeded the symbol boundaries, leading to ISI. Inter-symbol interference could also be eliminated by preceding each OFDM symbol with a guard interval in which no signal was transmitted. However, this results in ICI, due to the loss of the orthogonality condition between subcarriers. As can be seen from Figure 2.1(b), when a CP with duration T_g is used, the portion of the 'slow subcarrier' that has shifted out is replaced by an identical one, thus preserving the orthogonality condition. In conclusion, as long as the delay spread does not exceed the CP length, i.e.

$$t_d < T_g \tag{2.11}$$

and the receiver DFT window is properly aligned, then no ISI or ICI occurs [9].

2.1.5 Spectral efficiency

The spectral efficiency (η) of a system is defined as the ratio between the total bit rate (R_b) of the system and the bandwidth (B_w) occupied by the transmitted signal

$$\eta = \frac{R_b}{B_w} \tag{2.12}$$

In an OFDM system with N_{sc} subcarriers and symbol period T_s, the total bit rate is simply

$$R_b = \frac{N_{sc}}{T_s} \log_2 M \tag{2.13}$$

being M the size of the alphabet of the modulation used in all subcarriers. Therefore, $\log_2 M$ is the number of bits per subcarrier.

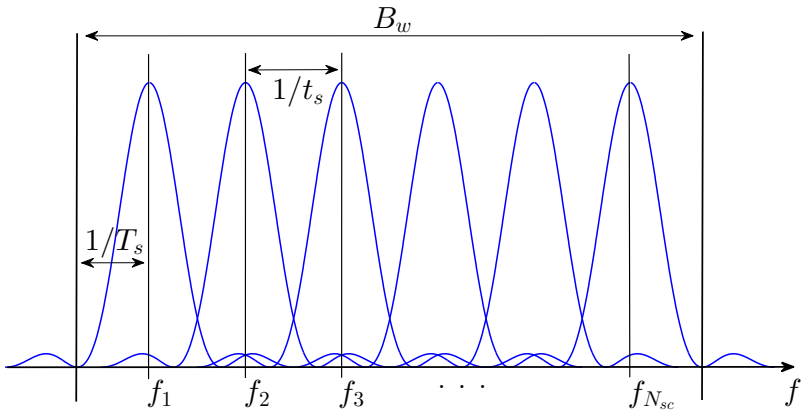

Figure 2.2: Typical OFDM spectrum and associated bandwidth when the spectrum of each subcarrier has a $|\sin(x)/x|^2$ form.

When each subcarrier waveform in the time domain is a windowed complex exponential, each subcarrier spectrum has a $|\sin(x)/x|^2$ form centered at the corresponding frequency, as depicted in Figure 2.2. With reference to Figure 2.2, and remembering that, if a cyclic prefix is used, the total symbol duration is $T_s = t_s + T_g$, the resulting bandwidth of the OFDM signal is

$$B_w = \frac{2}{T_s} + \frac{N_{sc} - 1}{t_s} \tag{2.14}$$

To obtain equation (2.14) we have neglected, for each subcarrier, the portion of the spectrum outside the two first nulls. If the number of subcarriers is sufficiently high (i.e. $N_{sc} - 1 \simeq N_{sc}$ and $N_{sc} T_s \gg 2t_s$), equation (2.14) can be approximated as

$$B_w \simeq \frac{N_{sc}}{t_s} \tag{2.15}$$

Substituting equation (2.13) and equation (2.14) in equation (2.12) we obtain

$$\eta_{OFDM} = \frac{N_{sc} t_s}{2t_s + T_s(N_{sc} - 1)} \log_2 M \tag{2.16}$$

Or, using the approximation of equation (2.15), the spectral efficiency can be written as

$$\eta_{OFDM} \simeq \frac{t_s}{T_s} \log_2 M = \left(1 - \frac{T_g}{T_s}\right) \log_2 M \tag{2.17}$$

Then, to achieve higher spectral efficiency, the cyclic prefix duration must be sufficiently small if compared to the total symbol duration.

It is worth noting that, sometimes, in real systems, some subcarriers do not transport information, as they are used for channel estimation purposes, thus further reducing the spectral efficiency (training sequences can also be employed for channel estimation).

2.2 MB-OFDM signals

An MB-OFDM signal consist of a number of independent - properly placed in frequency - OFDM signals. Different OFDM signals (also referred as OFDM bands) do not overlap in frequency. Therefore, each OFDM band does not interfere with the others.

2.2.1 Parameters of an MB-OFDM signal

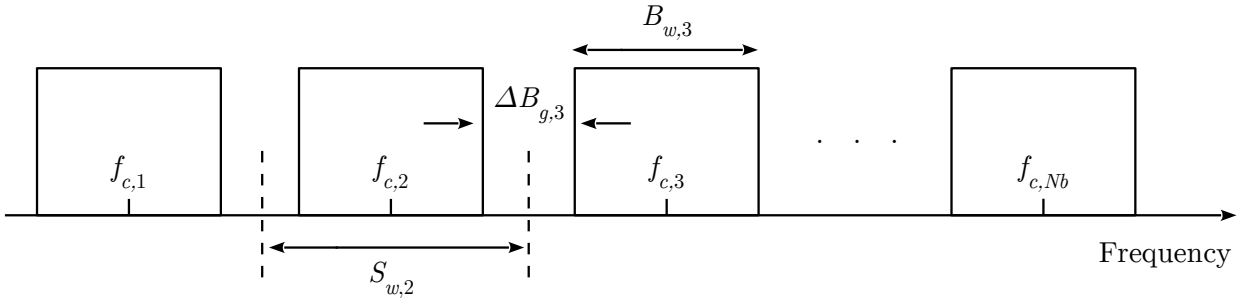

Figure 2.3: Illustration of the spectrum of an MB-OFDM signal

This subsection provides an overview of the most important MB-OFDM signal parameters, with particular emphasis on the relation between an MB-OFDM signal and a single OFDM signal. The spectrum of a typical MB-OFDM signal with N_b bands is illustrated in Figure 2.3. $B_{w,n}$ and $f_{c,n}$ are the bandwidth and the central frequency of the nth band respectively, $\Delta B_{g,n}$ is the width of the frequency gap between the $(n-1)$th and the nth band, $S_{w,n}$ is the bandwidth of the frequency slot that hosts the nth band. Let us define a slot as a range of frequencies that contains a single OFDM band and includes half of the guard intervals at both sides of the band. Then, the following relation holds

$$S_{w,n} = B_{w,n} + \frac{\Delta B_{g,n} + \Delta B_{g,n+1}}{2}. \tag{2.18}$$

Note that the number of slots is equal to the number of bands (N_b).

Since each band is an independent OFDM signal, most of the MB-OFDM signal parameters can be derived in a straightforward manner. The total bit rate of the MB-OFDM system is the sum of the bit rates of each band

$$R_{MB-OFDM} = \sum_{n=1}^{N_b} R_{b,n} \tag{2.19}$$

where $R_{b,n}$ in the bit rate of the nth band. $R_{b,n}$ for each band can be computed from equation (2.13).

The relation between the central frequency of the nth band and the central frequency of the $(n-1)$th band is

$$f_{c,n} = f_{c,n-1} + \frac{B_{w,n-1} + B_{w,n}}{2} + \Delta B_{g,n} \qquad n = 2, ..., N_b \tag{2.20}$$

If slots of fixed width (S_w) are considered, a possible choice for the central frequency of the nth OFDM band is

$$f_{c,n} = f_{c,1} + (n-1)S_w \qquad n = 1, 2, \ldots N_b \tag{2.21}$$

Note that central frequency of the first band ($f_{c,1}$) in equation (2.21) can be chosen with some degree of freedom. Once selected $f_{c,1}$, the choice of equation (2.21) ensure that each band is centred in the respective slot. In order to ensure that the first OFDM band is properly positioned in frequency, the following condition has to be satisfied:

$$f_{c,1} > \frac{B_{w,1}}{2} \tag{2.22}$$

The total band occupied by the MB-OFDM signal is

$$B_{MB-OFDM} = \sum_{n=1}^{N_b} B_{w,n} + \sum_{n=2}^{N_b} \Delta B_{g,n} \tag{2.23}$$

For each band, $B_{w,n}$ can be derived from equation (2.14).

If not otherwise specified, in this work, similar bandwidths and band gaps are considered, for each OFDM band. Moreover, slots of fixed width are addressed. With these assumptions, the previous equations can be written in a simplified form: equation (2.18) becomes

$$S_w = B_w + \Delta B_g \tag{2.24}$$

Equation (2.19) simplifies to

$$R_{MB-OFDM} = N_b R_b \tag{2.25}$$

Equation (2.23) can be written as

$$B_{MB-OFDM} = N_b B_w + (N_b - 1)\Delta B_g \tag{2.26}$$

Making use of equation (2.24), equation (2.26) can be rewritten as

$$B_{MB-OFDM} = N_b S_w - \Delta B_g \tag{2.27}$$

Equation (2.27) shows that, as was easily predictable, the bandwidth occupied by the MB-OFDM signal is comparable to $N_b S_w$.

2.2.2 Indicative numerical parameters for a real system

In this work, in accordance with the recommendations of [23] for the optical channel transport unit 4 (OTU4), a target bit rate ($R_{MB-OFDM}$) of 112 Gbit/s for the MB-OFDM signal is considered. This bit rate takes into account a 7% forward error correction (FEC) overhead associated to the OTU4 structure, and a 5% optical channel data unit 4 (ODU4) overhead (see [23]). Considering the use of the FEC and in accordance with the guidelines of [3], the optical signal-to-noise ratio (OSNR) required to achieve a bit error ratio (BER) of 10^{-3} is used as a figure of merit to assess the performances of the optical MB-OFDM system.

The MB-OFDM signal must fit into a single optical channel, also referred to as a wavelength, of a wavelength division multiplexing (WDM) system. Let us consider fixed spacing between optical channels. Spacing of 12.5, 25 and 50 GHz are addressed in this discussion, since, as described in [24], the current spacing between channel have historically evolved by subdividing the initial 100 GHz grid by successive factors of two. For the same reason, slots of 3.125 GHz to host a single OFDM band are considered. As an example, it can be observed that exactly 4 slots fit in the 12.5 GHz channel. However, in a real system, due to the finite selectivity of optical filters and add-drop multiplexers (ADMs), only a portion of the optical channel bandwidth (B_{ch}) can be used to carry the MB-OFDM signal. Let $r_c \in]0, 1]$ be the fraction of optical channel filling, e.g., if r_c is equal to 0.8, then only 3 slots can be placed in the 12.5 GHz channel. More precisely, the number of filled slots per optical channel is

$$N_b = \left\lfloor \frac{r_c B_{ch}}{S_w} \right\rfloor \tag{2.28}$$

where $\lfloor \cdot \rfloor$ indicates the down rounding function. The number of filled slots for each optical channel, for various values of r_c, is reported in Table 2.1.

A similar reasoning can be applied to a single slot: in order to allow the insertion and extraction of an OFDM band, only a portion of the slot can be occupied by the OFDM signal. Let $r_s \in]0, 1]$ be the fraction of the slot occupied by the OFDM signal, then the bandwidth of the signal can be written as

N_b	$r_c = 0.5$	$r_c = 0.6$	$r_c = 0.7$	$r_c = 0.8$	$r_c = 0.9$	$r_c = 1$
$B_{ch} = 12.5\,\text{GHz}$	2	2	2	3	3	4
$B_{ch} = 25\,\text{GHz}$	4	4	5	6	7	8
$B_{ch} = 50\,\text{GHz}$	8	9	11	12	14	16

Table 2.1: Number of filled slots for each optical channel, for various values of r_c.

$$B_w = r_s S_w \tag{2.29}$$

Table 2.2 reports some values of B_w and of t_s (the OFDM symbol duration without CP) as a function of r_s. Values of B_w are computed using equation (2.29). Values of t_s are computed solving equation (2.15) with respect to t_s itself, assuming $N_{sc} = 128$.

r_s	B_w (GHz)	t_s (ns)
0.5	1.563	81.9
0.6	1.875	68.3
0.7	2.188	58.5
0.8	2.500	51.2
0.9	2.813	45.5
1	3.125	41.0

Table 2.2: Bandwidth, B_w, and symbol duration, t_s, (with no CP) of each OFDM signal, for various values of r_s, assuming $N_{sc} = 128$.

Consider now the parameter M (the size of the alphabet of the modulation used in all subcarriers), or, equivalently, the number of bits per subcarrier, $n_{bit} = \log_2 M$. On the one hand, since the bandwidth is a system constrain, to achieve the required bit rate for the MB-OFDM system, a sufficiently high value of M must be selected. By solving equation (2.13) with respect to $\log_2 M$ and making use of equation (2.10), equation (2.15), equation (2.25), equation (2.28) and equation (2.29), a lower bound for the value of $n_{bit} = \log_2 M$ as a function of the main system requirements and constraints can be easily found:

$$n_{bit} = \log_2 M = \frac{R_{MB-OFDM}}{N_{sc} \left\lfloor \frac{r_c B_{ch}}{S_w} \right\rfloor} \left(\frac{N_{sc}}{r_s S_w} + T_g \right) \tag{2.30}$$

The value of n_{bit} of equation (2.30) must be rounded up to the next integer, and a lower bound for the value of M can be computed as $M = 2^{n_{bit}}$.

On the other hand, the value of M cannot grow indefinitely. For a square constellation ($M = 2^{2n}$, $n \in \mathbb{N}$), the BER of an M-QAM modulation format can be expressed as a function of M and the signal-to-noise ratio (SNR) [25]

$$\mathrm{BER}_M = \frac{4}{\log_2 M}\left(1 - \frac{1}{\sqrt{M}}\right) Q\left(\sqrt{\frac{3}{(M-1)}\mathrm{SNR}}\right) \tag{2.31}$$

where $Q(\cdot)$ is the complementary Gaussian distribution function. Values of the BER as a function of the SNR for different M are reported in Figure 2.4. Since in practice an SNR greater than 30 dB is very difficult to achieve, and for the considered target BER of 10^{-3}, from equation (2.31) an upper bound for the value of M can be derived. As shown in Figure 2.4 and from the above remarks, it is reasonable to consider only values of M smaller than or equal to 256 in real systems.

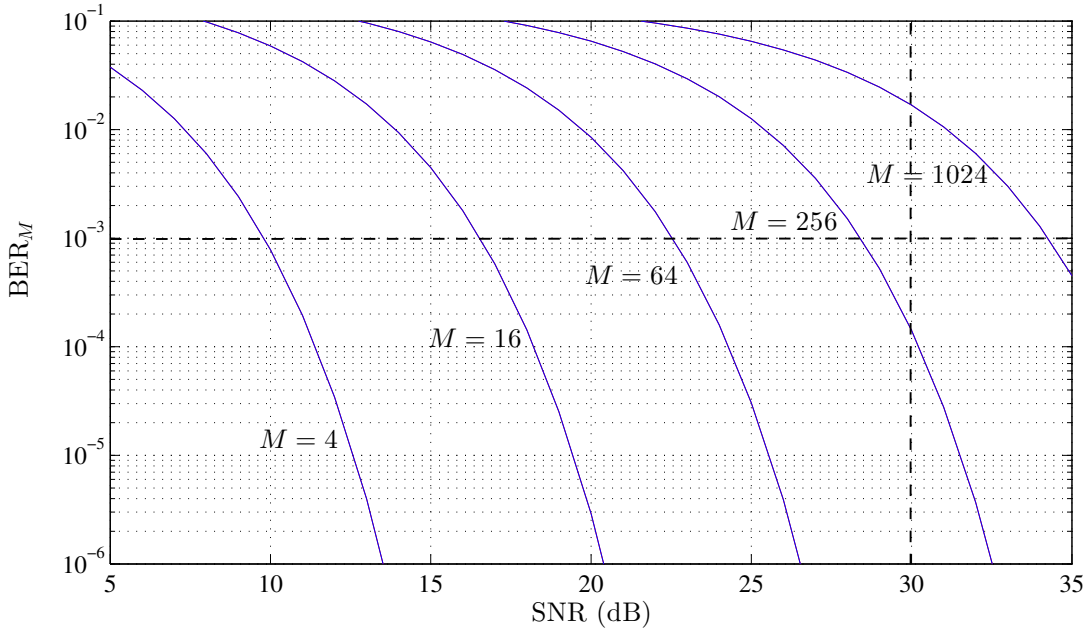

Figure 2.4: Bit error rate as a function of the SNR for M-QAM transmission with square constellation

Table 2.3 reports the lower bound for the value of M, computed from equation (2.30), to achieve a bit rate $\geq$112 Gbit/s for various values of r_c and r_s, for $N_{sc} = 128$, values of T_g taken from Table 2.4, (a) for the 25 GHz optical channel and (b) for the 50 GHz optical channel. Note that values of M greater than 256 are not reported in Table 2.3. For the 12.5 GHz optical channel, even in an ideal situation ($r_c = r_s = 1$), it is required $M = 512$ to achieve the target bit rate. Then the 12.5 GHz optical channel is no longer considered in our discussion.

2.2.3 Delay spread and cyclic prefix duration

In subsection 2.1.4, it was shown that, when a single OFDM signal is considered, to deal with ISI and ICI, a CP of proper duration (T_g) can be used. Since an MB-OFDM signal is composed of independent OFDM signals, the CP is individually introduced in each OFDM band. To choose a proper value for T_g, let us first compute the delay spread (t_d) experienced

$\boldsymbol{M}$	$r_c = 0.7$	$r_c = 0.8$	$r_c = 0.9$	$r_c = 1$
$r_s = 0.7$	-	-	256	128
$r_s = 0.8$	-	256	128	64
$r_s = 0.9$	-	128	64	64
$r_s = 1$	256	128	64	32

(a)

$\boldsymbol{M}$	$r_c = 0.5$	$r_c = 0.6$	$r_c = 0.7$	$r_c = 0.8$	$r_c = 0.9$	$r_c = 1$
$r_s = 0.5$	-	256	128	64	64	32
$r_s = 0.6$	256	128	64	32	32	16
$r_s = 0.7$	128	64	32	32	16	16
$r_s = 0.8$	64	32	32	16	16	8
$r_s = 0.9$	64	32	16	16	8	8
$r_s = 1$	32	32	16	16	8	8

(b)

Table 2.3: Minimum value of M to achieve a bit rate $\geq$112 Gbit/s for various values of r_c and r_s, for $N_{sc} = 128$, (a) for the 25 GHz optical channel and (b) for the 50 GHz optical channel. Values of T_g from Table 2.4. Values of M greater than 256 are not reported.

by an optical OFDM signal of bandwidth B_w travelling along a standard single-mode fibre (SSMF) of length L_f. In this work, only the delay spread due to chromatic dispersion (CD), the phenomenon for which different spectral components of an optical signal travel along an optical fibre with different velocities, is considered. The delay spread due to CD, for the considered optical OFDM signal, can be expressed as

$$t_d = D_\lambda L_f \Delta\lambda_S \tag{2.32}$$

where D_λ is the CD per unit length coefficient ($D_\lambda = 17\,\text{ps}/(\text{nm}\,\text{km})$ for a SSMF, if the optical carrier frequency is $\lambda_0 = 1552\,\text{nm}$), and $\Delta\lambda_S$ (expressed in meters) is the spectral width of the optical OFDM signal travelling into the fibre. $\Delta\lambda_S$ can be computed from B_w (expressed in Hertz) as

$$\Delta\lambda_S = \frac{\lambda_0^2}{c} B_w \tag{2.33}$$

being c the speed of light in the vacuum ($c \simeq 3 \times 10^8\,\text{m/s}$).

As stated in subsection 2.1.4, in order to obtain an ISI and ICI-free OFDM transmission, the cyclic prefix duration has to satisfy condition (2.11). Table 2.4 reports values of t_d and T_g for $L_f = 300\,\text{km}$ (indicative maximum extension of a metro network, as stated in subsection 1.1.1), as a function of the slot filling coefficient, r_s, or, in other words, as a function of B_w (see equation (2.29) and Table 2.2). In order to satisfy condition (2.11), values of T_g of Table 2.4 are computed as $T_g = 2t_d$.

r_s	t_d (ns)	T_g (ns)
0.5	0.06	0.12
0.6	0.08	0.16
0.7	0.09	0.18
0.8	0.10	0.20
0.9	0.12	0.24
1	0.13	0.26

Table 2.4: Delay spread (t_d) and cyclic prefix duration (T_g), for $L_f = 300\,\text{km}$, $D_\lambda = 17\,\text{ps}/(\text{nm}\,\text{km})$ and for various values of r_s.

Note that, in our case, the values of T_g of Table 2.4 are relatively small if compared to the values of t_s (see Table 2.2). Thus, the overhead due to the introduction of the CP is almost negligible in our system.

2.3 Optical MB-OFDM system description

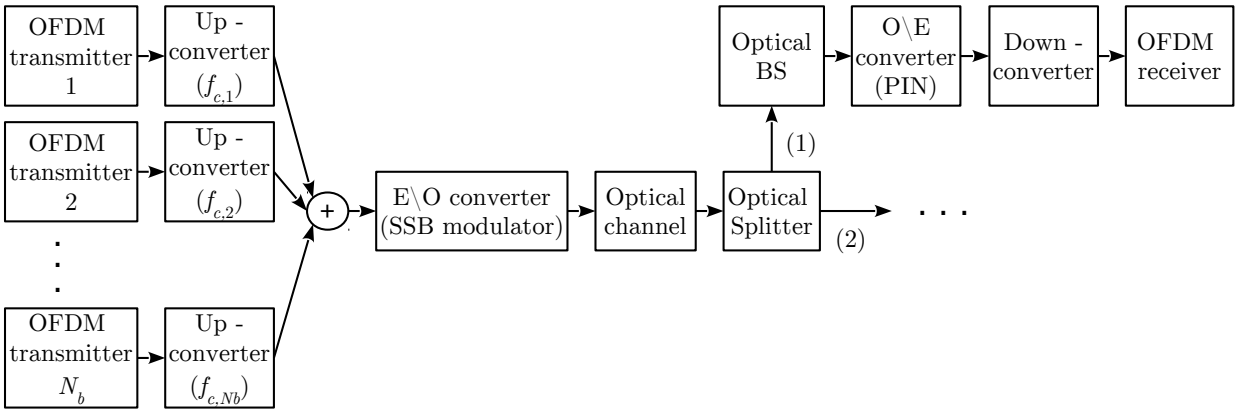

Figure 2.5: Block diagram of the optical MB-OFDM system considered in our work.

The basic scheme of the optical MB-OFDM system considered in this work is illustrated in Figure 2.5. Each OFDM transmitter block depicted in Figure 2.5 generates an independent OFDM signal which is then up-converted to a specific central frequency ($f_{c,i}$) by the corresponding up-converter. All the OFDM transmitters perform similar tasks and their implementation is detailed in subsection 2.3.1, together with the description of the up-conversion block structure. The resulting up-converted OFDM signals are summed together to generate the MB-OFDM signal.

Then, the MB-OFDM signal enters an electrical-to-optical (E/O) converter, also referred as optical modulator. Single sideband (SSB) modulators (modulators capable of generating SSB signals) are addressed in this work. More precisely, we consider the E/O converter presented in [1], also referred as Sieben's architecture or Sieben's modulator. The Sieben's architecture is described in detail in subsection 2.3.3. The output of the E/O converter is

a signal suitable for the transmission along the optical channel. The optical channel is usually composed of an optical fibre and an optical amplifier. The optical amplifier considered in this work is an erbium-doped fibre amplifier (EDFA). Besides amplifying the signal, an EDFA introduces optical noise called amplified spontaneous emission (ASE). The ASE noise is described in subsection 2.5.2.

At the receiver side, an optical splitter can be employed to obtain two or more equivalent replicas of the MB-OFDM signal. The replica at output (1) of the optical splitter of Figure 2.5 is delivered to an optical band selector (BS). The BS is simply an optical filter that is used to select a specific OFDM band. The combined use of the optical splitter and BS allows the receiver to extract a specific band from the whole MB-OFDM signal. The destination of the other replica (output (2) of the optical splitter) is of not relevance in this section. For instance, the replica at output (2) of the splitter could be delivered to another network node.

The output of the BS is connected to an optical-to-electrical (O/E) converter. In this work, the device considered to perform O/E conversion is the PIN photodetector. The behaviour of the PIN is detailed in subsection 2.3.4. Even if is not shown in Figure 2.5, an electrical amplifier is connected to the PIN output. As any other electrical device, the PIN and the electrical amplifier are sources of thermal noise (other kinds of electrical noise are not considered in this work). We assume that the whole thermal noise is added after the electrical amplifier, as detailed in subsection 2.5.1.

After photodetection and amplification, the selected OFDM signal enters a down-conversion block. The resulting signal is ready to be detected by the corresponding OFDM receiver. The implementation of the OFDM receiver is described in subsection 2.3.2, together with the illustration of the down-converter structure.

2.3.1 Basic OFDM transmitter scheme

The basic architecture of an OFDM transmitter and of an up-converter is illustrated in Figure 2.6. With reference to Figure 2.6, a step-by-step description of the OFDM signal generation is presented in this subsection.

The input bit stream is first mapped into an M-QAM symbol stream. A possible 16-QAM constellation is shown in Figure 2.7. The output of the M-QAM mapper is a series of complex symbols, each one representing a particular constellation point.

A serial-to-parallel (S/P) converter is needed to present a vector of symbols of proper dimension (N_{sc}) at the input of the IFFT block.

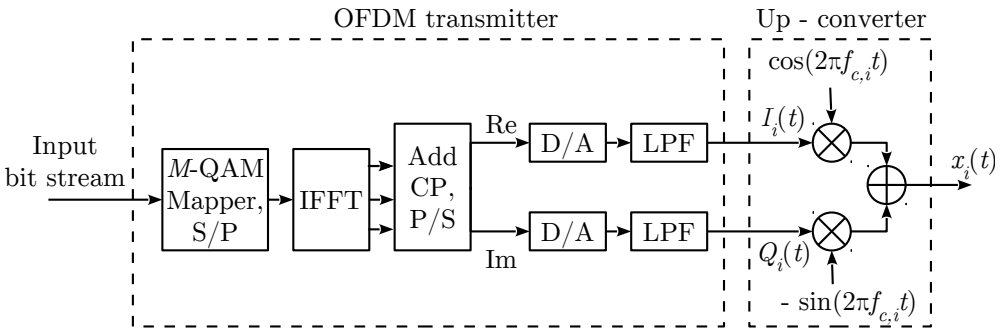

Figure 2.6: Block diagram of a basic OFDM transmitter and of a simple up-converter.

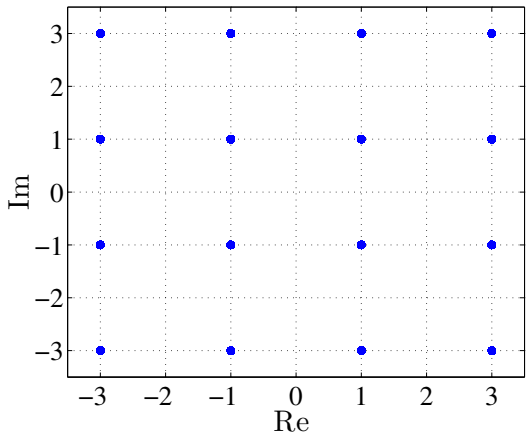

Figure 2.7: Example of M-QAM constellation with $M = 16$.

The IFFT block is responsible for the creation of each OFDM symbol in the digital domain. In every practical OFDM system, a cyclic prefix (CP) is added to each symbol, in order to make it robust against ISI and ICI.

After parallel-to-serial (P/S) conversion, the real (Re) and imaginary (Im) parts of the signal are separately converted into analogue waveforms using two digital-to-analogue (D/A) converters. A low pass filter (LPF) is usually required to eliminate aliasing components introduced by the D/A conversion process.
The analogue waveform resulting from the real part of the digital OFDM signal is referred as in-phase component, $I_i(t)$. The other one is called quadrature component, $Q_i(t)$. The complex baseband representation, $x_{B,i}(t)$, of the ith OFDM signal is defined as

$$x_{B,i}(t) = I_i(t) + jQ_i(t) \tag{2.34}$$

The $I_i(t)$ and $Q_i(t)$ components are then up-converted to a proper central frequency $f_{c,i}$ and combined together. The structure of the up-converter block is detailed in Figure 2.6. The signal at the up-converter output is given by

$$x_i(t) = I_i(t)\cos(2\pi f_{c,i}t) - Q_i(t)\sin(2\pi f_{c,i}t)\ . \tag{2.35}$$

The relation between the baseband signal, $x_{B,i}(t)$, and the up-converted signal, $x_i(t)$, is

$$x_i(t) = \Re\{x_{B,i}(t)\exp(j2\pi f_{c,i}t)\} \tag{2.36}$$

where $\Re\{\cdot\}$ denoted the real part of a signal.

2.3.2 Basic OFDM receiver scheme

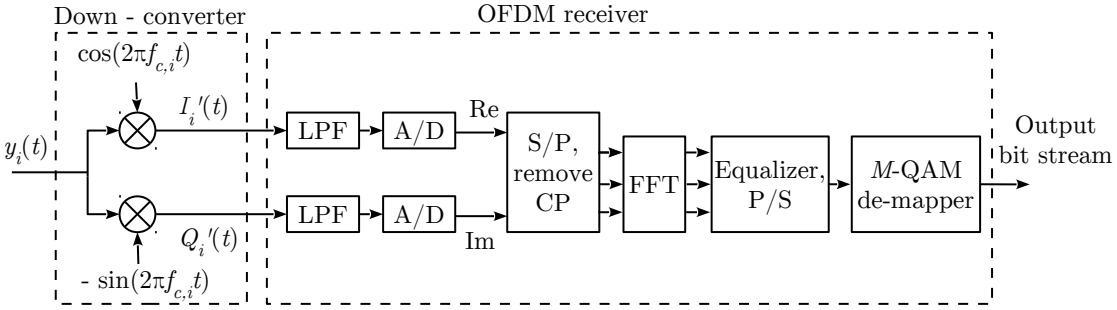

Figure 2.8: Block diagram of a down-converter and a basic OFDM receiver.

The basic OFDM receiver scheme and the basic down-converter structure are presented in Figure 2.8. Let $y_i(t)$ be the input of the down-converter. The down-conversion process consists in separately multiplying $y_i(t)$ by a cosine and a sine waveform. For detection purposes, it is important that the sinusoidal waveforms have frequency $f_{c,i}$ equal to the up-conversion frequency. If we assume $y_i(t) = x_i(t)$ (ideal system), the signal $I_i'(t)$ at the output of the down-converter can be written as $I_i'(t) = x_i(t)\cos(2\pi f_{c,i}t)$. Considering equation (2.35) and using some trigonometric identities, $I_i'(t)$ can be rewritten as

$$I_i'(t) = \frac{I_i(t)}{2} + \left[\frac{I_i(t)}{2}\cos(4\pi f_{c,i}t) - \frac{Q_i(t)}{2}\sin(4\pi f_{c,i}t)\right] \tag{2.37}$$

Equation (2.37) shows that $I_i'(t)$ consists of two terms: a baseband term, $I_i(t)/2$, and an "high frequency term", $1/2[I_i(t)\cos(4\pi f_{c,i}t) - Q_i(t)\sin(4\pi f_{c,i}t)]$. Then, a LPF can be used to cut off the high frequency term from $I_i'(t)$, and recover the transmitted in-phase term $I_i(t)$, except for a multiplicative constant 1/2. Following analogous steps, the transmitted quadrature component $Q_i(t)$ can be recovered.

Afterwards, the OFDM receiver performs a set of operations similar to those carried out by the OFDM transmitter, but in the reverse order. The two analogue-to-digital (A/D) converters simply extract samples from the analogue OFDM signal components at specific time instants. After S/P conversion, the CP is removed and the signal enters the FFT block, which is responsible for the demodulation process. In a real system, after the FFT block, equalization is needed to compensate for the distortion introduced by the channel. Finally, the M-QAM de-mapper converts the received information symbol stream in the output bit stream.

Single-tap equalizer

One of the advantages of the OFDM technique is that equalization can be performed in the digital domain. Usually, since ISI and ICI are removed by means of the CP, only a simple "single-tap" equalizer (i.e., an equalizer that perform only a single complex multiplication) for each subcarrier is required [9]. More precisely, in our work, for channel estimation purposes, a sequence of OFDM training symbols is transmitted before the information symbols (training symbols are not used for performance evaluation). These OFDM training symbols are known a priori by the receiver.

Assume that $\boldsymbol{c}$ (defined before the IFFT block) is an OFDM training symbol. As any other OFDM symbol, $\boldsymbol{c}$ is a vector of N_{sc} M-QAM symbols: $\boldsymbol{c} = (c_1, \ldots, c_{N_{sc}})$. Assume that $\tilde{\boldsymbol{c}} = (\tilde{c}_1, \ldots, \tilde{c}_{N_{sc}})$ is the received OFDM symbol (after the FFT block) associated to $\boldsymbol{c}$. Let us call $\boldsymbol{H_{eq}} = (H_{eq,1}, \ldots, H_{eq,N_{sc}})$ the equalizer transfer function. Each element, $H_{eq,k}$, of $\boldsymbol{H_{eq}}$ is associated to the kth subcarrier and is computed as

$$H_{eq,k} = \frac{c_k}{\tilde{c}_k} \tag{2.38}$$

It can be shown that, in this way, the resulting equalizer transfer function is the inverse of the channel transfer function. To make the equalizer transfer function robust to the noise, a number (N_{tr}) of OFDM training symbols is transmitted, N_{tr} transfer functions are computed and a mean is performed over all the transfer functions. After the training OFDM symbols, OFDM information symbols are transmitted. Let us call $\hat{c}_k$ a generic QAM received information symbol, associated to the kth subcarrier. In order to remove the channel effects from $\hat{c}_k$, the equalizer simply multiplies $\hat{c}_k$ by $H_{eq,k}$.

Figure 2.9(a) shows the constellation of the received QAM information symbols after the FFT block, when a filter with transfer function described by a Bessel function of the third order is interposed between the electrical OFDM transmitter and the electrical OFDM receiver (no optical modulator and optical channel are considered in this context). Details on the Bessel function are deliberately omitted, cause our aim is to test the equalizer when, as shown in Figure 2.9(a), distortion on both the amplitude and the phase of the QAM symbols is introduced. Notice that additional amplitude attenuation is introduced by the down-conversion process (see equation (2.37)). Figure 2.9(b) shows the QAM symbols constellation after equalization. By comparison between the received equalized constellation and the transmitted constellation (see Figure 2.7), we can infer that our equalizer properly corrects amplitude and phase distortion introduced by the channel.

2.3.3 Sieben's architecture to generate SSB optical signals

The single sideband (SSB) version, $x_{SSB}(t)$, of a generic signal $x(t)$ is given by

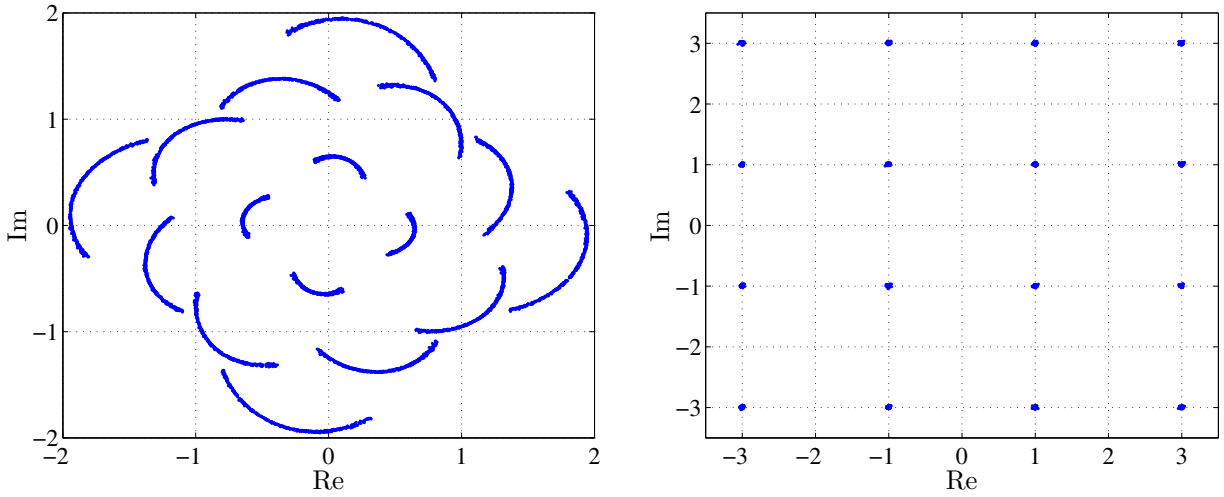

Figure 2.9: Constellation of the received QAM information symbols, when the channel transfer function is described by a Bessel function of the third order, (a) after FFT block and (b) after equalizer block.

$$x_{SSB}(t) = x(t) \pm j x_H(t) \tag{2.39}$$

where $x_H(t)$ is the Hilbert transform (HT) of $x(t)$ and j is the imaginary unit. The ideal HT transfer function is given by

$$H_H(f) = -j \ \mathrm{sgn}(f) \tag{2.40}$$

where $\mathrm{sgn}(f)$ is the sign function, defined as

$$\mathrm{sgn}(f) = \begin{cases} 1, & f > 0 \\ 0, & f = 0 \\ -1, & f < 0 \end{cases} \tag{2.41}$$

Among the different techniques presented in literature to generate a SSB optical signal, in this work, we focus on the architecture described in [1], henceforth referred as Sieben's architecture.

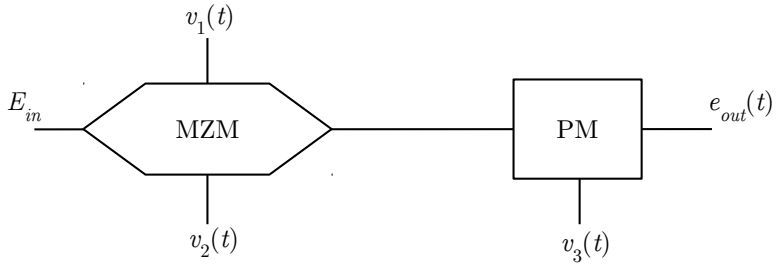

Figure 2.10: Schematic representation of the Sieben's architecture.

As depicted in Figure 2.10, the Sieben's architecture consists of a cascade of a Mach-Zehnder modulator (MZM) and a phase modulator (PM). The electric field at the output of the Sieben's architecture can be expressed as

$$e_{out}(t) = \frac{E_{in}}{2}\left[\exp\left(j\frac{\pi}{2V_x}v_1(t)\right) + \exp\left(j\frac{\pi}{2V_x}v_2(t)\right)\right]\exp\left(j\frac{\pi}{2V_x}v_3(t)\right) \tag{2.42}$$

where E_{in} is the electric field at the input of the architecture and V_x is the modulators switching voltage (voltage swing required to switch between the maximum and the minimum of the power transmission characteristic of the modulators). V_x is assumed to be the same for both the MZM and the PM. The electrical signals at the input of the MZM, $v_1(t)$ and $v_2(t)$, and at the input of the PM, $v_3(t)$, are [1] [26]

$$v_1(t) = -V_b + \alpha v(t) \tag{2.43}$$

$$v_2(t) = +V_b - \alpha v(t) \tag{2.44}$$

$$v_3(t) = v_H(t) \tag{2.45}$$

where V_b is the MZM bias voltage, $v(t)$ is the electrical (voltage) signal to be converted in the optical domain (in our case, $v(t)$ is usually the MB-OFDM signal), $v_H(t)$ is the HT of $v(t)$ and α is a coefficient used to adjust the voltage level of the signal $v(t)$ with respect to the voltage level of the signal $v_H(t)$. It will be shown in subsection 3.1.1 that, by choosing α in the proper way, it is possible to obtain a SSB signal at the output of the architecture of Figure 2.10.

2.3.4 O/E converter (PIN)

The O/E converter considered in this work is the positive-intrinsic-negative (PIN) photodetector. A PIN generates a current that is proportional to the optical power incident on its surface, or, in other words, proportional to the square of the absolute value of the incident electric field. More precisely, if $e_{PIN}(t)$ is the incident electric field, the current at the PIN output is given by

$$i_{PIN}(t) = R_\lambda |e_{PIN}(t)|^2 \tag{2.46}$$

where R_λ is a parameter called responsivity.

2.4 Photodetection process

The two main optical detection processes, coherent-detection, and direct-detection (DD) were introduced in chapter 1. In this work, DD is considered. When DD is employed, only one PIN is used in the photodetection process and an optical carrier is transmitted together with the optical signal to assist photodetection.

2.4.1 Carrier assisted photodetection

When DD is employed, to understand why an optical carrier is needed to assist photodetection, let us initially consider a single optical OFDM signal, $x(t)$, as the input of the PIN photodetector. Since the current at the PIN output is proportional to $|x(t)|^2$ (see equation (2.46)), part of the information carried by $x(t)$ is destroyed by the detection process: $x(t)$ cannot be recovered.
Consider now an optical signal, $s(t)$, (in baseband representation) composed by the sum of a single optical OFDM signal, $x(t)$, and an optical carrier, B,

$$s(t) = x(t) + B \tag{2.47}$$

Without loss of generality, suppose $x(t)$ real-valued. An illustration of the spectrum of $s(t)$ is depicted in Figure 2.11(a), where B_w is the bandwidth of $x(t)$ and the the optical carrier is represented as Dirac delta. Figure 2.11(a) also illustrates the presence of a frequency gap, Δf, between the optical carrier and the OFDM band. This frequency gap is usually needed for reasons that will be clear soon.
When $s(t)$ is photodetected, the current at the PIN output, $i_{PIN}(t)$, is proportional to:

$$i_{PIN}(t) \propto |s(t)|^2 = \underbrace{|B|^2}_{(1)} + \underbrace{2\Re\{B\}x(t)}_{(2)} + \underbrace{|x(t)|^2}_{(3)}. \tag{2.48}$$

where $\Re\{\cdot\}$ denotes the real part of a complex number. Let us analyse each term of equation (2.48). Term (1) is a DC component. Term (2) is the result of the beat between $x(t)$ and the optical carrier. From term (2) a replica of the information-bearing signal, $x(t)$, can be recovered, thus explaining the role of the optical carrier in the DD process. Term (3) is a second-order nonlinear product, also known as signal-to-signal beat interference (SSBI), which is a source distortion introduced by the PIN. In Figure 2.11(b), an illustration of the spectrum of $i_{PIN}(t)$ is shown. Figure 2.11(b) also illustrates the role of the frequency gap Δf: it is used to "accommodate" the SSBI term, i.e., to avoid that the information-bearing signal and the SSBI overlap in frequency, thus allowing to discard the SSBI term with simple filtering techniques. It can be shown that, to completely accommodate the SSBI term, Δf has to be typically as wider as B_w, leading to a considerable reduction of the spectral efficiency.
If high spectral efficiency is a main requirement, the optical carrier must be placed close to the OFDM band and alternative solutions to deal with the SSBI have to be used.
A first, partial, solution consists in properly increasing, if possible, the power of the optical carrier, if compared to the power of the OFDM signal, in order to make term (2) of equation (2.48) dominant with respect to term (3).
A second solution, that can be used together with the first one, consists in the development of a DSP algorithm, at the receiver side, to reconstruct the SSBI term and remove it from the photodetected signal [3].

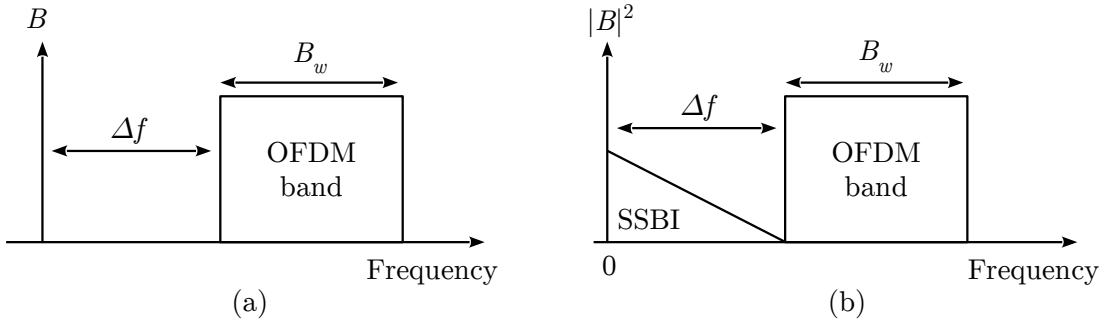

Figure 2.11: Illustration of the spectrum of (a) the signal $s(t)$ of equation (2.47) and (b) the signal $i_{PIN}(t)$ of equation (2.48), when a frequency gap Δf is used to accommodate the SSBI term. For simplicity, only positive frequencies are reported.

2.4.2 MB-OFDM signal detection and the virtual carrier concept

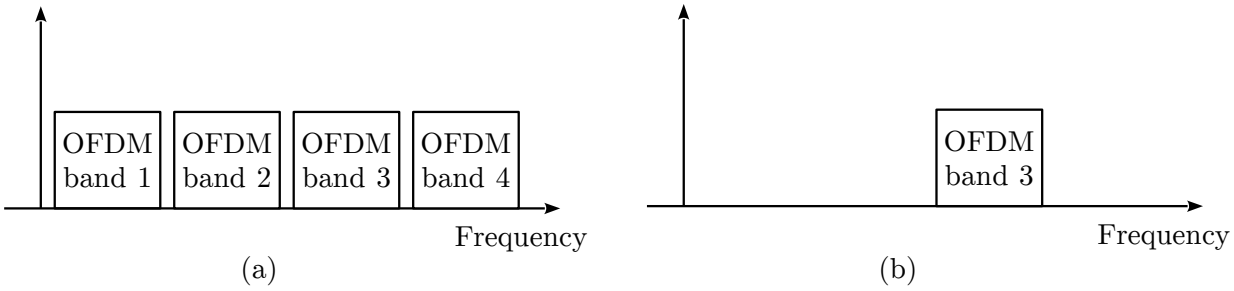

Figure 2.12: Illustration of the spectrum of an optical MB-OFDM signal with four bands and one optical carrier (a) before and (b) after a dual band optical filter.

When an optical MB-OFDM signal is considered, for networking purposes, it should be possible to detect each OFDM band (belongings to the MB-OFDM signal) independently from the other ones.

A first possible solution to achieve this requirement, if only one optical carrier is transmitted together with the MB-OFDM signal, is to use a dual band optical filter (before photodetection). In Figure 2.12(a), the spectrum of an optical MB-OFDM signal with four bands and one optical carrier is illustrated. The resulting spectrum, after the dual band optical filter, is illustrated in Figure 2.12(b). As illustrated in Figure 2.12, a dual band optical filter allows to select a desired OFDM band (band 3 in this case) together with the optical carrier, while discarding the other OFDM bands.
After the dual band optical filter, the selected optical OFDM band and the optical carrier are delivered to the PIN for photodetection. It should be noticed that the bandwidth of the signal at the dual band optical filter output depends on the central frequency of the selected OFDM band. In the worst case, when the band with highest central frequency is selected (band 4 in Figure 2.12(a)), the filtered signal has a bandwidth comparable to the bandwidth of the entire MB-OFDM signal. Consequently, the photodetector should have an electrical bandwidth at least as wide as the bandwidth of the MB-OFDM signal, even if

only one OFDM band is photodetected.
Another disadvantage of this solution is the high cost expected for the dual band optical filter [3].

An alternative solution, which allows to overcome the need for an expensive dual band optical filter, while maintaining networking flexibility, consists in the use of virtual carriers. One virtual carrier is placed close to each OFDM band as illustrated in Figure 2.13 ($f_{vc,i}$ is the frequency of the virtual carrier associated to the ith OFDM band). A standard (single band) optical filter can be used to filter the desired OFDM band (the band that has to be photodetected) together with the associated virtual carrier. The virtual carrier is used to assist in the detection process (in the way described in subsection 2.4.1).

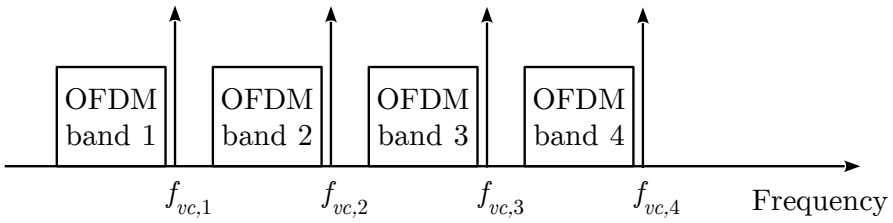

Figure 2.13: Illustration of the spectrum of an MB-OFDM signal with virtual carriers.

If compared with the first solution, the use of virtual carriers brings at least two advantages. First of all, no expensive dual band optical filter is needed. Second, the bandwidth requirements for the photodetector and for the receiver front-end are relaxed. If each virtual carrier is placed close the respective band, the electrical bandwidth required to the receiver is comparable to the bandwidth of a single OFDM signal.

The use of virtual carriers, generated in the electrical domain, with one virtual carrier placed close to each OFDM band, together with a SSBI mitigation method (described in section 4.3), is the solution considered in this work.

Parameters of an MB-OFDM signal comprising virtual carriers

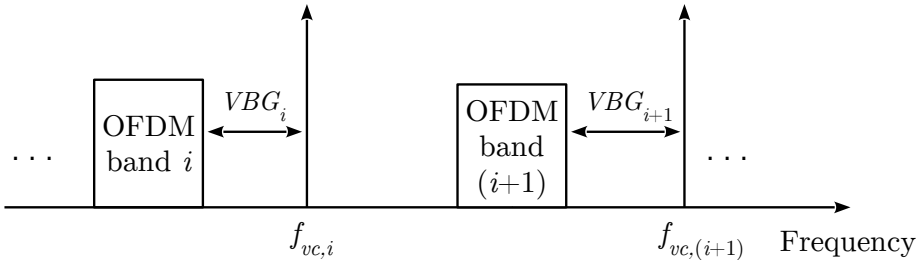

Figure 2.14: Illustration of the VBG concept.

Besides the parameters defined in subsection 2.2.1, when considering an MB-OFDM signal comprising virtual carriers, it is useful to define new parameters. The virtual carrier-to-band

gap (VBG) is the frequency gap between a certain OFDM band and the associated virtual carrier. VBG_i is the width of frequency gap between the ith band and the corresponding virtual carrier, as illustrated in Figure 2.14.

The virtual carrier-to-band power ratio (VBPR) between the ith virtual carrier and the corresponding band is defined as

$$\text{VBPR}_i = \frac{p_{vc,i}}{p_{b,i}} \tag{2.49}$$

where $p_{b,i}$ is the power of the ith OFDM band and $p_{vc,i}$ is the power of the associated virtual carrier.

From now on, if not differently specified, we will assume $VBG_1 = VBG_2 = \cdots = VBG_{N_b} = VBG$ and $\text{VBPR}_1 = \text{VBPR}_2 = \cdots = \text{VBPR}_{N_b} = \text{VBPR}$.

The frequency of the ith virtual carrier is called $f_{vc,i}$ (see Figure 2.14). A possible choice for $f_{vc,i}$ is

$$f_{vc,i} = f_{c,i} + \frac{B_w}{2} + VBG \qquad\qquad i = 1, 2, \ldots N_b \tag{2.50}$$

where $f_{c,i}$ is the central frequency of the ith OFDM band and B_w is the bandwidth of the OFDM band.

In agreement with the notation of [27], a generic MB-OFDM signal, $v(t)$, comprising virtual carriers, in the electrical domain, can be mathematically expressed as

$$v(t) = \underbrace{[s_b(t) + A_v s_v(t)]}_{s_e(t)} \frac{V_{RMS,imp}}{V_{RMS,s_e}} \tag{2.51}$$

with

$$s_b(t) = \sum_{i=1}^{N_b} \frac{s_{b,i}(t)}{V_{RMS,s_{b,i}}} \tag{2.52}$$

and

$$s_v(t) = \sum_{i=1}^{N_b} \frac{s_{v,i}(t)}{V_{RMS,s_{v,i}}} \tag{2.53}$$

where $s_{b,i}$ and $s_{v,i}$ are the ith up-converted OFDM band and the ith virtual carrier, respectively, $s_b(t)$ and s_v are the sum of all N_b OFDM bands and virtual carriers, respectively, $V_{RMS,s_{b,i}}$, $V_{RMS,s_{v,i}}$ and V_{RMS,s_e} are the RMS voltages of $s_{b,i}$, $s_{v,i}$ and $s_e(t)$, respectively, $V_{RMS,imp}$ is the RMS voltage imposed to $v(t)$, and A_v is the amplitude of each virtual carrier (assumed to be real). The notation of equation 2.51, equation 2.52 and equation 2.53 is useful when dealing with signal powers. The mean power of $v(t)$ can be written as

$$p_v = \left\langle |v(t)|^2 \right\rangle = V_{RMS,imp}^2 \tag{2.54}$$

where $\langle \cdot \rangle$ denotes the mean value of a signal. Remembering that both a generic OFDM signal and a virtual carrier are zero-mean signals, it results

$$\left\langle |s_b(t)|^2 \right\rangle = \left\langle |s_v(t)|^2 \right\rangle = N_b \tag{2.55}$$

and

$$V_{RMS,s_e}^2 = N_b(1 + A_v^2) \tag{2.56}$$

It is also not difficult to show that the VBPR can be written as

$$\text{VBPR} = A_v^2 \tag{2.57}$$

On the other hand, is some situations, the notation of equation 2.51, equation 2.52 and equation 2.53 may result heavy. Thus, another definition of $v(t)$ is also considered:

$$v(t) = \sum_{i=1}^{N_b} x_i(t) + \sum_{i=1}^{N_b} B\cos(\omega_{vc,i}t) \tag{2.58}$$

where $x_i(t)$ is the ith OFDM signal and $B\cos(\omega_{vc,i}t)$ is the associated virtual carrier. B and $\omega_{vc,i} = 2\pi f_{vc,i}$ are the amplitude and the angular frequency of the virtual carrier, respectively. The following relations hold:

$$x_i(t) = \frac{s_{b,i}(t)}{V_{RMS,s_{b,i}}} \frac{V_{RMS,imp}}{V_{RMS,s_e}} \tag{2.59}$$

$$B = \frac{A_v}{V_{RMS,s_{v,i}}} \frac{V_{RMS,imp}}{V_{RMS,s_e}} \tag{2.60}$$

$$\cos(\omega_{vc,i}t) = s_{v,i}(t) \tag{2.61}$$

From equation (2.60) and since A_v is assumed to be real, it follows that B is a real constant, as well.

2.5 Noise sources

Two kinds of noise are considered in this work, namely thermal noise and amplified spontaneous emission (ASE) noise. An electrical amplifier is used after photodetection. We assume that the whole thermal noise is added at the electrical amplifier output. An optical amplifier is used before the BS. We assume that the whole ASE noise is added at the optical amplifier output.

2.5.1 Thermal noise

Thermal noise is generated by the thermal agitation of electrons in an electrical conductor. It affects each real electrical device. Although other kinds of electrical noise exist (e.g. shot noise), thermal noise is the only electrical noise considered in this work. More precisely, we use an electrical amplifier after the PIN photodetector (see configuration of Figure 2.15), and we assume that the whole thermal noise is added at the electrical amplifier output. In Figure 2.15, V_{bias} and R_{bias} are the PIN bias voltage and bias resistance, respectively, $e_{PIN}(t)$ is the electrical field at PIN input, $i_{PIN}(t)$ is the current at PIN output, $f_{n,e}$ and g_e are the noise figure and gain of the electrical amplifier, respectively. The current at the electrical amplifier output, $i(t)$, can be expressed as

$$i(t) = g_e i_{PIN}(t) + i_{th}(t) \tag{2.62}$$

where $i_{th}(t)$ is the thermal noise current at the electrical amplifier output.
The two sided PSD of $i_{th}(t)$ can be expressed as

$$S_{th} = \frac{2k_B T_r f_{n,e}}{R_{bias}} g_e^2 \tag{2.63}$$

where k_B is the Boltzmann constant ($k_B \simeq 1.38\times10^{-23}$ J/K) and T_r is the room temperature. Typical values for the parameters of equation (2.63) are reported in Table 2.5

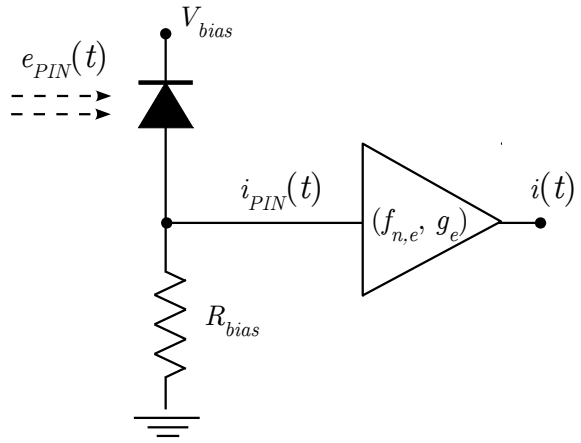

Figure 2.15: Electrical amplifier at PIN output.

Parameter	Symbol	Typical value	Unit
electrical amplifier noise figure	$f_{n,e}$	3-6	dB
electrical amplifier gain	g_e	10-20	dB
room temperature	T_r	298	K
bias resistance	R_{bias}	50	Ω

Table 2.5: Typical values for the parameters of equation (2.63).

2.5.2 ASE noise

Erbium doped fibre amplifiers (EDFAs) can be used to amplify an optical signal in the C-band of the optical spectrum. In our MB-OFDM system, an EDFA is assumed to be used before the BS. Besides amplifying the optical signal, the EDFA also introduces a kind of noise called ASE. The ASE is due to the amplification of photons generated by spontaneous emission inside the doped fibre. In this work, the ASE generated by the EDFA is the only optical noise considered.

Let us assume, for the sake of simplicity, that the electric field at the EDFA input, $e_{in,EDFA}(t)$, has parallel ($||$) polarization, i.e., it is oriented along the direction identified by the unit vector $\boldsymbol{u}_{||}$. Then, the electric field at the EDFA output, $\boldsymbol{e}_{out,EDFA}(t)$, can be expressed as

$$\boldsymbol{e}_{out,EDFA}(t) = [g_{EDFA} e_{in,EDFA}(t) + n_{ASE,||}(t)]\boldsymbol{u}_{||} + [n_{ASE,\perp}(t)]\boldsymbol{u}_{\perp} \tag{2.64}$$

where g_{EDFA} is the gain of the EDFA, $n_{ASE,||}(t)$ is the ASE noise component with parallel polarization and $n_{ASE,\perp}(t)$ is the ASE noise component with perpendicular ($\perp$) polarization, i.e., oriented along the direction identified by the unit vector $\boldsymbol{u}_{\perp}$.

In the baseband representation, the useful signal, $e_{in,EDFA}(t)$, and, in a similar way, the ASE noise components, $n_{ASE,||}(t)$ and $n_{ASE,\perp}(t)$, are characterized by an in-phase (I) component and a quadrature (Q) component:

$$e_{in,EDFA}(t) = e_{in,EDFA,I}(t) + j e_{in,EDFA,Q}(t) \tag{2.65}$$

$$n_{ASE,||}(t) = n_{ASE,||,I}(t) + j n_{ASE,||,Q}(t) \tag{2.66}$$

$$n_{ASE,\perp}(t) = n_{ASE,\perp,I}(t) + j n_{ASE,\perp,Q}(t) \tag{2.67}$$

We assume that each of the four ASE noise components is zero-mean additive white Gaussian, with constant PSD given by S_{ASE}.

Then, the mean power of the ASE (p_{ASE}) in a reference bandwidth, B_0, is given by

$$p_{ASE} = 4 S_{ASE} B_0 \tag{2.68}$$

S_{ASE} is a function of the optical frequency (ν_0):

$$S_{ASE} = S_{ASE}(\nu_0) = h\nu_0 f_{n,EDFA}(g_{EDFA} - 1) \tag{2.69}$$

where h is the Planck constant ($h = 6.62 \times 10^{-34}$ J·s) and $f_{n,EDFA}$ is the noise figure of the EDFA. In this work we assume $\nu_0 = 193.1$ THz. Typical values for the EDFA noise figure are 3-6 dB.

Chapter 3

Sieben's architecture and PIN combined nonlinearities

3.1 Sieben's architecture analysis

The Sieben's architecture is described in subsection 2.3.3. In subsection 3.1.1 we show that, with a proper selection of the coefficient α of equation (2.43) and equation (2.44), in a first-order approximation, the signal at the output of the Sieben's architecture is a SSB signal. In subsection 3.1.2, we identify the second-order nonlinearities introduced by the architecture under consideration. Our analysis is similar to the one developed in [1], but more general, since no constraints are imposed on V_b, the bias voltage of the MZM. Moreover, assuming that the electrical signal at the Sieben's architecture input is an MB-OFDM signal, different mixed products that emerge from second-order nonlinear terms are identified and analysed in subsection 3.1.3, subsection 3.1.4 and subsection 3.1.5. Some spectra, obtained by numerical simulation, of the signal at the Sieben's architecture output are presented in subsection 3.1.6. Cancellations between second-order terms are shown in subsection 3.1.7. The frequency location of each mixed products is identified and, in subsection 3.1.8, a general method to understand if such product is inside the nth OFDM band is given.

With reference to Figure 2.10, taking into account equations (2.43)-(2.45) and defining $z = \pi/(2V_x)$, equation (2.42) can be rewritten as

$$\begin{aligned} e_{out}(t) &= \frac{E_{in}}{2}\left[\exp\left(j\frac{\pi}{2V_x}(-V_b+\alpha v(t))\right)+\exp\left(j\frac{\pi}{2V_x}(V_b-\alpha v(t))\right)\right]\exp\left(j\frac{\pi}{2V_x}v_H(t)\right) \\ &= E_{in}\cos\Big(z\alpha v(t)-zV_b\Big)\exp\Big(jzv_H(t)\Big) \\ &= E_{in}\Big[\cos\Big(z\alpha v(t)\Big)\cos(zV_b)+\sin\Big(z\alpha v(t)\Big)\sin(zV_b)\Big]\exp\Big(jzv_H(t)\Big) \end{aligned} \tag{3.1}$$

Our analysis can be further developed taking the Taylor expansion around zero of the time dependent terms in equation (3.1). After some algebraic steps and discarding terms above the second-order, we obtain

$$\begin{aligned} e_{out}(t) \simeq E_{in}\Big[& \cos(zV_b)+ \\ & + z\alpha \sin(zV_b)v(t) + jz\cos(zV_b)v_H(t)+ \\ & - \frac{1}{2}z^2\alpha^2\cos(zV_b)v^2(t) - \frac{1}{2}z^2\cos(zV_b)v_H^2(t) + j\alpha z^2\sin(zV_b)v(t)v_H(t)\Big] \end{aligned} \tag{3.2}$$

In equation (3.2), zero-order, first-order and second-order terms of the expansion are reported on different lines.

3.1.1 Choice of the coefficient α

Discarding the second-order terms in equation (3.2) we obtain

$$e_{out}(t) \simeq E_{in}\Big[\cos(zV_b) + z\alpha\sin(zV_b)v(t) + jz\cos(zV_b)v_H(t)\Big] \tag{3.3}$$

Comparing equation (3.3) with equation (2.39), it immediately follows that, to obtain a SSB optical signal, at least in a first-order approximation, it has to be $z\alpha\sin(zV_b) = \pm z\cos(zV_b)$, i.e., the choice of the coefficient α to obtain a SSB optical signal at the output of the Sieben's architecture, as a function of the bias voltage (V_b), is

$$\alpha = \pm\frac{\cos\left(\dfrac{\pi}{2V_x}V_b\right)}{\sin\left(\dfrac{\pi}{2V_x}V_b\right)} \tag{3.4}$$

If not differently specified, in the following, we will consider the choice with the plus sign in equation (3.4).

It is interesting to note that, if $V_b = V_x$, i.e., working at minimum bias point (MBP), it results $\alpha = 0$. Then, at MBP, in is not possible to generate SSB signals with the Sieben's architecture.

If we choose $V_b = V_x/2$, i.e., working at quadrature bias point (QBP), it results $\cos(zV_b) = \sin(zV_b) = \sqrt{2}/2$, $\alpha = 1$ and the Taylor expansion of equation (3.2) takes a similar form to equation (8) in [1] (discarding third-order terms).

3.1.2 Analysis of second-order nonlinearities

With the choice (3.4), equation (3.2) becomes

$$
\begin{aligned}
e_{out}(t) \simeq E_{in}\Bigg[& \underbrace{\cos(zV_b)}_{(a)} + \\
& \underbrace{+z\cos(zV_b)\Big(v(t)+jv_H(t)\Big)}_{(b)} + \\
& \underbrace{-\frac{1}{2}z^2\frac{\cos^3(zV_b)}{\sin^2(zV_b)}v^2(t)}_{(c)} \; \underbrace{-\frac{1}{2}z^2\cos(zV_b)v_H^2(t)}_{(d)} + \underbrace{jz^2\cos(zV_b)v(t)v_H(t)}_{(e)}\Bigg]
\end{aligned}
\tag{3.5}
$$

Let us identify each term of equation (3.5). Term (a) is the zero-order term (optical carrier). Term (b) is a first-order SSB version of the information-bearing signal $v(t)$ (see equations (2.43)-(2.44) of subsection 2.3.3). Term (b) is thus the "useful" part of $e_{out}(t)$. Terms labelled as (c), (d) and (e) are second-order distortion terms or second-order nonlinear terms.

It is interesting to determine, if possible, which choice of the bias voltage (V_b) minimizes the second-order terms in equation (3.5).

Equation (3.5) shows that working near MBP ($V_b \simeq V_x$) seems to be convenient, since the second-order term depending on $\cos^3(zV_b)/\sin^2(zV_b)$ in equation (3.5) will be minimized. However, all the other terms in equation (3.5) are proportional to $\cos(zV_b)$, thus it seems that no further improvements can be achieved through a proper choice of V_b.
Furthermore, as V_b tends to V_x, $\cos(zV_b)$ tends to zero. As a consequence, the power of $e_{out}(t)$ tends to zero as well.

To further develop the analysis of second-order nonlinear terms, suppose that $v(t)$ is an MB-OFDM signal comprising virtual carriers. We focus now on $v^2(t)$, $v_H^2(t)$ and $v(t)v_H(t)$, which are second-order products that appear in terms (c), (d) and (e) of equation (3.5). Making use of equation 2.58, $v^2(t)$ can be written as

$$
\begin{aligned}
v^2(t) &= \left(\sum_{i=1}^{N_b} x_i(t) + \sum_{i=1}^{N_b} B\cos(\omega_{vc,i}t)\right)^2 = \\
&= \underbrace{\left(\sum_{i=1}^{N_b} x_i(t)\right)^2}_{(1)} + \underbrace{2B\left(\sum_{i=1}^{N_b} x_i(t)\right)\left(\sum_{i=1}^{N_b}\cos(\omega_{vc,i}t)\right)}_{(2)} + \underbrace{B^2\left(\sum_{i=1}^{N_b}\cos(\omega_{vc,i}t)\right)^2}_{(3)}
\end{aligned}
\tag{3.6}
$$

Exploiting the linearity of the Hilbert transform (HT) and the fact that $\mathrm{HT}\{\cos(t)\} = \sin(t)$, it is possible to express $v_H(t)$ as

$$v_H(t) = \sum_{i=1}^{N_b} x_{H,i}(t) + \sum_{i=1}^{N_b} B\sin(\omega_{vc,i}t) \tag{3.7}$$

where $x_{H,i}(t)$ denotes the HT of $x_i(t)$.
Using equation (3.7) and equation (2.58), terms $v_H^2(t)$ and $v(t)v_H(t)$ can be expressed as

$$v_H^2(t) = \underbrace{\left(\sum_{i=1}^{N_b} x_{H,i}(t)\right)^2}_{(1)} + \underbrace{2B\left(\sum_{i=1}^{N_b} x_{H,i}(t)\right)\left(\sum_{i=1}^{N_b}\sin(\omega_{vc,i}t)\right)}_{(2)} + \underbrace{B^2\left(\sum_{i=1}^{N_b}\sin(\omega_{vc,i}t)\right)^2}_{(3)} \tag{3.8}$$

$$\begin{aligned} v(t)v_H(t) = {} & \underbrace{\left(\sum_{i=1}^{N_b} x_i(t)\right)\left(\sum_{i=1}^{N_b} x_{H,i}(t)\right)}_{(1)} + \\ & + \underbrace{B\left(\sum_{i=1}^{N_b} x_i(t)\right)\left(\sum_{i=1}^{N_b}\sin(\omega_{vc,i}t)\right) + B\left(\sum_{i=1}^{N_b} x_{H,i}(t)\right)\left(\sum_{i=1}^{N_b}\cos(\omega_{vc,i}t)\right)}_{(2)} + \\ & + \underbrace{B^2\left(\sum_{i=1}^{N_b}\cos(\omega_{vc,i}t)\right)\left(\sum_{i=1}^{N_b}\sin(\omega_{vc,i}t)\right)}_{(3)} \end{aligned} \tag{3.9}$$

Considering terms (c), (d) and (e) of equation (3.5) and from equation (3.6), equation (3.8) and equation (3.9) it can be seen that the Sieben's architecture introduces, in the optical signal $e_{out}(t)$, different kinds of second-order distortion terms. Terms (1) in equation (3.6), equation (3.8) and equation (3.9) are mixed products between OFDM bands. These mixed products between bands do not depend on the constant B. Terms (2) in equation (3.6), equation (3.8) and equation (3.9) are mixed products between OFDM bands and virtual carriers. These mixed products between OFDM bands and virtual carriers are proportional to B. Terms (3) in equation (3.6), equation (3.8) and equation (3.9) are mixed products between virtual carriers. These mixed products between virtual carriers are proportional to B^2.
In turn, B is proportional to the VBPR and the VBPR is usually greater than 1. It is thus reasonable to expect that, as the VBPR increases, the impact of term (2) and, especially, of term (3) of equation (3.6), equation (3.8) and equation (3.9) on system performance also increases, as will be more rigorously shown in subsection 3.2.2.

Remembering that, before photodetection, the optical MB-OFDM signal passes through a band selector (BS) (see Figure 2.5), it is interesting to determine the "frequency location" of

each distortion term in equation (3.6), equation (3.8) and equation (3.9). Once determined the frequency location of a certain distortion component, it is possible to understand if this component is inside the band of the BS. If it is, it will introduce degradation after square-law photodetection, at the PIN output, as will be more rigorously shown in subsection 3.2.2.

3.1.3 Distortion tones

We focus now on the mixed products between virtual carriers, i.e., terms (3) of equation (3.6), equation (3.8) and equation (3.9). In the following, since the product between two sinusoidal signals can be expressed as the sum of two signals that are still sinusoidal, these mixed products between virtual carriers are called "second-order distortion tones" or simply "distortion tones".

We try now to determine the frequency location of a generic distortion tone. Omitting the coefficient B^2, and exploiting some trigonometric identities, term (3) of equation (3.6) can be rewritten as

$$\begin{aligned}\left(\sum_{i=1}^{N_b}\cos(\omega_{vc,i}t)\right)^2 &= \sum_{i=1}^{N_b}\sum_{j=1}^{N_b}\cos(\omega_{vc,i}t)\cos(\omega_{vc,j}t) = \\ &= \frac{1}{2}\underbrace{\sum_{i=1}^{N_b}\sum_{j=1}^{N_b}\cos\Big((\omega_{vc,i}-\omega_{vc,j})t\Big)}_{(1)} + \frac{1}{2}\underbrace{\sum_{i=1}^{N_b}\sum_{j=1}^{N_b}\cos\Big((\omega_{vc,i}+\omega_{vc,j})t\Big)}_{(2)}\end{aligned} \tag{3.10}$$

From equation (3.10), and developing a similar analysis for terms (3) of equation (3.8) and equation (3.9) (see Appendix A.3.1), two types of distortion tones can be identified. They are reported in Table 3.1 and they are called type 1 and type 2 distortion tones respectively.

Type	Distortion tones	Frequency location
1	$\cos\Big((\omega_{vc,i}-\omega_{vc,j})t\Big),\ \sin\Big((\omega_{vc,i}-\omega_{vc,j})t\Big)$	$f_{vc,i}-f_{vc,j}$
2	$\cos\Big((\omega_{vc,i}+\omega_{vc,j})t\Big),\ \sin\Big((\omega_{vc,i}+\omega_{vc,j})t\Big)$	$f_{vc,i}+f_{vc,j}$

Table 3.1: Two types of distortion tones that emerge from second-order Sieben's architecture nonlinearities, and their respective frequency locations. $i, j = 1, 2, \ldots N_b$.

As shown in Table 3.1, type 1 tones are centred at $f_{vc,i} - f_{vc,j}$, type 2 tones are centred at $f_{vc,i} + f_{vc,j}$. Making use of equation (2.21) and equation (2.50), we obtain

$$f_{vc,i} - f_{vc,j} = (i-j)S_w \tag{3.11}$$

$$f_{vc,i} + f_{vc,j} = (i + j - 2)S_w + 2\left(f_{c,1} + \frac{B_w}{2} + VBG\right) \tag{3.12}$$

where S_w is the width of a frequency slot ($S_w = 3.125\,\text{GHz}$, as stated in subsection 2.2.2), $f_{c,1}$ is the central frequency of the first OFDM band, B_w is the OFDM signal bandwidth and VBG is the virtual carrier-to-band gap width.
From equation (3.11), it can be seen that type 1 distortion tones are located at frequencies multiples of the slot width, S_w, and their location does not depend on the central frequency of the first OFDM band, $f_{c,1}$. On the other hand, from equation (3.12), it can be seen that type 2 distortion tones are located at frequencies multiples of S_w, plus a constant "offset" ($2f_{c,1} + B_w + 2VBG$), and their location depends on $f_{c,1}$.

Equation (3.10) shows that N_b^2 type 1 and N_b^2 type 2 distortion tones are introduced by term (3) of equation (3.6). However, it is worth to notice that some of these tones are placed at the same frequency (equal-frequency tones). In the following, equal-frequency tones will be regarded as a single (equivalent) tone.
We are going now to rearrange equation (3.10) to determine the number, the amplitude and the frequency position of (equivalent) distortion tones.
Substituting equation (3.11) into term (1) of equation (3.10), observing that $f_{vc,i} - f_{vc,j}$ does not separately depend on i and j, but only depends on their difference, $i - j$, and exploiting the fact that the cosine is an even function, we obtain

$$\sum_{i=1}^{N_b}\sum_{j=1}^{N_b}\cos\Big(2\pi(i-j)S_w t\Big) = N_b + 2\sum_{k=1}^{N_b-1}(N_b-k)\cos\Big(2\pi k S_w t\Big) \tag{3.13}$$

Equation (3.13) shows that N_b (equivalent) type 1 distortion tones originate from term (3) of equation (3.6), they are located at frequencies kS_w ($k = 0, \ldots, N_b - 1$) and, except for the tone at zero frequency, their amplitude is proportional to $2(N_b - k)$. Then, the lower the index k, the higher the amplitude of the tone.
Furthermore, equation (3.13) shows that the frequency range occupied by type 1 tones is $[0,\ (N_b - 1)S_w]$. This frequency range has width comparable to the bandwidth of the MB-OFDM signal, $B_{MB-OFDM}$ (see equation (2.27)), especially for sufficiently a high value of N_b.

Substituting equation (3.12) into term (2) of equation (3.10), defining $\delta_1 = 2f_{c,1} + B_w + 2VBG$ and observing that $f_{vc,i} + f_{vc,j}$ does not separately depend on i and j, but only depends on their sum , $i + j$, we obtain

$$\begin{aligned}\sum_{i=1}^{N_b}\sum_{j=1}^{N_b}\cos\Big(2\pi\Big((i+j-2)S_w + \delta_1\Big)t\Big) &= \sum_{k=0}^{N_b-1}(k+1)\cos\Big(2\pi\Big(kS_w + \delta_1\Big)t\Big) \\ &+ \sum_{k=1}^{N_b-1}(N_b-k)\cos\Big(2\pi\Big((N_b+k-1)S_w + \delta_1\Big)t\Big)\end{aligned} \tag{3.14}$$

Equation (3.14) shows that $2N_b - 1$ type 2 (equivalent) distortion tones originate from term (3) of equation (3.6). N_b of them are located at frequencies $kS_w + \delta_1$ $(k = 0, \ldots, N_b - 1)$ and their amplitude is proportional to $(k + 1)$. Let us call them type (2.a) distortion tones. The higher the frequency of a type (2.a) tone, the higher the amplitude of the tone itself. $N_b - 1$ of them are located at frequencies $(N_b + k - 1)S_w + \delta_1$ $(k = 1, \ldots, N_b - 1)$ and their amplitude is proportional to $(N_b - k)$. Let us call them type (2.b) distortion tones. The higher the frequency of a type (2.b) distortion tone, the lower the amplitude of the tone itself. It will be shown in subsection 3.1.8 that type (2.b) tones are always outside the MB-OFDM signal band.
Furthermore, equation (3.14) shows that the frequency range occupied by type 2 tones is $[\delta_1,\ 2(N_b - 1)S_w + \delta_1]$. This frequency range has width comparable to two times the bandwidth of the MB-OFDM signal, $2B_{MB-OFDM}$ (see equation (2.27)), especially for sufficiently a high value of N_b.

A similar analysis can be developed for term (3) of equation (3.8) to show that the same number of tones are introduced by this term at the same frequency positions, as term (3) of equation (3.6). Term (3) of equation (3.9) also introduces the same number of type 2 tones, at the same frequency positions; whereas no type 1 tones originate from this term, as will be more rigorously shown in subsection 3.1.7.

Placing distortion tones outside the OFDM bands

It is interesting to determine, if it exists, a choice of $f_{c,1}$ of equation (2.21) for which both type 1 and type 2 distortion tones are located outside the OFDM bands (i.e., they are located in the gaps between bands). The most interesting choice for the parameter $f_{c,1}$ we have found is

$$f_{c,1} = mS_w - \frac{B_w}{2} - VBG \tag{3.15}$$

with m a positive integer.
With the choice (3.15), equation (3.12) and equation (2.50) become respectively

$$f_{vc,i} + f_{vc,j} = (i + j + 2m - 2)S_w \tag{3.16}$$

$$f_{vc,i} = (i + m - 1)S_w \tag{3.17}$$

Equation (3.16) and equation (3.17) show that, with the choice (3.15), both a generic type 2 tone and a generic virtual carrier are located at frequencies multiples of S_w. Remembering that also type 1 tones are located at multiples of S_w, it is not difficult to show that both types of tones are positioned outside the OFDM bands (since, by construction, virtual carriers are placed outside OFDM bands).

3.1.4 Mixed products between bands and virtual carriers

In this subsection, we focus our analysis on the mixed products between OFDM bands and virtual carriers, i.e., terms (2) of equation (3.6), equation (3.8) and equation (3.9). In the following, we will refer to these products as "band-to-virtual carrier mixed products" or simply "band-to-carrier products". Our aim is to determine the frequency location of a generic band-to-carrier product.

Omitting the coefficient B, and using equation (A.11) of Appendix A.3.2, term (2) of equation (3.6) can be rewritten as

$$\begin{aligned}\left(\sum_{i=1}^{N_b} x_i(t)\right)\left(\sum_{i=1}^{N_b}\cos(\omega_{vc,i}t)\right) &= \sum_{i=1}^{N_b}\sum_{k=1}^{N_b} x_i(t)\cos(\omega_{vc,k}t) = \\ &= \underbrace{\frac{1}{2}\sum_{i=1}^{N_b}\sum_{k=1}^{N_b}\Re\Big\{x_{B,i}(t)\exp\big(j(\omega_{c,i}-\omega_{vc,k})t\big)\Big\}}_{(1)} + \\ &+ \underbrace{\frac{1}{2}\sum_{i=1}^{N_b}\sum_{k=1}^{N_b}\Re\Big\{x_{B,i}(t)\exp\big(j(\omega_{c,i}+\omega_{vc,k})t\big)\Big\}}_{(2)}\end{aligned} \tag{3.18}$$

where $\Re\{\cdot\}$ denotes the real part of a complex signal and $x_{B,i}(t)$ (see equation (2.34)) is the baseband representation of the ith (up-converted) OFDM signal, $x_i(t)$.

By comparison with equation (2.36) it is possible to note that, for example, the term

$$\Re\Big\{x_{B,i}(t)\exp\big(j(\omega_{c,i}-\omega_{vc,k})t\big)\Big\}$$

of equation (3.18) is simply the up-converted version of $x_{B,i}(t)$, centred in frequency at $f_{c,i}-f_{vc,k}$, and its bandwidth is thus comparable to B_w (the OFDM signal bandwidth).

From equation (3.18), and developing a similar analysis for terms (2) of equation (3.8) and equation (3.9) (see Appendix A.3.2), it can be shown that each product between the ith band and the kth virtual carrier leads to the introduction of two kinds of distortion terms. They are reported in Table 3.2 and they are called, with little abuse of terminology, type 1 and type 2 band-to-carrier products, respectively.
Table 3.2 shows that type 1 band-to-carrier products are centred in frequency at $f_{c,i}-f_{vc,k}$, type 2 band-to-carrier products are centred at $f_{c,i}+f_{vc,k}$. Making use of equation (2.21) and equation (2.50), we obtain

$$f_{c,i}-f_{vc,k} = (i-k)S_w - \frac{B_w}{2} + VBG \tag{3.19}$$

Type	Band-to-carrier products	Frequency location
1	$\Re\Big\{x_{B,i}(t)\exp\big(j(\omega_{c,i}-\omega_{vc,k})t\big)\Big\}$, $\Re\Big\{jx_{B,i}(t)\exp\big(j(\omega_{c,i}-\omega_{vc,k})t\big)\Big\}$	$f_{c,i}-f_{vc,k}$
2	$\Re\Big\{x_{B,i}(t)\exp\big(j(\omega_{c,i}+\omega_{vc,k})t\big)\Big\}$, $\Re\Big\{jx_{B,i}(t)\exp\big(j(\omega_{c,i}+\omega_{vc,k})t\big)\Big\}$	$f_{c,i}+f_{vc,k}$

Table 3.2: Two types of band-to-carrier products that emerge from second-order Sieben's architecture nonlinearities, and their respective frequency locations. $i,k=1,2,\dots N_b$.

$$f_{c,i}+f_{vc,k}=(i+k-2)S_w+2f_{c,1}+\frac{B_w}{2}+VBG \tag{3.20}$$

Similarly to type 1 distortion tones, from equation (3.19), it can be seen that type 1 band-to-carrier products are located at frequencies multiples of the slot width, S_w, (plus a constant offset, $-B_w/2+VBG$) and their location does not depend on the central frequency of the first OFDM band, $f_{c,1}$. Symilarly to type 2 distortion tones, from equation (3.20), it can be seen that type 2 band-to-carrier products are located at frequencies multiples of S_w, plus a constant offset ($2f_{c,1}+B_w/2+VBG$), and their location depends on $f_{c,1}$.

Observing that $f_{c,i}-f_{vc,k}$ does not separately depend on i and k, but only on their difference, $i-k$, from equation (3.19), we can conclude that a generic type 1 band-to-carrier product is centred at frequency $kS_w+\delta_2$ ($k=0,\dots,N_b-1$), with $\delta_2=-B_w/2+VBG$. Similarly, from equation (3.20), we can conclude that a generic type 2 band-to-carrier product is centred at frequency $kS_w+\delta_3$ ($k=0,\dots,2(N_b-1)$), with $\delta_3=2f_{c,1}+B_w/2+VBG$.

Let us try to rearrange term (2) of equation (3.18) (a similar rearrangement is valid for term (1) of equation (3.18)), in order to determine how many type 2 band-to-carrier products sum together at the same frequency location. Unlike distortion tones, it is not possible to regard equal-(central)-frequency band-to-carrier products as a single equivalent term. Nevertheless, omitting the $\Re\{\cdot\}$ operator, term (2) of equation (3.18) can be rearranged as

$$\begin{aligned}\sum_{i=1}^{N_b}\sum_{k=1}^{N_b}x_{B,i}(t)\exp\big(j(\omega_{c,i}+\omega_{vc,k})t\big)=\\ =\underbrace{\sum_{k=0}^{N_b-1}\exp\Big(j2\pi(kS_w+\delta_3)t\Big)\left(\sum_{i=1}^{k+1}x_{B,i}(t)\right)}_{(1)}+\\ +\underbrace{\sum_{k=1}^{N_b-1}\exp\Big(j2\pi\big((N_b+k-1)S_w+\delta_3\big)t\Big)\left(\sum_{i=k+1}^{N_b}x_{B,i}(t)\right)}_{(2)}\end{aligned} \tag{3.21}$$

As an example, term (1) of equation (3.21) shows that only one (type 2) band-to-carrier product is centred at δ_3 (obtained for $k = 0$), whereas N_b band-to-carrier products sum together at $(N_b - 1)S_w + \delta_3$ (obtained for $k = N_b - 1$). In general, the higher the index k in term (1) of equation (3.21), the higher the number of bands that sum together around the frequency $kS_w + \delta_3$ ($k = 0, \ldots, N_b - 1$).

It is not difficult to show that, similarly to type 1 and 2 distortion tones, the width of the frequency range occupied by type 1 and type 2 band-to-carrier products is comparable to $B_{MB-OFDM}$ and $2B_{MB-OFDM}$ respectively.

A similar analysis can be developed for term (2) of equation (3.8) to show that the same number of band-to-carrier products are introduced by this term at the same frequency positions, as term (2) of equation (3.6). Term (2) of equation (3.9) also introduces the same number of type 2 band-to-carrier products, at the same frequency positions; however, no type 1 band-to-carrier products originate from this term, as will be more rigorously shown in subsection 3.1.7.

3.1.5 Mixed products between bands

In this subsection, we focus our analysis on the mixed products between OFDM bands, i.e., terms (1) of equation (3.6), equation (3.8) and equation (3.9). In the following, we will refer to these products as "band-to-band mixed products" or simply "band-to-band products". Our aim is to determine the frequency location of a generic band-to-band product.

Using equation (A.19) of Appendix A.3.3, term (1) of equation (3.6) can be rewritten as

$$\begin{aligned}\left(\sum_{i=1}^{N_b} x_i(t)\right)^2 &= \sum_{i=1}^{N_b}\sum_{k=1}^{N_b} x_i(t)x_k(t) = \\ &= \frac{1}{2}\sum_{i=1}^{N_b}\sum_{k=1}^{N_b} \Re\Big\{ x_{B,i}(t)x^*_{B,k}(t)\exp\big(j(\omega_{c,i} - \omega_{c,k})t\big)\Big\} + \\ &+ \frac{1}{2}\sum_{i=1}^{N_b}\sum_{k=1}^{N_b} \Re\Big\{ x_{B,i}(t)x_{B,k}(t)\exp\big(j(\omega_{c,i} + \omega_{c,k})t\big)\Big\}\end{aligned} \tag{3.22}$$

It is possible to note that, for example, the term

$$\Re\Big\{ x_{B,i}(t)x^*_{B,k}(t)\exp\big(j(\omega_{c,i} - \omega_{c,k})t\big)\Big\}$$

of equation (3.22) is the up-converted version of $x_{B,i}(t)x^*_{B,k}(t)$, centred at frequency $f_{c,i} - f_{c,k}$. It is not difficult to show that the (two-sided) bandwidth of $x_{B,i}(t)x^*_{B,k}(t)$ is comparable to $2B_w$.

From equation (3.22), and developing a similar analysis for terms (1) of equation (3.8) and equation (3.9) (see Appendix A.3.3), it can be shown that each product between the ith and the kth OFDM band leads to the introduction of two kinds of distortion terms.
They are reported in Table 3.3 and they are called, with little abuse of terminology, type 1 and type 2 band-to-band products, respectively.

Type	Band-to-band products	Frequency location
1	$\Re\Big\{x_{B,i}(t)x^*_{B,k}(t)\exp\big(j(\omega_{c,i}-\omega_{c,k})t\big)\Big\}$, $\Re\Big\{jx_{B,i}(t)x^*_{B,k}(t)\exp\big(j(\omega_{c,i}-\omega_{vc,k})t\big)\Big\}$	$f_{c,i}-f_{c,k}$
2	$\Re\Big\{x_{B,i}(t)x_{B,k}(t)\exp\big(j(\omega_{c,i}+\omega_{c,k})t\big)\Big\}$ $\Re\Big\{jx_{B,i}(t)x_{B,k}(t)\exp\big(j(\omega_{c,i}+\omega_{c,k})t\big)\Big\}$	$f_{c,i}+f_{c,k}$

Table 3.3: Two types of band-to-band products that emerge from second-order Sieben's architecture nonlinearities, and their respective frequency locations. $i,k=1,2,\dots N_b$.

Table 3.3 shows that type 1 band-to-band products are centred in frequency at $f_{c,i}-f_{c,k}$, type 2 band-to-band products are centred at $f_{c,i}+f_{c,k}$. Making use of equation (2.21), we obtain

$$f_{c,i}-f_{c,k}=(i-k)S_w \tag{3.23}$$

$$f_{c,i}+f_{c,k}=(i+k-2)S_w+2f_{c,1} \tag{3.24}$$

Similarly to type 1 distortion tones and type 1 band-to-carrier products, from equation (3.23), it can be seen that type 1 band-to-band products are centred at frequencies multiples of the slot width, S_w, and their location does not depend on the central frequency of the first OFDM band, $f_{c,1}$. Symilarly to type 2 distortion tones and type 2 band-to-carrier products, from equation (3.24), it can be seen that type 2 band-to-band products are centred at frequencies multiples of S_w, plus a constant offset ($2f_{c,1}$), and their location depends on $f_{c,1}$.

Observing that $f_{c,i}-f_{c,k}$ does not separately depend on i and k, but only on their difference, $i-k$, from equation (3.23), we can conclude that a generic type 1 band-to-band product is centred at frequency kS_w ($k=0,\dots,N_b-1$). Similarly, from equation (3.24), we can conclude that a generic type 2 band-to-band product is centred at frequency $kS_w+2f_{c,1}$ ($k=0,\dots,2(N_b-1)$).

It is not difficult to show that, similarly to type 1 and 2 distortion tones and band-to-carrier products, the width of the frequency range occupied by type 1 and type 2 band-to-band products is comparable to $B_{MB-OFDM}$ and $2B_{MB-OFDM}$ respectively.

A similar analysis can be developed for term (1) of equation (3.8) to show that the same number of band-to-band products are introduced by this term at the same frequency positions. Term (2) of equation (3.9) also introduces the same number of type 2 band-to-band products, at the same frequency positions; however, no type 1 band-to-band products originate from this term, as will be more rigorously shown in subsection 3.1.7.

3.1.6 Type 1 and type 2 second-order distortion

From the analysis developed in subsection 3.1.3, subsection 3.1.4 and subsection 3.1.5 it was possible to identify two main kind of distortion, namely type 1 distortion and type 2 distortion. In this subsection, some spectra of the signal $e_{out}(t)$ of equation (3.5) are presented, to show that they are in agreement with the analysis of subsection 3.1.3, subsection 3.1.4 and subsection 3.1.5.

To simplify the notation let us rewrite equation (3.5) as

$$\begin{aligned} e_{out}(t) \simeq E_{in}\Big[& a_{0,1} + \\ & + a_{1,1} v_{SSB}(t) + \\ & + a_{2,1} v^2(t) + a_{2,2} v_H^2(t) + j a_{2,3} v(t) v_H(t) \Big] \end{aligned} \tag{3.25}$$

where

$$a_{0,1} = \cos(zV_b), \quad a_{1,1} = z\cos(zV_b) \tag{3.26}$$

$$a_{2,1} = -\frac{1}{2} z^2 \frac{\cos^3(zV_b)}{\sin^2(zV_b)}, \quad a_{2,2} = -\frac{1}{2} z^2 \cos(zV_b), \quad a_{2,3} = z^2 \cos(zV_b) \tag{3.27}$$

$$v_{SSB}(t) = v(t) + j v_H(t) \tag{3.28}$$

Figure 3.1 shows, in black, the spectrum of the useful MB-OFDM signal ($a_{1,1} v_{SSB}(t)$ of equation (3.25)), and, in gray, the spectrum of the distortion that originates from term $a_{2,1} v^2(t)$ of equation (3.25). Notice, first of all, that a relatively high central frequency for the first band is selected ($f_{c,1} = 3S_w$) in order to clearly distinguish type 1 and type 2 distortion. For lower values of $f_{c,1}$, the spectra of type 1 and type 2 distortion may overlap in frequency, and it is not easy to distinguish them. Consequences of the choice of $f_{c,1}$ are more rigorously analysed in subsection 3.1.8.
It is not difficult to verify that the spectra of Figure 3.1 are in agreement with the analysis developed in subsection 3.1.3, subsection 3.1.4 and subsection 3.1.5. As an example, the number of (equivalent) distortion tones, their frequency positions and their relatively amplitudes are in agreement with what predicted from equation (3.13) and equation (3.14).

Figure 3.2 shows, in black, the spectrum of the useful MB-OFDM signal ($a_{1,1}v_{SSB}(t)$ of equation (3.25)), and, in gray, the spectrum of the distortion that originates from term $a_{2,2}v_H^2(t)$ of equation (3.25). Notice that, as expected, term $a_{2,2}v_H^2(t)$ introduces the same kinds of distortion, at the same frequencies, as term $a_{2,1}v^2(t)$.

Figure 3.3 shows, in black, the spectrum of the useful MB-OFDM signal ($a_{1,1}v_{SSB}(t)$ of equation (3.25)), and, in gray, the spectrum of the distortion that originates from term $a_{2,3}v(t)v_H(t)$ of equation (3.25). Notice that, as will be proved in subsection 3.1.7, no type 1 distortion is introduced by $a_{2,3}v(t)v_H(t)$.

Moreover, Figure 3.1, Figure 3.2 and Figure 3.3 confirm that the bandwidth of type 1 distortion is comparable to $B_{MB-OFDM}$ and the bandwidth of type 2 distortion is comparable to $2B_{MB-OFDM}$.

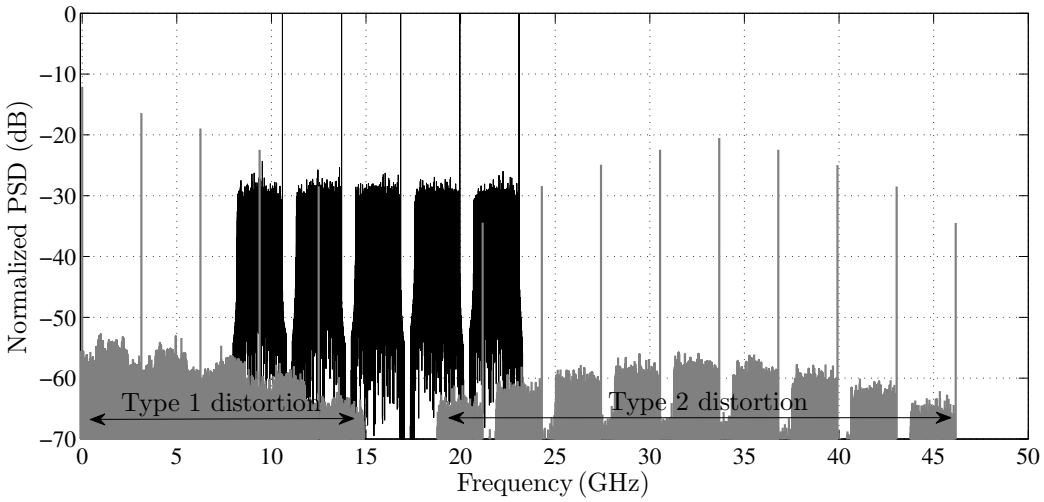

Figure 3.1: Normalized PSD of $a_{1,1}v_{SSB}(t)$ (black) and $a_{2,1}v^2(t)$ (gray). $N_b = 5$, $f_{c,1} = 3S_w$, $B_w \simeq 2.3\,\text{GHz}$, $VBG \simeq 0.04\,\text{GHz}$, $V_b = 0.5V_x$, $m_{PM} = 7\%$, VBPR $= 5\,\text{dB}$.

3.1.7 Distortion components cancellation

In this section we show that, in some circumstances, cancellation occurs between distortion terms.

Let us show that, for any bias voltage, no type 1 distortion originates from term $v(t)v_H(t)$ of equation (3.9). First of all, consider type 1 distortion tones. Type 1 tones that originate from term (3) of equation (3.9) are described by term (2) of equation (A.7) of Appendix A.3.1. Exploiting the fact that the sine function is an odd function, it is not difficult to prove that term (2) of equation (A.7) is equal to zero:

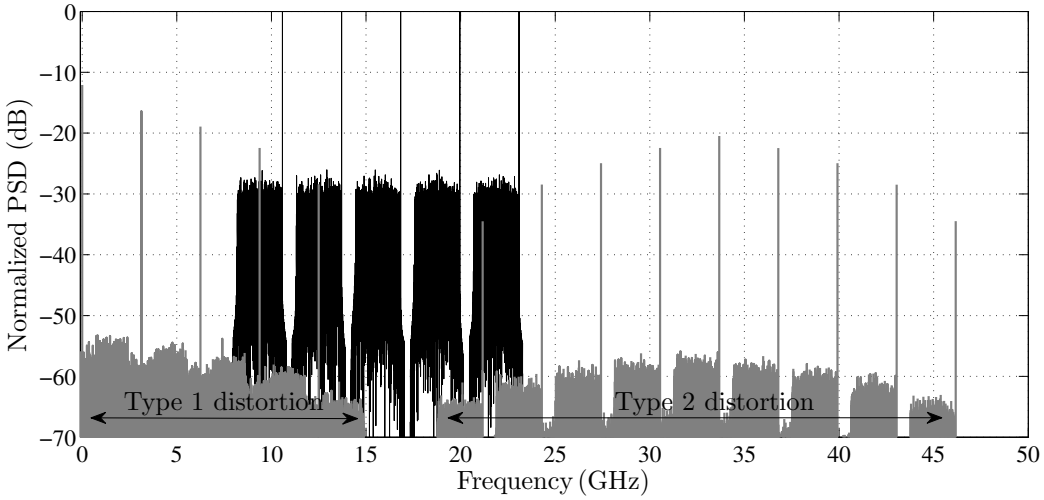

Figure 3.2: Normalized PSD of $a_{1,1}v_{SSB}(t)$ (black) and $a_{2,2}v_H^2(t)$ (gray). $N_b = 5$, $f_{c,1} = 3S_w$, $B_w \simeq 2.3\,\text{GHz}$, $VBG \simeq 0.04\,\text{GHz}$, $V_b = 0.5V_x$, $m_{PM} = 7\%$, VBPR $= 5\,\text{dB}$.

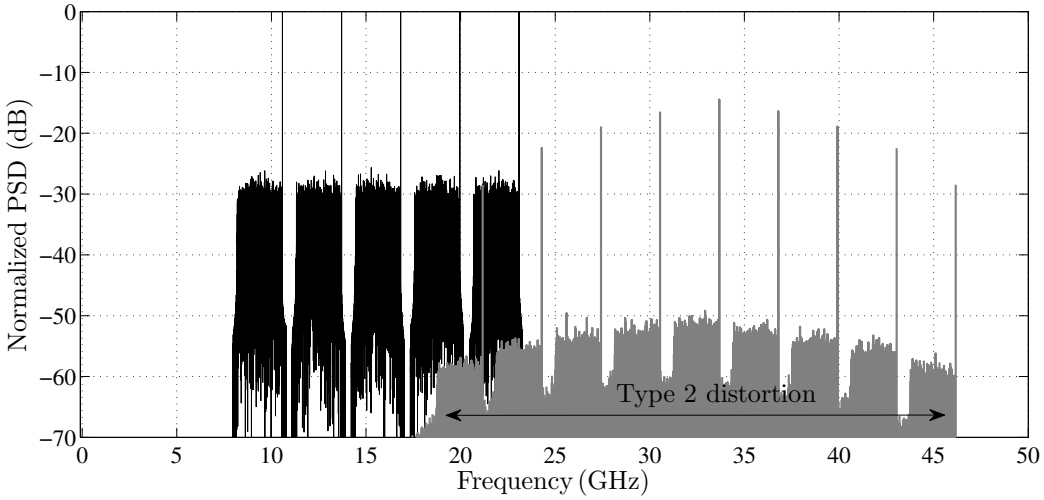

Figure 3.3: Normalized PSD of $a_{1,1}v_{SSB}(t)$ (black) and $ja_{2,3}v(t)v_H(t)$ (gray). $N_b = 5$, $f_{c,1} = 3S_w$, $B_w \simeq 2.3\,\text{GHz}$, $VBG \simeq 0.04\,\text{GHz}$, $V_b = 0.5V_x$, $m_{PM} = 7\%$, VBPR $= 5\,\text{dB}$.

$$\sum_{i=1}^{N_b}\sum_{j=1}^{N_b}\sin\Big((\omega_{vc,i}-\omega_{vc,j})t\Big) = 0 \tag{3.29}$$

Thus, only type 2 distortion tones originate from $v(t)v_H(t)$.

Band-to-carrier products that originate from term (2) of equation (3.9) are described by equation (A.14) and equation (A.15) of Appendix A.3.1. To show that no type 1 band-to-carrier products originates from term $v(t)v_H(t)$ is sufficient to notice that the sum of equation (A.14) and equation (A.15) is equal to

$$x_i(t)\sin(\omega_{vc,k}t) + x_{H,i}(t)\cos(\omega_{vc,k}t) = -\Re\Big\{jx_{B,i}(t)\exp\big(j(\omega_{c,i}+\omega_{vc,k})t\big)\Big\} \tag{3.30}$$

Thus, only type 2 band-to-carrier products originate from $v(t)v_H(t)$.

A similar kind of cancellation occurs inside term (1) of equation (3.9) (see equation (A.24) of Appendix A.3.3). In conclusion, no type 1 distortion originates from term $v(t)v_H(t)$, as shown in Figure 3.3.

A second kind of cancellation occurs for type 2 distortion of terms $a_{2,1}v^2(t)$ and $a_{2,2}v_H^2(t)$ of equation (3.25), when the bias voltage is

$$V_b = \frac{1}{2}V_x \tag{3.31}$$

i.e., when $a_{2,1} = a_{2,2}$ in equation (3.25). This second cancellation is shown in Figure 3.4 (a) and can be mathematically proved using equation (A.8), equation (A.16) and equation (A.23) of Appendix A.2. Observe that, even if in Figure 3.4 (a) is not shown, type 2 distortion from term $v(t)v_H(t)$ is still present for $V_b = (1/2)V_x$.

A third kind of cancellation occurs, for all type 2 distortion, when the coefficients of equation (3.27) are properly balanced. More precisely, we have to impose

$$a_{2,1} - a_{2,2} + a_{2,3} = 0 \tag{3.32}$$

Solving equation (3.32) with respect to V_b, we obtain

$$V_b = \frac{1}{3}V_x \tag{3.33}$$

Without going into the details, to mathematically prove this third cancellation, the results achieved in Appendix A can be used. More precisely, it can be shown that the cancellation occurs only in the positive part of the frequency spectrum. As shown in Figure 3.4 (b), no type 2 distortion appears when $V_b = (1/3)V_x$.

When the choice of equation (3.33) is considered, an interesting choice of $f_{c,1}$ is

$$f_{c,1} = (2m - 1)\frac{S_w}{2} \tag{3.34}$$

where m is a positive integer. Observing that no type 2 distortion tones appears when $V_b = (1/3)V_x$, the choice of equation (3.34) allows to place type 1 distortion tones exactly in the middle between two OFDM bands, as shown, for $f_{c,1} = (3/2)S_w$, in Figure 3.4 (b).

In subsection 3.1.2 it was noticed that, in order to minimize second order distortion, it is convenient to work near MBP (i.e., $V_b \simeq V_x$). From this point of view, even if type 2 distortion cancels for $V_b = (1/3)V_x$, type 1 distortion can result intolerable.

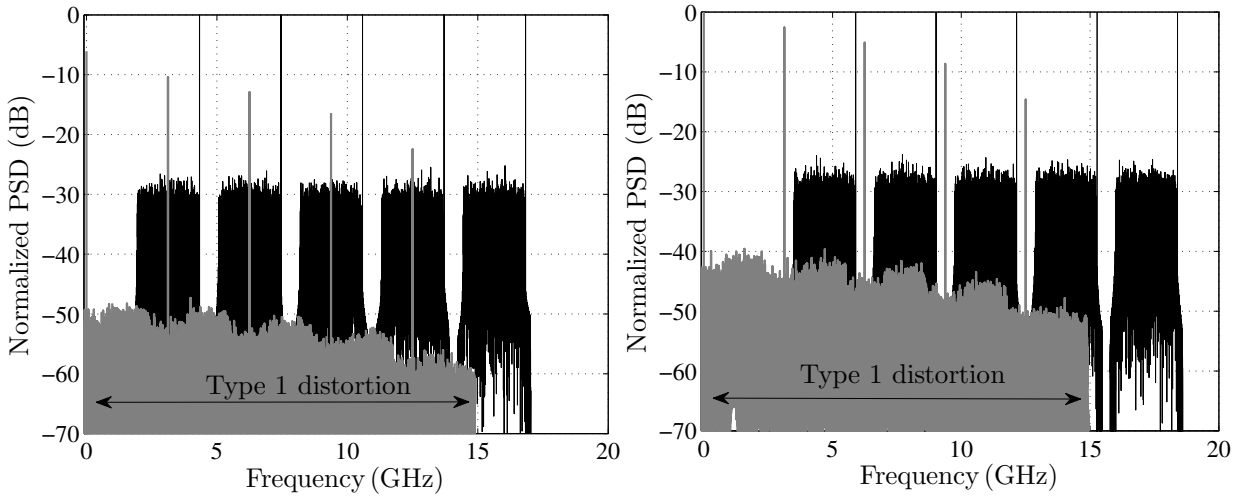

Figure 3.4: In black: normalized PSD of $a_{1,1}v_{SSB}(t)$. In gray: (a) normalized PSD of $a_{2,1}v^2(t) + a_{2,2}v_H^2(t)$, cancellation of type 2 distortion for $V_b = (1/2)V_x$ is shown ($f_{c,1} = S_w$). In gray: (b) normalized PSD of $a_{2,1}v^2(t) + a_{2,2}v_H^2(t) + ja_{2,3}v(t)v_H(t)$, cancellation of type 2 distortion for $V_b = (1/3)V_x$ is shown ($f_{c,1} = (3/2)S_w$). Common parameters: $N_b = 5$, $B_w \simeq 2.3\,\text{GHz}$, $VBG \simeq 0.04\,\text{GHz}$, $m_{PM} = 7\%$, VBPR $= 5\,\text{dB}$.

3.1.8 Distortion components inside the nth OFDM band

Using the results achieved in subsection 3.1.3, subsection 3.1.4 and subsection 3.1.5, we are going now to determine which second-order distortion components are inside a generic OFDM band (comprising, if not differently specified, the virtual carrier). A similar analysis can be developed to understand which distortion components are inside the passband of the BS, or inside a generic frequency slot.

Let us introduce here the definitions of "first distortion tone" and "last distortion tone", which will be useful in the following.
Upon a set of tones, we call "first tone" the tone with lower frequency inside the set, we call "last tone" the tone with higher frequency inside the set.
Similarly, it is possible to define the first and last band-to-carrier product and the first and last band-to-band product.
Analogously, the first OFDM band is the band with lower central frequency, the last OFDM band is the band with higher central frequency (the N_bth band).

Frequency boundaries of the nth OFDM band

To determine exactly which distortion components are (eventually) inside the nth OFDM band, it is important to identify the frequency range occupied by the nth band itself. Let us call $[B_{w,n}]$ the frequency interval occupied by the nth OFDM band (comprising the virtual

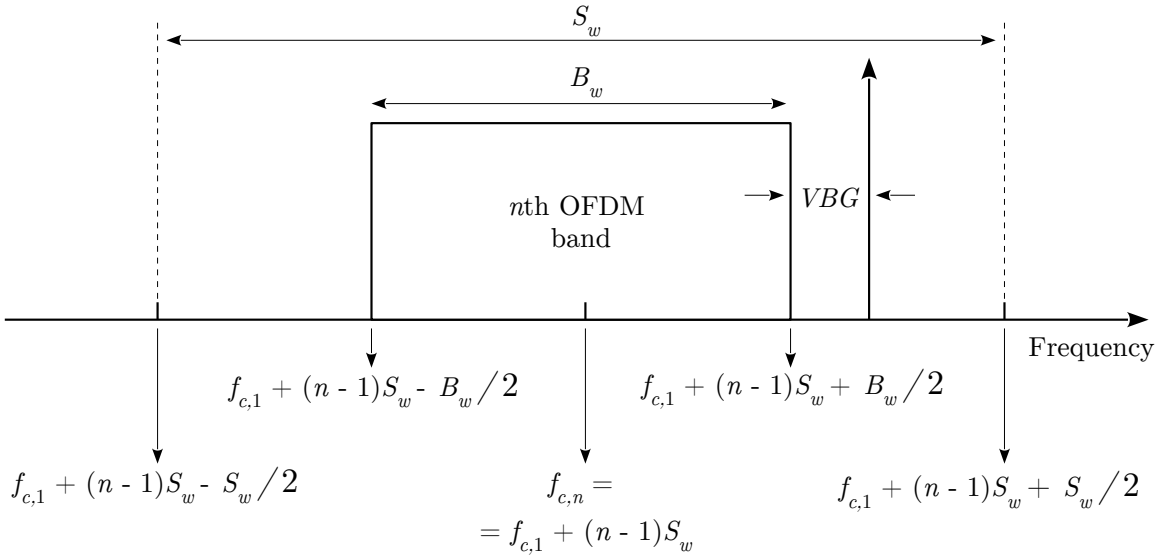

Figure 3.5: Frequency boundaries of the nth OFDM band and of the nth slot. Dependence on $f_{c,1}$ and the index n are explicitly highlighted.

carrier). When choice (2.21) is considered, it is not difficult to show that (see Figure 3.5)

$$[B_{w,n}] = \left[f_{c,1} + (n-1)S_w - \frac{B_w}{2} \ , \ f_{c,1} + (n-1)S_w + \frac{B_w}{2} + VBG \right] \tag{3.35}$$

Similarly, we can define $[S_{w,n}]$ and $[BS_n]$ as the frequency intervals occupied by the nth slot and by (the passband of) a BS used to select the nth band. For the frequency, slot it results (see Figure 3.5)

$$[S_{w,n}] = \left] f_{c,1} + (n-1)S_w - \frac{S_w}{2} \ , \ f_{c,1} + (n-1)S_w + \frac{S_w}{2} \right] \tag{3.36}$$

It is more difficult uniquely define $[BS_n]$. In our discussion, we will consider an ideal BS, for which $[BS_n] = [B_{w,n}]$; however, we should be aware that, in a real system, $[BS_n]$ is usually wider than $[B_{w,n}]$.

Distortion tones inside the nth OFDM band

We are now able to determine if the kth type 1 distortion tone of equation (3.13) is inside the nth OFDM band: it is sufficient to determine if exists an index $k = 0, \ldots, N_b - 1$ such that

$$kS_w \in [B_{w,n}] \tag{3.37}$$

Similarly, remembering that $\delta_1 = 2f_{c,1} + B_w + 2VBG$, the kth type (2.a) distortion tone of equation (3.14) is located inside the nth OFDM band if

$$kS_w + \delta_1 \in [B_{w,n}] \tag{3.38}$$

for an index $k = 0, \ldots, N_b - 1$.

Observe that (i) the first type (2.b) tone of equation (3.14) is located in frequency at $f = N_b S_w + \delta_1$, (ii) the higher frequency occupied by the last OFDM band (comprising the virtual carrier) is $f = (N_b - 1)S_w + \frac{\delta_1}{2}$. Thus, since $N_b S_w + \delta_1 > (N_b - 1)S_w + \frac{\delta_1}{2}$, no type (2.b) tones can be inside the MB-OFDM signal band.

Band-to-carrier and band-to-band products inside the nth OFDM band

From the analysis developed in subsection 3.1.4, remembering that $\delta_2 = -\frac{B_w}{2} + VBG$, the central frequency of a generic type 1 band-to-carrier product is inside the nth OFDM band if

$$kS_w + \delta_2 \in [B_{w,n}] \tag{3.39}$$

for an index $k = 0, \ldots, N_b - 1$.

Similarly, remembering that $\delta_3 = 2f_{c,1} + \frac{B_w}{2} + VBG$, the central frequency of a generic type 2 band-to-carrier product is inside the nth OFDM band if

$$kS_w + \delta_3 \in [B_{w,n}] \tag{3.40}$$

for an index $k = 0, \ldots, 2(N_b - 1)$.

From the analysis developed in subsection 3.1.5, the central frequency of a generic type 1 band-to-band product is inside the nth OFDM band if

$$kS_w \in [B_{w,n}] \tag{3.41}$$

for an index $k = 0, \ldots, N_b - 1$.

Similarly, the central frequency of a generic type 2 band-to-band product is inside the nth OFDM band if

$$kS_w + 2f_{c,1} \in [B_{w,n}] \tag{3.42}$$

for an index $k = 0, \ldots, 2(N_b - 1)$.

When considering band-to-carrier and band-to-band products instead of distortion tones, it has to be taken into account that these products have a non negligible bandwidth (comparable to B_w and $2B_w$, respectively).

Distortion tone position with respect to $f_{c,1}$

It is interesting to find a relation between the choice of $f_{c,1}$ and the frequency position of the distortion tones (with respect to the nth band).
Notice that the last type 1 tone of equation (3.13) has frequency $(N_b - 1)S_w$ and the lower frequency of the nth OFDM band is $f_{c,1} + (n-1)S_w - B_w/2$ (see Figure 3.5). Then, if we choose

$$f_{c,1} > (N_b - n)S_w + \frac{B_w}{2} \tag{3.43}$$

no type 1 distortion tones are inside the nth band (and in the bands with index higher than n). Choosing $n = 1$ in equation (3.43), we obtain (a lower bound for) the value of $f_{c,1}$ for which no type 1 tones are inside the MB-OFDM signal band. Such a value of $f_{c,1}$ is comparable to $B_{MB-OFDM}$.

Similarly, since the first type 2 tone of equation (3.14) has frequency δ_1 and the higher frequency of the nth OFDM band is $f_{c,1} + (n-1)S_w + B_w/2 + VBG$ (see Figure 3.5), then, choosing

$$f_{c,1} > (n-1)S_w - \frac{B_w}{2} - VBG \tag{3.44}$$

no type 2 distortion tones are inside the nth band (and in the bands with index lower than n). Choosing $n = N_b$ in equation (3.44), we obtain (a lower bound for) the value of $f_{c,1}$ for which no type 2 tones are inside the MB-OFDM signal band. Such a value of $f_{c,1}$ is comparable to $B_{MB-OFDM}$.

Similar considerations are valid for band-to-carrier and band-to-band products.

In other words, we have proved that, for a sufficiently high value of $f_{c,1}$ (typically $f_{c,1}$ comparable with $B_{MB-OFDM}$), it is possible to place all the second-order distortion outside the band of the MB-OFDM signal. However, such a choice of $f_{c,1}$ is usually not acceptable in real systems, e.g., due to the significant reduction of spectral efficiency and the increased bandwidth requirements for the optical modulator.

3.2 Analysis of Sieben's architecture and PIN combined nonlinearities

In the following subsections, the current at the PIN output is analysed in different cases. The Sieben's architecture is assumed to be used to generate the optical signal delivered to the PIN.

3.2.1 PIN output in back-to-back configuration when no band selector is used

The band selector (BS) is a fundamental component of our system (see Figure 2.5). Nevertheless, from a mathematical point of view, it is interesting to analyse the current at the PIN output when no BS is interposed between the Sieben's architecture and the PIN. No hypothesis are made on the nature of the signal $v(t)$ (see equations (2.43)-(2.44) of subsection 2.3.3) at the input of the Sieben's architecture ($v(t)$ is not necessarily an MB-OFDM signal).

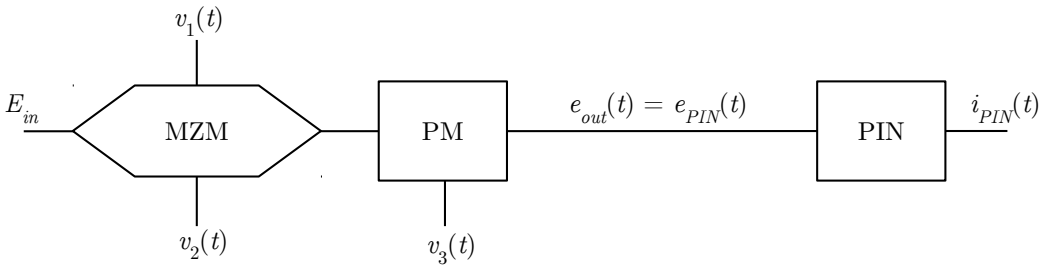

Figure 3.6: Schematic representation of the Sieben's architecture directly connected to the PIN photodetector input.

When the Sieben's architecture is directly connected to the PIN input (see Figure 3.6), considering equation (3.1) and equation (2.46), the current generated by the PIN can be computed as

$$\begin{aligned} i_{PIN}(t) &= R_\lambda |e_{PIN}(t)|^2 = R_\lambda |e_{out}(t)|^2 \\ &= R_\lambda |E_{in}|^2 |\cos(z\alpha v(t) - zV_b)|^2 |\exp(jzv_H(t))|^2 \\ &= R_\lambda \frac{|E_{in}|^2}{2}[1 + \cos(2z\alpha v(t) - 2zV_b)] \\ &= R_\lambda \frac{|E_{in}|^2}{2}[1 + \cos(2z\alpha v(t))\cos(2zV_b) + \sin(2z\alpha v(t))\sin(2zV_b)] \end{aligned} \tag{3.45}$$

By carrying out the Taylor expansion of the time-dependent terms of equation (3.45) and after some algebraic rearrangements, we obtain

$$\begin{aligned} i_{PIN}(t) \simeq R_\lambda \frac{|E_{in}|^2}{2} \Bigg[& 1 + \cos(2zV_b) + 2z\alpha \sin(2zV_b)v(t) + \\ & - 2z^2\alpha^2 \cos(2zV_b)v^2(t) - \frac{4}{3}z^3\alpha^3 \sin(2zV_b)v^3(t) \Bigg] \end{aligned} \tag{3.46}$$

From equation (3.46), it can be seen that a first-order version of $v(t)$, the information-bearing signal, is recovered after opto-electric conversion, along with higher-order terms representing the distortion introduced by the combined nonlinearities of the Sieben's architecture and the PIN photodetector.

It can be noted that, when the MZM works at QBP ($V_b = V_x/2$), the coefficient of the

second-order term in equation (3.46) goes to zero. Then, at QBP, the next significant term in equation (3.46) after the first-order one is the third-order one [1] and equation (3.46) becomes similar to equation (11) in [1]. Thus, if the configuration of Figure 3.6 is considered, working at QBP seems to be a good choice to minimize the nonlinear effects at the PIN output.

3.2.2 PIN output in back-to-back configuration considering the band selector presence

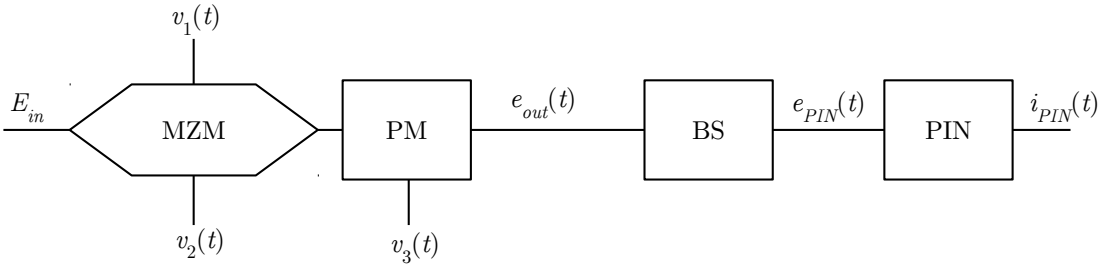

Figure 3.7: Schematic representation of the Sieben's architecture directly connected to the band-selector input.

The analysis of the configuration without BS (illustrated in Figure 3.6) is simplified by the fact that the effects of the phase-modulator disappear after square-law photodetection (i.e., $|\exp(jzv_H(t))|^2 = 1$). However, if a BS is interposed between the Sieben's transmitter and the PIN, such an analysis is not valid any more.

In this subsection, we explicitly assume that the signal $v(t)$ (see equations (2.43)-(2.44) of subsection 2.3.3) is an MB-OFDM signal comprising virtual carriers. We suppose to work is back-to-back configuration (no optical fibre between transmitter and receiver). We assume the presence of a BS before photodetection (see Figure 3.7). In other words, only a single OFDM band (including the associated virtual carrier) is dropped from the MB-OFDM signal and delivered to the PIN.

SSBI term identification

The SSBI term, introduced by the PIN, when DD is employed, was already identified in subsection 2.4.1, for a simple, real-valued signal ($s(t)$ of equation (2.47)).

With reference to the scheme of Figure 3.7, we now identify the SSBI term considering an optical SSB MB-OFDM signal as the input of the BS. More precisely, since the SSBI is a term due to the PIN nonlinearity, only the first-order approximation of the signal at the Sieben's architecture output ($e_{out}(t)$ of equation (3.5)) is considered, i.e., we assume

$$e_{out}(t) = E_{in}\left[\cos(zV_b) + c\Big(v(t) + jv_H(t)\Big)\right] \tag{3.47}$$

where $v(t)$ and $v_H(t)$ are defined by equation (2.58) and equation (3.7), respectively, and c is a constant, $c = z\cos(zV_b)$.

From equation (3.47), considering equation (2.58) and equation (3.7), after the BS, assuming that the nth band is selected, we obtain

$$e_{PIN}(t) = cE_{in}\left[x_n(t) + jx_{H,n}(t) + B\exp(j\omega_{vc,n}t)\right] \tag{3.48}$$

where $x_n(t) + jx_{H,n}(t)$ is the SSB version of the nth OFDM signal and $B\exp(j\omega_{vc,n}t)$ is the (SSB version of the) nth virtual carrier.

After square-law detection, we obtain

$$\begin{aligned} i_{PIN}(t) &= R_\lambda |e_{PIN}(t)|^2 \\ &= c^2|E_{in}|^2 R_\lambda \Big[\underbrace{B^2}_{(1)} + \underbrace{2Bx_n(t)\cos(\omega_{vc,n}t) + 2Bx_{H,n}(t)\sin(\omega_{vc,n}t)}_{(2)} + \underbrace{x_n^2(t) + x_{H,n}^2(t)}_{(3)}\Big] \end{aligned} \tag{3.49}$$

Term (1) of equation (3.49) is a DC component due to the virtual carrier-to-virtual carrier beat. Term (2) is due to the beat between the virtual carrier and the nth OFDM band (and its HT). Term (3) represents the SSBI in the case of an optical MB-OFDM signal at the input of the BS.

Observe that, omitting some constant coefficients, term (2) of equation (3.49) can be rewritten as

$$x_n(t)\cos(\omega_{vc,n}t) + x_{H,n}(t)\sin(\omega_{vc,n}t) = \Re\Big\{x_{B,n}(t)\exp\Big(j(\omega_{c,n} - \omega_{vc,n})t\Big)\Big\} \tag{3.50}$$

From equation (3.50), it is immediately clear that term (2) of equation (3.49) is a replica of the baseband information bearing signal, $x_{B,n}(t)$, shifted in frequency to $f_{c,n} - f_{vc,n}$. Then, $f_{c,n} - f_{vc,n}$ is the frequency that has to be considered for the down-conversion process (see Figure 2.8).

Observe that the SSBI term of equation (3.49) can be rewritten as

$$x_n^2(t) + x_{H,n}^2(t) = |x_{B,n}(t)|^2 \tag{3.51}$$

From equation (3.50), it is clear that the SSBI term is located around the zero frequency

and has a (double-side) bandwidth comparable to $2B_w$. Thus, in accordance with what was stated is subsection 2.4.1, to place the useful signal outside SSBI band, $|f_{c,n} - f_{vc,n}|$ has to be, in general, larger than $(3/2)B_w$.

Distortion components effect at PIN output

In subsection 3.1.8, a general method was given to identify which distortion components are inside the passband of an ideal BS used to select the nth OFDM band. We analyse now the effects of these distortion components at the PIN output. Although we consider only distortion tones, our analysis may be extended to the other kinds of distortion, taking into account that band-to-carrier and band-to-band products have non-negligible bandwidth.

Let us assume that the signal at the PIN input is composed of the SSB version of the nth band, the nth virtual carrier and an arbitrary number, N_{DT}, of distortion tones, each one with amplitude $A_{DT,i}$ and angular frequency $\omega_{DT,i}$. Thus, the signal at the PIN input has the form

$$e_{PIN}(t) \propto c\Big(x_n(t) + jx_{H,n}(t)\Big) + cB\exp(j\omega_{vc,n}t) + \sum_{i=1}^{N_{DT}} A_{DT,i}\exp(j\omega_{DT,i}t) \tag{3.52}$$

After some mathematical steps, assuming for simplicity that $A_{DT,i}$, at the PIN output, we obtain

$$\begin{aligned} i_{PIN}(t) \propto\ & c^2\Bigg(\underbrace{B^2}_{(1)} + \underbrace{2B\,\Re\Big\{x_{B,n}(t)\exp\Big(j(\omega_{c,n}-\omega_{vc,n})t\Big)\Big\}}_{(2)} + \underbrace{|x_{B,n}(t)|^2}_{(3)}\Bigg) + \\ & + c\sum_{i=1}^{N_{DT}} \underbrace{A_{DT,i}\,\Re\Big\{x_{B,n}(t)\exp\Big(j(\omega_{c,n}-\omega_{DT,i})t\Big)\Big\}}_{(4)} + \\ & + cB\sum_{i=1}^{N_{DT}} \underbrace{A_{DT,i}\cos\Big((\omega_{vc,n}-\omega_{DT,i})t\Big)}_{(5)} + \\ & + \sum_{i=1}^{N_{DT}}\sum_{j=1}^{N_{DT}} \underbrace{A_{DT,i}A_{DT,j}\cos\Big((\omega_{DT,i}-\omega_{DT,j})t\Big)}_{(6)} \end{aligned} \tag{3.53}$$

Let us analyse each term of equation (3.53). Terms (1)-(3) were already described (see equations (3.49), (3.50) and (3.51)). Terms (4)-(6) are new distortion terms due to the distortion tones presence. Term (4) is due to the beat between the ith distortion tone and the nth band. This term is clearly a replica of the baseband signal, $x_{B,i}(t)$, shifted in frequency to $f_{c,n} - f_{DT,i}$. Term (5) is due to the beat between the ith distortion tone and the virtual carrier, and is centred in frequency at $f_{vc,n} - f_{DT,i}$. Term (6) is due to the

beat between the ith and the jth distortion tones, and is located in frequency at $f_{DT,i} - f_{DT,j}$.

A similar result can be obtained if, instead of the distortion tones, band-to-carrier products or band-to-band products are considered. Obviously, when all kind of distortion components are considered together, additional distortion beats appear at the PIN output and their number can be very high. It is thus reasonable to quantitative evaluate the performance degradation due to the combined nonlinearities of the Sieben's architecture and PIN on virtual-carrier assisted single sideband direct-detection MB-OFDM signals through numerical simulation, as it is done in Chapter 4.

Equivalent distortion tones at PIN output

When equivalent distortion tones (i.e., when equal-frequency tone are regarded as a single equivalent one) are considered, the previous analysis can be greatly simplified. In particular it is possible to show that no more that one (equivalent) type 1 and no more that one (equivalent) type 2 tones can be inside the nth OFDM band at the same time (then we can impose $N_{DT} = 2$ in equation (3.53)), due to the fact that they are spaced in frequency of multiples of S_w, the slot width. Let us call $A_{DT,1}$ and $A_{DT,2}$ the amplitude of the type 1 and type 2 equivalent tones respectively. Using equation (3.5), equation (3.6), equation (3.8), equation (3.9), equation (A.5), equation (A.6), equation (A.7) and considering the presence of the BS, it can be shown that $A_{DT,1}$ and $A_{DT,2}$ are proportional to

$$A_{DT,1} \propto \left(-\frac{1}{8}B^2z^2\right)\left[\cos(zV_b) + \frac{\cos^3(zV_b)}{\sin^2(zV_b)}\right] \tag{3.54}$$

$$A_{DT,2} \propto \left(\frac{1}{8}B^2z^2\right)\left[3\cos(zV_b) - \frac{\cos^3(zV_b)}{\sin^2(zV_b)}\right] \tag{3.55}$$

To exactly determine the values of $A_{DT,1}$ and $A_{DT,2}$, the number of equal-frequency tones that sums together to generate the equivalent tone has to be considered, as will be shown in the following numerical example. Consider an optical MB-OFDM signal with 12 OFDM bands, $f_{c,1} = S_w$, $B_w \simeq 2.3\,\text{GHz}$ and $VBG \simeq 0.04\,\text{GHz}$ (see Figure 3.8). First of all, Figure 3.8 shows that no more than two equivalent distortion tones are inside the same OFDM band. Assume, for example, that the band of index $n = 6$ is selected. Substituting $n = 6$ in equation (3.35), we obtain

$$\Delta B_{w,6} = [17.6,\ 20.0]\,\text{GHz} \tag{3.56}$$

Thus, equation (3.37) is satisfied for $k = 6$, and, as shown in Figure 3.8, the frequency of the type 1 tone in the 6th band is $f_{DT,1} = 18.75\,\text{GHz}$. From equation (3.13), the amplitude of the type 1 tone of index $k = 6$ is proportional to $2(N_b - k) = 12$. To obtain the exact amplitude of the type 1 tone in the 6th band (after the BS), $A_{DT,1}$ of equation (3.54) has to be multiplied by $2(N_b - k) = 12$.

Still considering $n = 6$, equation (3.38) is satisfied for $k = 3$, and, as shown in Figure 3.8, the frequency of the type 2 tone in the 6th band is $f_{DT,2} = 18.04\,\text{GHz}$. From equation (3.14), the amplitude of the type (2.a) tone of index $k = 3$ is proportional to $(k+1) = 4$. To obtain the exact amplitude of the type 2 tone in the 6th band (after the BS), $A_{DT,2}$ of equation (3.54) has to be multiplied by $(k + 1) = 4$.
Finally, the effect of distortion tones at the PIN output can be evaluated substituting in equation (3.53) the amplitude and frequency values computed in the numerical example.

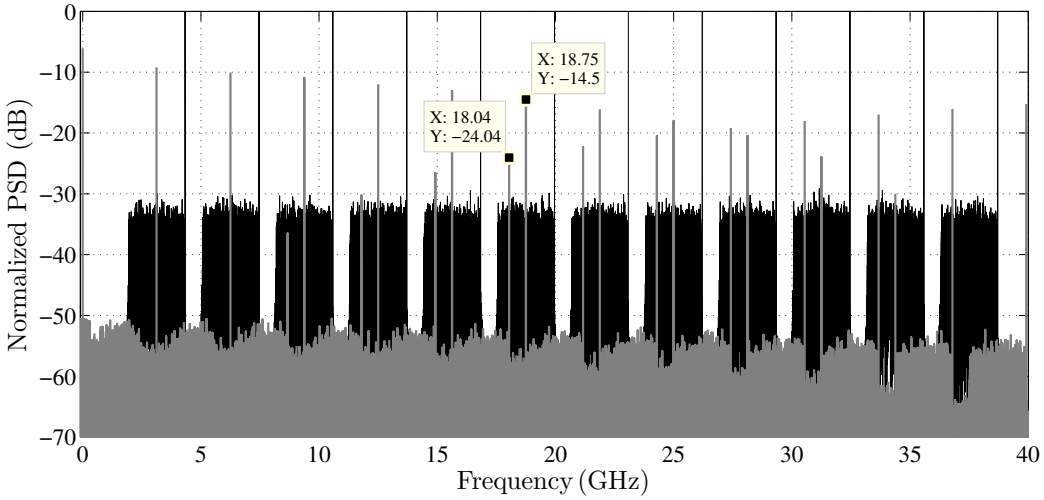

Figure 3.8: In black: normalized PSD of $a_{1,1}v_{SSB}(t)$ of equation (3.25). In gray: normalized PSD of $a_{2,1}v^2(t) + a_{2,2}v_H^2(t) + ja_{2,3}v(t)v_H(t)$ of equation (3.25). Parameters: $N_b = 12$, $f_{c,1} = S_w$, $B_w \simeq 2.3\,\text{GHz}$, $VBG \simeq 0.04\,\text{GHz}$, $V_b = 0.5V_x$, $m_{PM} = 7\%$, VBPR $= 5\,\text{dB}$.

Notice that in equation (3.53), term (2) is proportional B, while term (3) does not depend on B.
$A_{DT,1}$ and $A_{DT,2}$ of equation (3.54) and equation (3.55) are proportional to B^2. Thus, in general, in equation (3.53), term (4) depends on B^2, and term (5) is proportional to B^3 and term (6) depends on B^4 (being B the amplitude of the virtual carrier, which, in turn, is proportional to the VBPR). Consequently, incrementing the VBPR, the information-bearing term (term (2)) becomes dominant, if compared to the SSBI (term (3)). On the other hand, an increment of the VBPR can lead to the introduction of significant distortion at the PIN output, due to term (4), term (5) and term (6).

Chapter 4

Performance assessment of the MB-OFDM system

4.1 System parameters

The parameters of an OFDM signal and of an MB-OFDM signal are introduced and described in section 2.1 and section 2.2, respectively. If not differently specified, each OFDM signal considered in this chapter has $N_{sc} = 128$ subcarriers, a bandwidth $B_w \simeq 2.34\,\text{GHz}$ (which corresponds to a slot filling fraction $r_s \simeq 0.75$), and a bit rate $R_b \simeq 9.34\,\text{Gbit/s}$. Each OFDM symbol has a duration (with no CP) $t_s \simeq 54.6\,\text{ns}$ and M-QAM modulation format with $M = 16$ is used in each subcarrier. A $VBG \simeq 40\,\text{MHz}$ is used in each band and $f_{c,1}$ is set as in equation 3.15 (with $m = 1$), in order to place distortion tones outside each OFDM band.
If not differently specified, the generic MB-OFDM signal considered in this chapter has $N_b = 12$ bands, which corresponds to a channel filling fraction $r_c \in [0.75, 0.8125[$. In agreement with the target of subsection 2.2.2, the MB-OFDM signal has thus a bit rate $R_{MB-OFDM} \simeq 112.1\,\text{Gbit/s}$.

4.2 Performance evaluation methods

As stated in subsection 2.2.2, the OSNR required to achieve a BER of 10^{-3} is used as a figure of merit to assess the performances of the optical MB-OFDM system. Several approaches exist to evaluate the BER. The direct error counting (DEC) method consists of computing the BER comparing each transmitted bit with each received bit. Through the DEC method, accurate BER estimations can be achieved, however, unacceptable computation time may be required, especially when low values of the BER have to be evaluated.
In our work, two different methods to evaluate the BER are considered, namely, evaluation from the error vector magnitude (EVM), as described in subsection 4.2.1, and evaluation using an exhaustive Gaussian approach (EGA), as described in subsection 4.2.2. Note that

the EVM itself can be used as a figure of merit to asses the performance of a transmission system.

4.2.1 Error vector magnitude (EVM)

Considering a general transmission system, the error vector (EV) for each information symbol is defined as the difference between the received information symbol vector and the corresponding transmitted information symbol vector, in the constellation plane (see Figure 4.1).

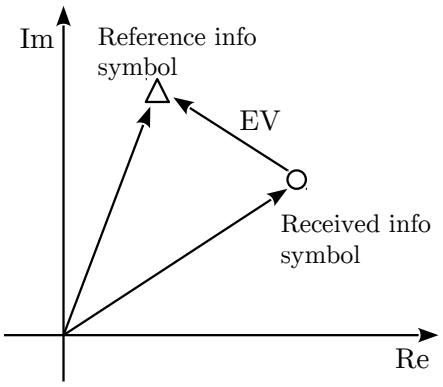

Figure 4.1: Illustration of the error vector (EV) concept.

The EVM is a normalized version of the square of the absolute value of the EV. For an OFDM signal, the EVM must first be computed for each subcarrier. The EVM for the kth subcarrier can be written as [28]

$$\mathrm{EVM}_k = \frac{\sum_{i=0}^{N_I-1} |\tilde{c}_{k,i} - c_{k,i}|^2}{\sum_{i=0}^{N_I-1} |c_{k,i}|^2} \tag{4.1}$$

where N_I is the number of transmitted OFDM information symbols, $c_{k,i}$ is the ith transmitted QAM information symbol at the kth subcarrier and $\tilde{c}_{k,i}$ is the ith received QAM information symbol (at the equalizer output) associated to the kth subcarrier.

The EVM for the whole OFDM signal is given by

$$\mathrm{EVM} = \frac{1}{N_{sc}} \sum_{k=0}^{N_{sc}-1} \mathrm{EVM}_k \tag{4.2}$$

The EVM itself can be used as a figure of merit to asses the performances of an (MB)-OFDM system. Moreover, if the degradation experienced by each subcarrier is mainly imposed by (Gaussian distributed) noise, the value of the EVM is related to the value of the SNR by the following relation [28]

$$\text{SNR}=\text{EVM}^{-1} \tag{4.3}$$

In turn, when an M-QAM modulation format is employed, the substitution of equation (4.3) into equation (2.31) allows the computation of the BER from the EVM.

As a main advantage, the analytical evaluation of the BER using the EVM allows to overcome the long computation time required by the DEC method.
As a main disadvantage, the value of the BER, estimated through the EVM, can be not accurate if the distortion experienced by each subcarrier is not Gaussian distributed [28].

4.2.2 Exhaustive Gaussian approach (EGA)

An exhaustive Gaussian approach (EGA) to compute the value of the BER in experimental DD-OFDM systems is presented in [29]. Excellent agreement between the BER computed by DEC and the BER computed using the EGA method is obtained in [29]. The EGA method provides rigorous estimation of the BER in a way that is faster than the DEC and more accurate than the EVM method. When the EGA method is considered, the BER of a given subcarrier is evaluated from the mean and standard deviation of the subcarrier itself. In turn, mean and standard deviation are computed from a set of experimental runs, which leads to a small increase in the computational requirements, if compared to the EVM approach.

4.3 SSBI mitigation method

A number of methods have been proposed in the literature to mitigate the SSBI effects [16] [30] [12] [17]. In this work, we consider the method proposed in [16] and schematically represented in Figure 4.2. Spectra of the optical and electrical signals at different points of the scheme are also illustrated in Figure 4.2, as insets. With reference to Figure 4.2, the optical signal from the BS, composed of one OFDM band and one virtual carrier (see inset (1)), is split into two parallel branches by an optical splitter. The optical signal in the upper branch is directly sent to a PIN photodetector. Thus, at the output of the PIN in the upper branch, the electrical signal is composed of a DC component, the useful signal and the SSBI term (see inset (2)). The optical signal in the lower branch passes through an optical filter, which removes the virtual carrier (see inset (3)). The filtered signal is then delivered to a PIN. At the output of the PIN in the lower branch, the electrical signal is only composed of the SSBI term (see inset (4)). By subtracting the output of the upper branch from that of the lower branch, the SSBI term is removed (see inset (5)). In our system, an ideal optical filter is used in the lower branch to remove the virtual carrier. It should be noted that, if a non-ideal optical filter is used, the virtual carrier is not completely cancelled, which, in

turn, leads to system performance degradation. The effects of a non-ideal optical filter are analysed in [16].

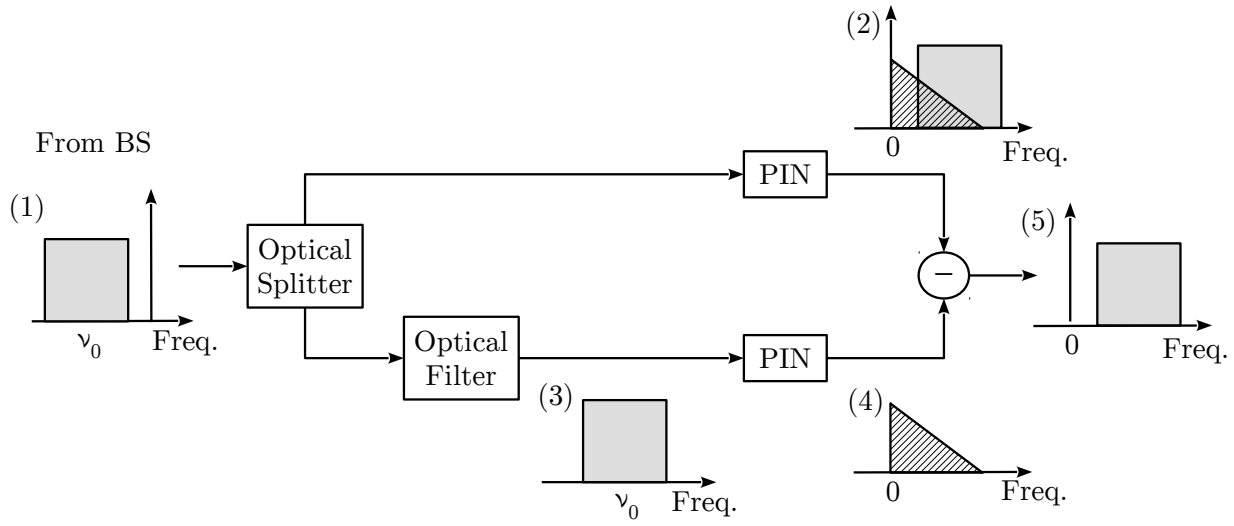

Figure 4.2: Scheme of the SSBI cancellation method proposed in [16]. Spectra of the signals, at different points of the scheme, are also shown as insets.

4.4 Performance assessment

In this section, the performances of the optical MB-OFDM system illustrated in Figure 2.5 and described in section 2.3 are assessed. Transmission in back-to-back configuration (no optical fibre) is considered. The Sieben's architecture is used as SSB modulator. It is useful to introduce now the concept of modulation index of a modulator. The modulation index can be viewed as a measure of "how much linear" is the behaviour of the modulator. The smaller the modulation index, the more linear the behaviour. Before mathematically defining the modulation index, remember that the Sieben's modulator is the cascade of a Mach-Zehnder modulator (MZM) and a phase modulator (PM), as described in subsection 2.3.3. The signals at the MZM input are

$$v_1(t) = -V_b + \alpha v(t) \tag{4.4}$$

$$v_2(t) = +V_b - \alpha v(t) \tag{4.5}$$

and the signal at the PM input is

$$v_3(t) = v_H(t) \tag{4.6}$$

where $v(t)$ in the electrical MB-OFDM signal described by equation (2.51), V_b is the MZM bias voltage, $v_H(t)$ is the Hilbert transform (HT) of $v(t)$, and α is the coefficient defined in equation (3.4). Remember that, by choosing α as in equation (3.4), we ensure that the

optical signal at the Sieben's architecture output is a SSB signal. Equation (3.4) shows that α depends on the ratio V_b/V_x, where V_x is the switching voltage (voltage swing required to switch between the maximum and the minimum of the power transmission characteristic of the modulators) of both the PM and MZM . Table 4.1 reports some values of α as a function of the ratio V_b/V_x. Table 4.1 shows that, as V_b tends to V_x (i.e., the ratio V_b/V_x goes to 1), α goes to zero.

V_b/V_x	α
0.5	1
0.6	0.73
0.7	0.51
0.8	0.32
0.9	0.16

Table 4.1: Coefficient α as a function of the ratio V_b/V_x.

Let us define the PM modulation index, m_{PM}, as

$$m_{PM} = \frac{V_{RMS,imp}}{V_x} \tag{4.7}$$

where $V_{RMS,imp}$ is the RMS voltage of the signal at the PM input, $v_H(t)$, (notice that, for the HT properties, $v(t)$ and $v_H(t)$ have the same RMS voltage). Since, before entering the MZM, $v(t)$ is multiplied by α, the MZM modulation index, m_{MZ}, is defined as

$$m_{MZ} = \alpha \frac{V_{RMS,imp}}{V_x} \tag{4.8}$$

and the following relation holds:

$$m_{MZ} = \alpha m_{PM} \tag{4.9}$$

Equation (4.9) shows that m_{MZ} is not independent from m_{PM}.

Two cases are considered in the following: transmission in the presence and in the absence of noise.

4.4.1 Distortion impairments

In this subsection, transmission in the absence of noise is considered. Since the SSBI term is cancelled using the ideal method of section 4.3, the distortion introduced by the Sieben's modulator is the major impairment on system performance.
In this subsection, the required EVM is used as a figure of merit to evaluate the system performance. Observe that, using equation (2.31) and equation (4.3), the required EVM to achieve a BER $= 10^{-3}$ (EVM$_{req}$) can be computed. For a 16-QAM, it results

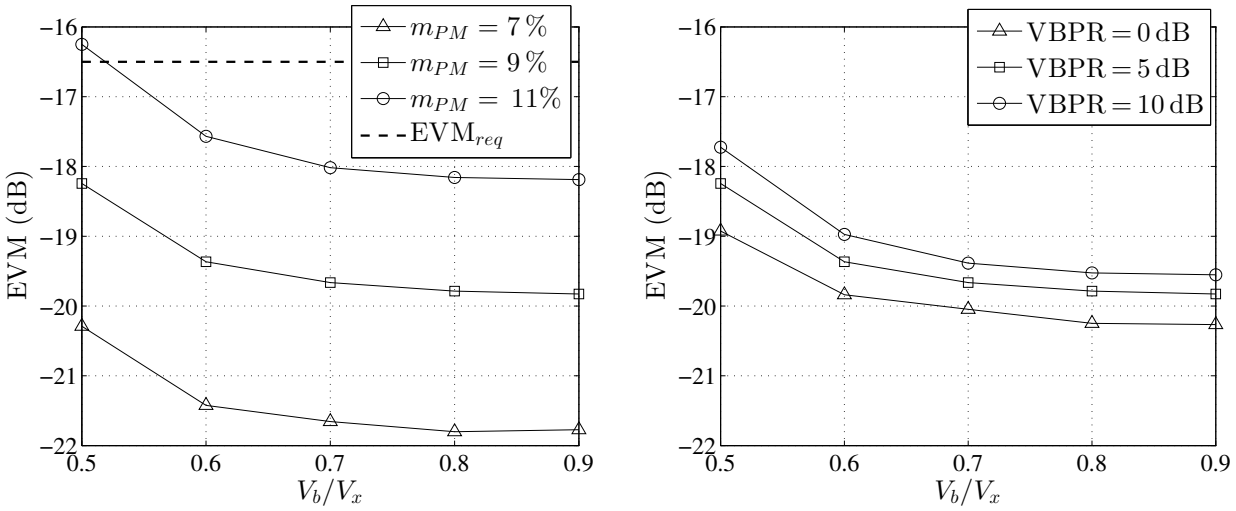

Figure 4.3: EVM as a function of the ratio V_b/V_x, in the absence of noise, (a) for various values of m_{PM} and VBPR = 5 dB; (b) for various values of VBPR and $m_{PM} = 9\,\%$. The required EVM to achieve a BER = 10^{-3} (EVM$_{req}$), when $M = 16$, is also shown in (a).

$$\text{EVM}_{req} \simeq -16.5\,\text{dB} \tag{4.10}$$

Our target is thus achieving a better (i.e., smaller) EVM than EVM$_{req}$.

Figure 4.3 (a) shows the EVM as a function of the ratio V_b/V_x, in the absence of noise, for various values of m_{PM} and for a fixed value of the virtual carrier-to-band power ration (VBPR = 5 dB). For low values of m_{PM}, we achieve better performances, since, the smaller m_{PM}, the more linear is the behaviour of the modulator. However, it is worth to notice that, in the presence of noise, smaller values of modulation index not always means better performances.

Furthermore, as predicted in subsection 3.1.2, better performances are achieved when V_b tends to V_x (i.e., working near minimum bias point (MBP)). On the other hand, remember that, when V_b tends to V_x, the output of the Sieben's modulator goes to zero. From Figure 4.3(a) it could be noticed that, for $V_b > 0.7V_x$, the performance improvement is not particularly significant. In Figure 4.3(a), EVM$_{req}$ is also reported. Notice that, except for $V_b = 0.5V_x$ and $m_{PM} = 11\%$, all the values of EVM reported in Figure 4.3(a) are smaller than EVM$_{req}$.

Figure 4.3 (b) shows the EVM as a function of the ratio V_b/V_x, in the absence of noise, for various values of VBPR and $m_{PM} = 9\,\%$. In agreement with the theoretical results of subsection 3.1.2, for lower values of the VBPR we achieve better performances, since second order distortion terms introduced by the Sieben's modulator are less significant. It is worth to notice however, that, when a non-ideal method to cancel the SSBI term is used, lower VBPR not always means better performances.

4.4.2 Noise impairments

In this subsection, transmission in back-to-back configuration (no optical fibre) and in the presence of ASE noise is considered. The required OSNR to achieve a BER of 10^{-3} (OSNR_{req}) is used as a figure of merit. It is worth to remember that, in a real system, achieving an OSNR higher than 30 dB is really difficult. In this section, as a main result, we show that, for the system under analysis, OSNR_{req} is in general too high to allow transmission on a real system. To prove this result, both an analytical method (AM) and numerical simulations (NS) are considered. The optical carrier generated by the Sieben's modulator and the high value of optical carrier-to-band power ratio (OBPR) are identified as main constraints to system performances, in the presence of ASE noise.

Analytical method

An AM for performance evaluation of amplified spontaneous emission noise-impaired direct detection SSB MB-OFDM system is proposed in [27]. In this paragraph, the AM of [27] is adopted to our case. Figure 4.4 shows the MB-OFDM system model considered to develop the AM. The main purpose is to obtain a relation between the OSNR and the electrical SNR (ESNR). With reference to Figure 4.4, the OSNR is evaluated after noise loading and the ESNR is evaluated at the output of the low pass filter (LPF) used after down-conversion.

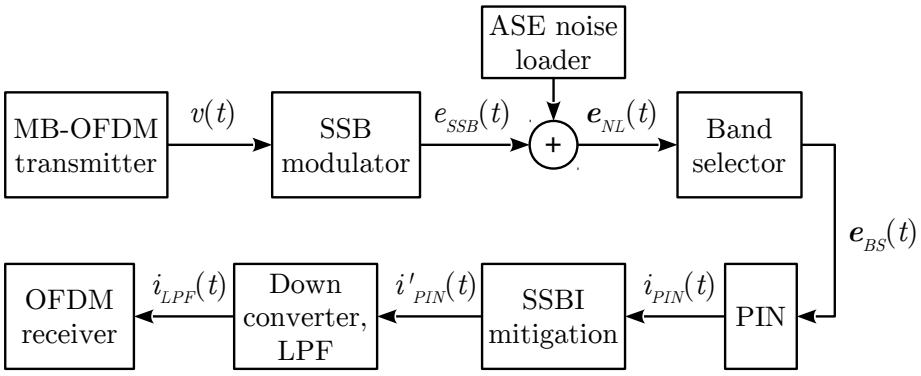

Figure 4.4: MB-OFDM system model considered to develop the analytical method for performance evaluation.

The signal $v(t)$ at the input of the SSB modulator (Sieben's modulator) is the MB-OFDM signal defined by equation (2.51). From equation (2.51), considering equation (2.55) and equation (2.56) the mean power of $v(t)$ can be expressed as

$$\left\langle |v(t)|^2 \right\rangle = V_{RMS,imp}^2 = \frac{V_{RMS,imp}^2}{1+A_v^2} + \frac{V_{RMS,imp}^2 A_v^2}{1+A_v^2} \tag{4.11}$$

where $\langle \cdot \rangle$ denotes the mean value of signal, A_v is the amplitude of each virtual carrier, and $V_{RMS,imp}$ is the RMS voltage of $v(t)$. A linearised version of the Sieben's modulator is considered. Discarding second-order terms from equation (3.5), at the modulator output, we obtain

$$e_{SSB}(t) = E_{in}\cos(zV_b)[1 + zv_{SSB}(t)] \tag{4.12}$$

where $z = \pi/(2V_x)$ and $v_{SSB}(t) = v(t) + jv_H(t)$ is the SSB version of $v(t)$. The constant term in equation (4.12) identifies the optical carrier introduced by the Sieben's modulator.

For the properties of the HT, it results

$$\left\langle |v(t)|^2 \right\rangle = \left\langle |v_H(t)|^2 \right\rangle \tag{4.13}$$

From equation (4.11), equation (4.12) and equation (4.13), the mean power (p_{SSB}) of $e_{SSB}(t)$ can be computed. It results

$$\begin{aligned} p_{SSB} &= \left\langle |e_{SSB}(t)|^2 \right\rangle \\ &= \underbrace{|E_{in}|^2 q^2}_{p_o} + \underbrace{2|E_{in}|^2 q^2 z^2 \frac{V_{RMS,imp}^2}{1 + A_v^2}}_{p_b} + \underbrace{2|E_{in}|^2 q^2 z^2 \frac{V_{RMS,imp}^2 A_v^2}{1 + A_v^2}}_{p_v} \end{aligned} \tag{4.14}$$

where $q = \cos(zV_b)$ is a constant, p_o is the optical carrier power, p_b is the powers of all the OFDM bands and p_v is the power of all the virtual carriers. With reference to equation (4.14), we define the virtual carrier-to-band power ratio (VBPR) and the optical carrier-to-band power ratio (OBPR) as

$$\text{VBPR} = \frac{p_v}{p_b} = \frac{p_{v,i}}{p_{b,i}} = A_v^2 \tag{4.15}$$

$$\text{OBPR} = \frac{p_o}{p_b} = \frac{2V_x^2(1 + \text{VBPR})}{\pi^2 V_{RMS,imp}^2} = \frac{2(1 + \text{VBPR})}{\pi^2 m_{PM}^2} \tag{4.16}$$

where $p_{b,i} = p_b/N_b$, $p_{v,i} = p_v/N_b$ are the mean powers of the ith band and the ith virtual carrier, respectively.

The noise introduced by the ASE noise loader can be expressed as (see subsection 2.5.2)

$$\boldsymbol{n}(t) = [n_{I,||}(t) + jn_{Q,||}(t)]\boldsymbol{u}_{||} + [n_{I,\perp}(t) + jn_{Q,\perp}(t)]\boldsymbol{u}_{\perp} \tag{4.17}$$

where the unit vectors $\boldsymbol{u}_{||}$ and $\boldsymbol{u}_{\perp}$ define the parallel and the perpendicular direction, respectively. Assuming that each one of the four noise components has constant power spectral density (PSD) given by S_{ASE}, the mean power of the ASE noise in a reference bandwidth B_0 can be expressed as

$$p_{ASE} = 4S_{ASE}B_0 \tag{4.18}$$

Assuming that $e_{SSB}(t)$ is polarised along the parallel direction, the signal $\boldsymbol{e}_{NL}(t)$, after noise loading, can be expressed as

$$\boldsymbol{e}_{NL}(t) = e_{SSB}(t)\boldsymbol{u}_{||} + \boldsymbol{n}(t) \tag{4.19}$$

The OSNR is given by

$$\text{OSNR} = \frac{p_{SSB}}{p_{ASE}} = \frac{p_o + p_b + p_v}{4S_{ASE}B_0} \tag{4.20}$$

Let us call $h_{BS,i}(t)$ the impulse response of the band selector (BS) used to filter the ith band and virtual carrier. An ideal BS, with rectangular frequency response, $H_{BS,i}(f)$, and bandwidth $B_{BS} = B_w + VBG$, is considered. From equation (4.19), equation (4.17) and denoting with $\circledast$ the convolution operation, the signal at the BS output can be written as

$$\begin{aligned}\boldsymbol{e}_{BS}(t) &= \boldsymbol{e}_{NL}(t) \circledast h_{BS,i} \\ &= [\underbrace{e_{SSB}(t) \circledast h_{BS,i}(t)}_{e_{BS,s}(t)} + \underbrace{n_{I,||}(t) \circledast h_{BS,i}(t)}_{n_1(t)} + j\,\underbrace{n_{Q,||}(t) \circledast h_{BS,i}(t)}_{n_2(t)}]\boldsymbol{u}_{||} + \\ &+ [\underbrace{n_{I,\perp}(t) \circledast h_{BS,i}(t)}_{n_3(t)} + j\,\underbrace{n_{Q,\perp}(t) \circledast h_{BS,i}(t)}_{n_4(t)}]\boldsymbol{u}_{\perp}\end{aligned} \tag{4.21}$$

where $e_{BS,s}(t)$ is the useful signal after band selection and that $n_k(t)$ $(k = 1, .., 4)$ are complex signals representing the filtered versions of the four noise components. The mean power of $n_1(t)$ (and similarly for the other noise components) can be computed as

$$\begin{aligned}\left\langle |n_1(t)|^2 \right\rangle &= \left\langle |n_{I,||}(t) \circledast h_{BS,i}(t)|^2 \right\rangle \\ &= \int_{-\infty}^{+\infty} S_{ASE}|H_{BS,i}(f)|^2 df \\ &= S_{ASE}B_{BS}\end{aligned} \tag{4.22}$$

Since the BS is designed to filter the ith OFDM band and the ith virtual carrier, from equation (4.12) and considering equation (2.51), equation (2.52) and equation (2.52), it results

$$\begin{aligned}&e_{BS,s}(t) = e_{SSB}(t) \circledast h_{BS,i} \\ &= E_{in}qz\frac{V_{RMS,imp}}{V_{RMS,s_e}}\left[\frac{1}{V_{RMS,s_{b,i}}}\Big(s_{b,i}(t) + js_{b,H,i}(t)\Big) + \frac{A_v}{V_{RMS,s_{v,i}}}\Big(s_{v,i}(t) + js_{v,H,i}(t)\Big)\right]\end{aligned} \tag{4.23}$$

where $s_{b,i}(t)$ is the ith OFDM band, $s_{v,i}(t)$ is the ith virtual carrier, $s_{b,H,i}(t)$ and $s_{v,H,i}(t)$ are the HTs of $s_{b,i}(t)$ and $s_{v,i}(t)$, respectively, $V_{RMS,s_{b,i}}$, $V_{RMS,s_{v,i}}$ and V_{RMS,s_e} are RMS voltages of $s_{b,i}(t)$, $s_{v,i}(t)$ and $s_e(t)$ (see equation (2.51)), respectively. Notice that, for the properties of the HT, it results

$$\left\langle |s_{b,i}(t)|^2 \right\rangle = \left\langle |s_{b,H,i}(t)|^2 \right\rangle \tag{4.24}$$

$$\left\langle |s_{v,i}(t)|^2 \right\rangle = \left\langle |s_{v,H,i}(t)|^2 \right\rangle \tag{4.25}$$

The current at the PIN output can be computed as

$$i_{PIN}(t) = |e_{BS}(t)|^2 = |e_{BS,s}(t) + n_1(t) + jn_2(t)|^2 + |n_3(t) + jn_4(t)|^2 \tag{4.26}$$

It is possible to show that i_{PIN} can be written as the sum of a signal-dependent current, $i_{PIN,s}$, and a noise-dependent current, $i_{PIN,n}(t)$,

$$i_{PIN}(t) = i_{PIN,s}(t) + i_{PIN,n}(t) \tag{4.27}$$

From equation (4.26), considering equation (4.23), and after some algebraic steps, $i_{PIN,s}(t)$ can be written as

$$\begin{aligned} i_{PIN,s}(t) = & \underbrace{b_1^2\Big(s_{b,i}^2(t) + s_{b,H,i}^2(t)\Big)}_{i_{SSBI}(t)} + \\ & + \underbrace{2b_1b_2\Big(s_{b,i}(t)s_{v,i}(t) + s_{b,H,i}(t)s_{v,H,i}(t)\Big)}_{i_{PIN,u}(t)} + \\ & + \underbrace{b_2^2\Big(s_{v,i}^2(t) + s_{v,H,i}^2(t)\Big)}_{i_{DC}(t)} \end{aligned} \tag{4.28}$$

where $i_{SSBI}(t)$ is the SSBI term, $i_{PIN,u}(t)$ is the useful signal, $i_{DC}(t)$ is the direct current component, b_1 and b_2 are constant coefficients:

$$b_1 = E_{in}qz\frac{V_{RMS,imp}}{V_{RMS,s_e}V_{RMS,s_{b,i}}}, \qquad b_2 = A_v b_1 \tag{4.29}$$

For the independence of the signals $s_{b,i}(t)$ and $s_{v,i}(t)$, we can compute the mean power of the product $s_{b,i}(t)s_{v,i}(t)$ as the product of the mean powers:

$$\begin{aligned} \left\langle |s_{b,i}(t)s_{v,i}(t)|^2 \right\rangle &= \left\langle |s_{b,i}(t)|^2 \right\rangle \left\langle |s_{v,i}(t)|^2 \right\rangle \\ &= V_{RMS,s_{b,i}}^2 V_{RMS,s_{v,i}}^2 \end{aligned} \tag{4.30}$$

From equation (4.28), using equation (4.24), equation (4.25) and equation (4.30), and after some calculations, the mean power of the useful signal, $i_{PIN,u}(t)$, can be expressed as

$$p_{PIN,u} = 2p_{b,i}p_{v,i} \tag{4.31}$$

Consider now the noise dependent current $i_{PIN,n}(t)$. From equation (4.26), considering equation (4.23), after some calculations and discarding noise-to-noise mixed products, we obtain

$$i_{PIN,n} \simeq \underbrace{2b_1\Big[s_{b,i}(t)\Big(\Re\{n_1(t)\} - \Im\{n_2(t)\}\Big) + s_{b,H,i}(t)\Big(\Im\{n_1(t)\} + \Re\{n_2(t)\}\Big)\Big]}_{(1)} + \\ + \underbrace{2b_2\Big[s_{v,i}(t)\Big(\Re\{n_1(t)\} - \Im\{n_2(t)\}\Big) + s_{v,H,i}(t)\Big(\Im\{n_1(t)\} + \Re\{n_2(t)\}\Big)\Big]}_{(2)} \tag{4.32}$$

where $\Re\{\cdot\}$ and $\Im\{\cdot\}$ denote the real and imaginary part of a signal, respectively. Term (1) of equation (4.32) is due to the beat between the ASE noise and the ith OFDM band. Term (2) of equation (4.32) is due to the beat between the ASE noise and the ith virtual carrier. The mean power of the real and imaginary part of $n_k(t)$, $k = 1, 2$ can be computed from equation (4.22). It result

$$\Big\langle |\Re\{n_k(t)\}|^2 \Big\rangle = \Big\langle |\Im\{n_k(t)\}|^2 \Big\rangle = \frac{\Big\langle |n_1(t)|^2 \Big\rangle}{2} = \frac{S_{ASE}}{2} B_{BS} \tag{4.33}$$

Due to the independence between the OFDM signal and the ASE noise, we can compute the mean power of the product $s_{b,i}(t)\Re\{n_1(t)\}$ as

$$\begin{aligned} \Big\langle |s_{b,i}(t)\Re\{n_1(t)\}|^2 \Big\rangle &= \Big\langle |s_{b,i}(t)|^2 \Big\rangle \Big\langle |\Re\{n_1(t)\}|^2 \Big\rangle \\ &= V^2_{RMS,s_{b,i}} \frac{S_{ASE}}{2} B_{BS} \end{aligned} \tag{4.34}$$

Similarly, we can compute the mean power of the other products between signals that appear in equation (4.32).
Using equation (4.32), equation (4.33) and equation (4.34), and after some calculations, it results

$$p_{PIN,n} = (p_{b,i} + p_{v,i}) 4 S_{ASE} B_{BS} \tag{4.35}$$

After the SSBI mitigation block, term $i_{SSBI}(t)$ is cancelled from $i_{PIN,s}(t)$, while $i_{PIN,n}(t)$ remains unchanged. Then, after the SSBI mitigation block, we have

$$i'_{PIN}(t) = i_{PIN,u}(t) + i_{DC}(t) + i_{PIN,n} \tag{4.36}$$

Let us call $i_{DW}(t)$ the current at the down-conversion process output. $i_{DW}(t)$ can be expressed as

$$i_{DW}(t) = i'_{PIN}(t) e^{-j2\pi f_{DW} t} \tag{4.37}$$

where f_{DW} is the frequency used for down-conversion. Notice that the down-conversion process does not alter the power of $i'_{PIN}(t)$.
Let us call $h_{LPF}(t)$ the LPF impulse response. An ideal LPF, with rectangular frequency response and bandwidth B_w, is considered. The current $i_{LPF}(t)$, at the LPF output, can

be expressed a the sum of signal-dependent term, $i_{LPF,s}(t)$, and a noise-dependent term $i_{LPF,n}(t)$:

$$\begin{aligned} i_{LPF}(t) &= i_{DW}(t) \circledast h_{LPF}(t) \\ &= \underbrace{[i_{PIN,u}(t)e^{-j2\pi f_{DW}t}] \circledast h_{LPF}(t)}_{i_{LPF,s}(t)} \\ &+ \underbrace{[i_{PIN,n}(t)e^{-j2\pi f_{DW}t}] \circledast h_{LPF}(t)}_{i_{LPF,n}(t)} \end{aligned} \tag{4.38}$$

Term $i_{DC}(t)$ does not appear in equation (4.38), cause, after up-conversion, it is cancelled by the LPF.

Remembering that, after down-conversion, a baseband component and a high frequency component can be identified and that the LPF is used to cancel the high frequency term (see subsection 2.3.2), it is possible to show that:

$$p_{LPF,s} = \frac{p_{PIN,u}}{2} \tag{4.39}$$

and

$$p_{LPF,n} = \frac{p_{PIN,n}}{2}\frac{B_w}{B_{BS}} \tag{4.40}$$

where $p_{LPF,s}$ and $p_{LPF,n}$ are the mean powers of $i_{LPF,s}(t)$ and $i_{LPF,n}(t)$, respectively. Observe that term B_w/B_{BS} in equation (4.40) takes into account the fact that the LPF is more selective than the BS. Using equation (4.39), equation (4.40), equation (4.31), and equation (4.35), the ESNR can be expressed as

$$\text{ESNR} = \frac{p_{LPF,s}}{p_{LPF,n}} = \frac{2p_{b,i}p_{v,i}}{(p_{b,i}+p_{v,i})4S_{ASE}B_w} \tag{4.41}$$

Finally, using equation (4.41), equation (4.20) and observing that $p_o/p_{b,n} = N_b\text{OBPR}$, $p_v/p_{b,n} = N_b\text{VBPR}$, $p_b/p_{b,n} = N_b$, the ESNR can be expressed as a function of the OSNR:

$$\text{ESNR} = \frac{1}{N_b}\frac{2}{(\text{OBPR}+\text{VBPR}+1)}\frac{\text{VBPR}}{(\text{VBPR}+1)}\frac{B_0}{B_w}\text{OSNR} \tag{4.42}$$

Analytical and numerical results comparison

Figure 4.5 shows the required OSNR to achieve a BER of 10^{-3} (OSNR_{req}) as a function of m_{PM} for various values of VBPR. In Figure 4.5, solid lines are obtained using the previously developed AM (i.e., solving equation (4.42) with respect to OSNR). Dashed lines are obtained from NS, considering the linearised model (LM), described by equation (4.12), for the Sieben's modulator.

Good agreement between NS and AM is shown in Figure 4.5, thus validating the AM itself. Observe that, as the VBPR increases, better agreement between the AM and NS is reached. This is due to the fact that, as the VBPR increases, noise-to-noise products (which are not

considered in the AM) become less significant.

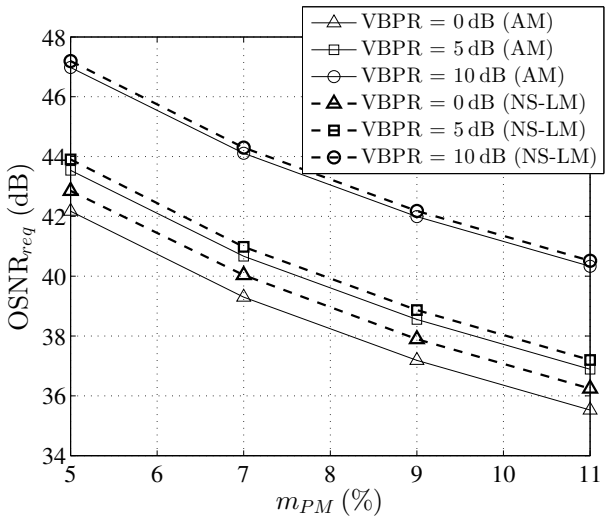

Figure 4.5: OSNR$_{req}$ as a function of m_{PM} for various values of VBPR, for $V_b = 0.7V_x$. Solid lines: analytical model (AM). Dashed lines: numerical simulations-linearised model (NS-LM).

To achieve better performance, Figure 4.5 suggests to decrease the VBPR and increase m_{PM}. On the other hand, as observed in subsection 4.4.1, when a real model (RM) for the Sieben's modulator (i.e., the model described by equation (2.42)) is used, as m_{PM} increases, distortion introduced by the modulator causes higher degradation.

Figure 4.6 shows the required OSNR, obtained from numerical simulations, as a function of m_{PM}, for various values of VBPR, considering both the LM (dashed lines) and the RM (solid lines) for the Sieben's modulator.

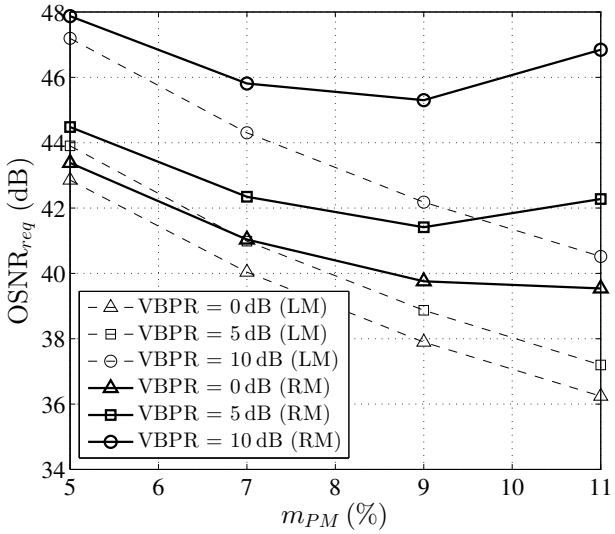

Figure 4.6: OSNR$_{req}$ as a function of m_{PM} for various values of VBPR, for $V_b = 0.7V_x$, from numerical simulation. Dashed lines: linearised model (LM). Solid lines: real model (RM).

In Figure 4.6, similar values of required OSNR, for the LM and for the RM, are obtained

when $m_{PM} = 5\%$, i.e., when noise is the main impairment, whereas, as m_{PM} increases, (i.e., when distortion becomes dominant over noise) the LM (and thus the AM) does not provide reliable results.

Let us consider the RM. Figure 4.6 shows that the minimum OSNR_{req} is obtained for m_{PM} around 9%, for VBPR $= [5, 10]$ dB, and for m_{PM} around 11%, for VBPR $= 0$ dB. However, even for VBPR $= 0$ dB, OSNR_{req} is in general to high to allow transmission on a real system. Figure 4.6 suggests that, acting only on m_{PM} and VBPR, we cannot achieve further performance improvements.

Keeping in mind that the AM has a limited range of validity, to achieve better performances, equation (4.42) suggests to decrease the OBPR. Table 4.2 reports some values of the OBPR, computed from equation (4.16). Table 4.2 shows that, actually, the OBPR is quite high in our system.

m_{PM} (%)	OBPR (dB)
5	25.3
7	22.4
9	20.2
11	18.4

Table 4.2: OBPR for some values of m_{PM} and VBPR $= 5$.

Equation (4.16) shows that the OBPR depends only on VBPR and m_{PM}. Moreover, the OBPR does not depend on V_b. Then, in a first order approximation, changing the bias voltage of the MZM, we are not able to reduce the ratio between the power of the optical carrier and the band power.
The optical carrier introduced by the Sieben's modulator was identified as the constant term in equation (4.12). The optical carrier does not transport useful information and is not needed for photodetection. Therefore, it only subtracts power to the useful signal. From the remarks of subsection 4.4.1 and subsection 4.4.2, it is possible to conclude that, in the presence of ASE noise, the optical carrier is the main impairment on system performance.

An alternative MB-OFDM system design, which allows the transmission of the MB-OFDM optical signal without the optical carrier, is presented in section 4.5.

4.5 Alternative MB-OFDM system design

In subsection 4.4.2, it was proved that, when the MB-OFDM system illustrated in Figure 2.5 is considered, the optical carrier generated by the Sieben's modulator is the main performance impairment. It was also shown that, even optimizing the system parameters,

the required OSNR results too high to allow transmission in a real system. Remember that, when the scheme of Figure 2.5 is used, only one optical modulator and one laser are needed, and virtual carriers can be generated in the electrical domain.

In this section, an alternative optical MB-OFDM transmitter design, which allows to overcome the impairments due to the optical carrier, is proposed.
Instead of generating the virtual carriers in the electrical domain, the key idea is to use the optical carrier generated by the Sieben's modulator as a virtual carrier (to assist in the photodetection process). In this case, we can define the optical carrier-to-band gap (OBG) as the frequency gap between the optical carrier and the associated OFDM band. Figure 4.7 shows the alternative optical MB-OFDM transmitter design. Notice that this new design requires one laser and one SSB optical modulator for each OFDM band. It is thus more expensive that the design of Figure 2.5.

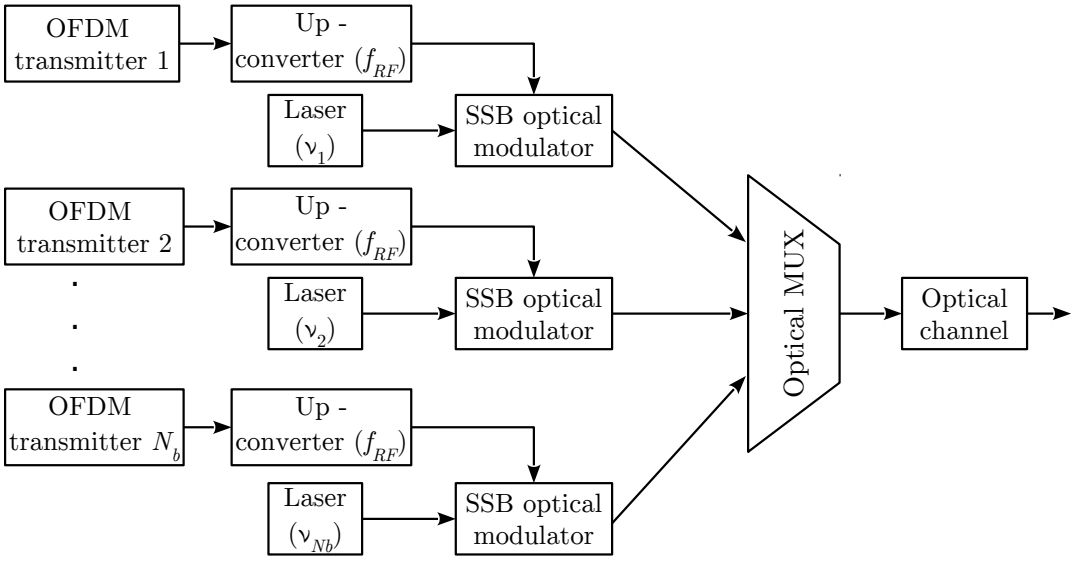

Figure 4.7: Alternative MB-OFDM transmitter scheme.

With reference to Figure 4.7, each OFDM band, generated by the OFDM transmitter, is up-converted to a fixed frequency, f_{RF}. This up-conversion is needed to properly adjust the optical OBG. A possible choice for f_{RF} is

$$f_{RF} = B_w/2 + OBG \tag{4.43}$$

When f_{RF} is chosen as in equation (4.43), the width of the gap between the OFDM band and the optical carrier is exactly OBG. Each OFDM band is then delivered to a different SSB modulator. Notice that each laser, used to feed the optical modulator, has a different optical frequency, $\nu_k,\ k = 1, \ldots, N_b$. At each SSB modulator output, we have a SSB OFDM signal plus an optical carrier.
The output of each SSB modulator is then delivered to an optical multiplexer (MUX). By properly choosing $\nu_k,\ k = 1, \ldots, N_b$, each OFDM band does not overlap in frequency with

the others, and, at the MUX output, an optical MB-OFDM signal is obtained. A possible choice for ν_k is

$$\nu_k = \nu_1 + (k-1)S_w \tag{4.44}$$

With the choice of optical frequency given by equation (4.44), each OFDM band is placed in a frequency slot of proper width, $S_w = 3.125\,\mathrm{GHz}$.

Chapter 5

Conclusions and future work

5.1 Conclusions

In this dissertation, the degradation introduced by the Sieben's architecture and PIN nonlinearities in DD virtual carrier-assisted SSB MB-OFDM systems is evaluated and optimized. In the following, the main outcomes of each chapter are presented.

In Chapter 2, a basic scheme of an MB-OFDM system, highlighting the functional blocks required to generate and detect an OFDM signal, is proposed, together with a review of basic OFDM concepts. The main parameters of an MB-OFDM system, namely VBPR, VBG and central frequency of the first OFDM band, are identified.

With reference to these parameters and to the MZM bias voltage, in Chapter 3, a theoretical analysis of Sieben's modulator and PIN nonlinearities is proposed. The analysis successfully identifies the frequency location and bandwidth of different distortion terms introduced by the Sieben's modulator, in order to understand which terms are inside the passband of a BS used to select a generic OFDM band. Nonlinear terms inside the passband of the BS cause distortion after photodetection and are a source of performance degradation. With the aim of minimizing distortion, the developed analysis suggests to select a proper central frequency for the first band. Moreover, it is proved that, working near MBP, second-order distortion can be partially reduced. However, as we approach MBP, the output of the modulator under consideration tends to zero. The impact of the VBPR on system performance is qualitatively analysed. It is shown that, increasing the VBPR, the SSBI term becomes less significant. On the other hand, as the VBPR increases, the degradation due to nonlinear terms, introduced by Sieben's modulator, increases.

In Chapter 4, the performance of a 112 Gbit/s MB-OFDM system comprising 12 OFDM bands is assessed when an ideal SSBI cancellation algorithm is employed. The optical carrier generated by the Sieben's modulator is identified as the main impairment on system performance. It is analytically proved that the OBPR does not depend on the MZM bias voltage. Then, by varying the bias voltage, it is not possible to reduce the impact of the optical carrier. To achieve a BER of 10^{-3}, a minimum required OSNR of about 40 dB for

VBPR = 0 dB, of about 42 dB for VBPR = 5 dB and of about 45 dB for VBPR = 10 dB is shown. Considering that (i) such values of OSNR are almost impossible to achieve in a real system and (ii) there exist different solutions (such as the one proposed in [3]) which require lower values of OSNR, the study on the proposed MB-OFDM system is concluded. A different optical MB-OFDM transmitter design, which allows to overcome the impairments due to the optical carrier, is proposed. Although better performances are envisioned, this alternative transmitter design requires a laser and an optical modulator for each OFDM band and it thus results more expensive than the previous one.

5.2 Future work

From the work performed in this dissertation and from the above conclusions, some topics are suggested as future work.

- Extend the analysis of Chapter 3 to systems employing different optical modulators, such as the dual-parallel Mach-Zehnder modulator (DP-MZM) used in [3].
- Assess more rigorously the effects of the non-negligible bandwidth of virtual carrier-to-band products and band-to-band products on system performances.
- Develop an analytical expression to relate the power of the information-bearing signal with the powers of distortion terms, at PIN output, to provide a deeper insight on the SSB MB-OFDM system employing DD.
- Evaluate the performance of the alternative MB-OFDM transmitter design (proposed in Chapter 4), especially identifying the penalty due to a non-ideal band-selector and a non-ideal hybrid coupler to implement the Hilbert transform.

Bibliography

[1] M. Sieben, J. Conradi, and D. Dodds, "Optical single sideband transmission at 10 Gb/s using only electrical dispersion compensation", *Journal of Lightwave Technology*, vol. 17, no. 10, pp. 1742–1749, Oct. 1999.

[2] I. Tomkos, "Metropolitan area optical networks", *IEEE Circuits and Devices Magazine*, vol. 19, no. 4, pp. 24–30, July 2003.

[3] T. Alves, L. Mendes, and A. Cartaxo, "High Granularity Multiband OFDM Virtual Carrier-Assisted Direct-Detection Metro Networks", *Journal of Lightwave Technology*, vol. 33, no. 1, pp. 42–54, Jan. 2015.

[4] N. Madamopoulos, D. Friedman, I. Tomkos, and A. Boskovic, "Study of the performance of a transparent and reconfigurable metropolitan area network", *Journal of Lightwave Technology*, vol. 20, no. 6, pp. 937–945, June 2002.

[5] A. Saleh and J. Simmons, "Architectural principles of optical regional and metropolitan access networks", *Journal of Lightwave Technology*, vol. 17, no. 12, pp. 2431–2448, Dec. 1999.

[6] W. Shieh and I. Djordjevic, *OFDM for optical communications*, Elsevier Science, 2009, URL: `http://books.google.pt/books?id=ViPrzMHnY8EC`.

[7] B. Mukherjee, "WDM optical communication networks: progress and challenges", *IEEE Journal on Selected Areas in Communications*, vol. 18, no. 10, pp. 1810–1824, Oct. 2000.

[8] S. Blouza, J. Karaki, N. Brochier, E. Le Rouzic, E. Pincemin, and B. Cousin, "Multiband OFDM networking concepts", *Networks and Optical Communications* 2012.

[9] J. Armstrong, "OFDM for optical communications", *Journal of Lightwave Technology*, vol. 27, no. 3, pp. 189–204, Feb. 2009.

[10] W. Shieh, "OFDM for flexible high-speed optical networks", *Journal of Lightwave Technology*, vol. 29, no. 10, pp. 1560–1577, May 2011.

[11] W. Peng, X. Wu, V. Arbab, K. Feng, B. Shamee, L. Christen, J. Yang, A. Willner, and S. Chi, "Theoretical and Experimental Investigations of Direct-Detected RF-Tone-Assisted Optical OFDM Systems", *Lightwave Technology, Journal of*, vol. 27, no. 10, pp. 1332–1339, May 2009.

[12] W. Peng, B. Zhang, K. Feng, X. Wu, A. Willner, and S. Chi, "Spectrally Efficient Direct-Detected OFDM Transmission Incorporating a Tunable Frequency Gap and an Iterative Detection Techniques", *Journal of Lightwave Technology*, vol. 27, no. 24, pp. 5723–5735, Dec. 2009.

[13] J. Armstrong, "Analysis of new and existing methods of reducing intercarrier interference due to carrier frequency offset in OFDM", *Communications, IEEE Transactions on*, vol. 47, no. 3, pp. 365–369, Mar. 1999.

[14] Xingwen Yi, William Shieh, and Yan Tang, "Phase Estimation for Coherent Optical OFDM", *Photonics Technology Letters, IEEE*, vol. 19, no. 12, pp. 919–921, June 2007.

[15] B. Schmidt, A. Lowery, and J. Armstrong, "Experimental Demonstrations of Electronic Dispersion Compensation for Long-Haul Transmission Using Direct-Detection Optical OFDM", *Journal of Lightwave Technology*, vol. 26, no. 1, pp. 196–203, Jan. 2008.

[16] S. Nezamalhosseini, L. Chen, Q. Zhuge, M. Malekiha, F. Marvasti, and D. Plant, "Theoretical and experimental investigation of direct detection optical OFDM transmission using beat interference cancellation receiver", *Optics express*, vol. 21, no. 13, pp. 15237–15246, 2013.

[17] A. Li, D. Che, X. Chen, Q. Hu, Y. Wang, and W. Shieh, "61 Gbits/s direct-detection optical OFDM based on blockwise signal phase switching with signal-to-signal beat noise cancellation", *Optics Letters*, vol. 38, no. 14, pp. 2614–2616, July 2013.

[18] H. Takahashi, S. Jansen, A. Amin, I. Morita, and H. Tanaka, "Comparison between single-band and multi-band optical OFDM at 120-Gb/s", in: *7th International Conference on Optical Internet, 2008. COIN 2008.* Oct. 2008.

[19] R. Dischler, F. Buchali, and A. Klekamp, "Demonstration of bit rate variable ROADM functionality on an optical OFDM superchannel", in: *Optical Fiber Communication (OFC), collocated National Fiber Optic Engineers Conference, 2010 Conference on (OFC/NFOEC)*, Mar. 2010.

[20] W. Peng, I. Morita, H. Takahashi, and T. Tsuritani, "Transmission of High-Speed (>100Gb/s) Direct-Detection Optical OFDM Superchannel", *Journal of Lightwave Technology*, vol. 30, no. 12, pp. 2025–2034, June 2012.

[21] Z. Li, X. Xiao, T. Gui, Q. Yang, R. Hu, Z. He, M. Luo, C. Li, X. Zhang, D. Xue, S. You, and S. Yu, "432-Gb/s Direct-Detection Optical OFDM Superchannel Transmission Over 3040-km SSMF", *IEEE Photonics Technology Letters*, vol. 25, no. 15, pp. 1524–1526, Aug. 2013.

[22] J. Salz and S. Weinstein, "Fourier transform communication system", in: *Proceedings of the first ACM symposium on Problems in the optimization of data communications systems*, ACM, 1969, pp. 99–128.

[23] ITU-T recommendation G.709, *Interfaces for the optical transport network (OTN)*, Feb. 2012.

[24] ITU-T recommendation G.694.1, *Spectral grids for WDM applications: DWDM frequency grid*, Feb. 2012.

[25] N. Benvenuto and G. Cherubini, *Algorithms for communications systems and their applications*, John Wiley & Sons, 2002.

[26] Tiago Alves, "Ultra Wideband Radio Signal Systems Along Optical Fibre", PhD thesis, Instituto Superior Técnico, Nov. 2011.

[27] P. Cruz, T. Alves, and A. Cartaxo, "Analytical modeling for performance evaluation of ASE noise-impaired direct-detection single-sideband multi-band optical OFDM systems", in: *International conference on photonics, optics and laser technology*, Jan. 2014.

[28] T. Alves and A. Cartaxo, "Analysis of methods of performance evaluation of direct-detection orthogonal frequency division multiplexing communication systems.", *Fiber and Integrated Optics,* vol. 29, no. 3, pp. 170–186, May 2010.

[29] T. Alves and A. Cartaxo, "Extension of the exhaustive Gaussian approach for BER estimation in experimental direct-detection OFDM setups", *Microwave and Optical Technology Letters*, vol. 52, no. 12, pp. 2772–2775, 2010.

[30] T. Alves, A. Alberto, and A. Cartaxo, "Direct-detection multi-band OFDM metro networks employing virtual carriers and low receiver bandwidth", in: *Optical Fiber Communications Conference and Exhibition (OFC), 2014*, Mar. 2014.

[31] S. Hahn, *Hilbert transform in signal processing*, Artech House, 1996.

[32] N. Cvijetic, "OFDM for next-generation optical access networks", *Journal of Lightwave Technology*, vol. 30, no. 4, pp. 384–398, Feb. 2012.

[33] T. Alves, A. Alberto, and A. Cartaxo, "Direct-detection multi-band OFDM metro networks employing virtual carriers and low receiver bandwidth", in: *Optical Fiber Communications Conference and Exhibition (OFC)*, Mar. 2014.

[34] J. Rebola and A. Cartaxo, "Gaussian approach for performance evaluation of optically preamplified receivers with arbitrary optical and electrical filters", *IEE Proceedings - Optoelectronics*, vol. 148, no. 3, pp. 135–142, June 2001.

[35] T. Alves and A. Cartaxo, "Semi-analytical approach for performance evaluation of direct-detection OFDM optical communication systems", *Optics Express*, vol. 17, no. 21, pp. 18714–18729, Oct. 2009.

[36] T. Alves and A. Cartaxo, "On the BER estimation of experimental direct detection OFDM systems", in: *Proceedings of the 2010 International Conference on Optical Communication Systems (OPTICS)*, July 2010.

[37] E. Bedrosian, "A product theorem for Hilbert transforms", *Proceedings of the IEEE*, vol. 51, no. 5, pp. 868–869, May 1963.

[38] T. Alves and A. Cartaxo, "Performance Degradation Due to OFDM-UWB Radio Signal Transmission Along Dispersive Single-Mode Fiber", *IEEE Photonics Technology Letters*, vol. 21, no. 3, pp. 158–160, Feb. 2009.

[39] R. Davey, D. Grossman, M. Wiech, D. Payne, D. Nesset, A. Kelly, A. Rafel, S. Appathurai, and S. Yang, "Long-Reach Passive Optical Networks", *Lightwave Technology, Journal of*, vol. 27, no. 3, pp. 273–291, Feb. 2009.

[40] W. Shieh, H. Bao, and Y. Tang, "Coherent optical OFDM: theory and design", *Opt. Express*, vol. 16, no. 2, pp. 841–859, Jan. 2008.

Appendix A

Useful theorems and equations

A.1 Bedrosian's theorem

The Bedrosian's theorem was stated for the first time by E. Bedrosian in 1962 [37].

Theorem: let $r(t)$ and $s(t)$ denote generally complex functions of the real variable t. If

1. the Fourier transform, $R(f)$, of $r(t)$ vanishes for $|f| > f_0$ and the Fourier transform, $S(f)$, of $s(t)$ vanishes for $|f| < f_0$, where f_0 is an arbitrary positive constant, or

2. $r(t)$ and $s(t)$ are analytic (i.e., their real and imaginary parts are Hilbert pairs),

then the Hilbert transform (HT) of the product of $r(t)$ and $s(t)$ is given by

$$HT\{r(t)s(t)\} = r(t)HT\{s(t)\}. \tag{A.1}$$

where $HT\{\cdot\}$ is the HT operator. In other words, part 1. of the Bedrosian's theorem states that the HT of the product of a low-pass signal, $r(t)$, and a high-pass signal, $s(t)$, is equal to the low-pass signal times the HT of the high-pass signal.

A.2 Hilbert Transform of an up-converted signal

Let us consider the up-converted OFDM signal, $x_i(t)$, of equation (2.36), reported here for the reader's convenience:

$$x_i(t) = \Re\{x_{B,i}(t)\exp(j2\pi f_{c,i}t)\} \tag{A.2}$$

where $x_{B,i}(t)$ (see equation (2.34)) is the baseband version of $x_i(t)$, $f_{c,i}$ is the central frequency of the ith OFDM band and $\Re\{\cdot\}$ denotes the real part of a signal.

Let us find a relation between $x_{B,i}(t)$ and $x_{H,i}(t)$ (the HT of $x_i(t)$). Using the property $HT\{\Re\{\cdot\}\} = \Re\{HT\{\cdot\}\}$, applying the Bedrosian's theorem [37], and remembering that the HT of a complex exponential is [31]

$$HT\{\exp(j2\pi f_0 t)\} = -j\exp(j2\pi f_0 t), \tag{A.3}$$

$x_{H,i}(t)$ can be written as

$$x_{H,i}(t) = \Re\{-jx_{B,i}(t)\exp(j2\pi f_{c,i}t)\} \tag{A.4}$$

A.3 Second-order mixed products

A.3.1 Mixed products between virtual carriers (distortion tones)

Let us rewrite terms (3) of equation (3.6), equation (3.8) and equation (3.9). Term (3) of equation (3.6) can be expressed as

$$\begin{aligned}\left(\sum_{i=1}^{N_b}\cos(\omega_{vc,i}t)\right)^2 &= \sum_{i=1}^{N_b}\sum_{j=1}^{N_b}\cos(\omega_{vc,i}t)\cos(\omega_{vc,j}t) = \\ &= \underbrace{\frac{1}{2}\sum_{i=1}^{N_b}\sum_{j=1}^{N_b}\cos\Big((\omega_{vc,i}-\omega_{vc,j})t\Big)}_{(1)} + \underbrace{\frac{1}{2}\sum_{i=1}^{N_b}\sum_{j=1}^{N_b}\cos\Big((\omega_{vc,i}+\omega_{vc,j})t\Big)}_{(2)}\end{aligned} \tag{A.5}$$

Term (3) of equation (3.8) can be expressed as

$$\begin{aligned}\left(\sum_{i=1}^{N_b}\sin(\omega_{vc,i}t)\right)^2 &= \\ &= \underbrace{\frac{1}{2}\sum_{i=1}^{N_b}\sum_{j=1}^{N_b}\cos\Big((\omega_{vc,i}-\omega_{vc,j})t\Big)}_{(1)} - \underbrace{\frac{1}{2}\sum_{i=1}^{N_b}\sum_{j=1}^{N_b}\cos\Big((\omega_{vc,i}+\omega_{vc,j})t\Big)}_{(2)}\end{aligned} \tag{A.6}$$

Term (3) of equation (3.9) can be expressed as

$$\begin{aligned}\left(\sum_{i=1}^{N_b}\cos(\omega_{vc,i}t)\right)\left(\sum_{i=1}^{N_b}\sin(\omega_{vc,i}t)\right) &= \\ = \underbrace{\frac{1}{2}\sum_{i=1}^{N_b}\sum_{j=1}^{N_b}\sin\Big((\omega_{vc,i}+\omega_{vc,j})t\Big)}_{(1)} - \underbrace{\frac{1}{2}\sum_{i=1}^{N_b}\sum_{j=1}^{N_b}\sin\Big((\omega_{vc,i}-\omega_{vc,j})t\Big)}_{(2)}\end{aligned} \tag{A.7}$$

Notice that, summing equation (A.5) to equation (A.6), terms centred at $(\omega_{vc,i}+\omega_{vc,j})$ cancel each others:

$$\left(\sum_{i=1}^{N_b}\cos(\omega_{vc,i}t)\right)^2+\left(\sum_{i=1}^{N_b}\sin(\omega_{vc,i}t)\right)^2= \\ =\sum_{i=1}^{N_b}\sum_{j=1}^{N_b}\cos\Big((\omega_{vc,i}-\omega_{vc,j})t\Big) \tag{A.8}$$

Notice that, due to the fact that the sine function is an odd function, term (2) of equation (A.7) is equal to zero:

$$\sum_{i=1}^{N_b}\sum_{j=1}^{N_b}\sin\Big((\omega_{vc,i}-\omega_{vc,j})t\Big)=0 \tag{A.9}$$

A.3.2 Mixed products between virtual carriers and OFDM bands

In this subsection, we rewrite some band-to-carrier products that emerge from terms (2) of equation (3.6), equation (3.8) and equation (3.9). Our aim is to express them as a function of the baseband signal $x_{B,i}(t)$.

Considering that the cosine function is a real function, exploiting the well known identity

$$\cos(x)=\frac{e^{jx}+e^{-jx}}{2} \tag{A.10}$$

and using equation (A.2), the product $x_i(t)\cos(\omega_{vc,k}t)$ (that emerge from term (2) of equation (3.6)) can be rewritten as

$$x_i(t)\cos(\omega_{vc,k}t)=\frac{1}{2}\Re\Big\{x_{B,i}(t)\exp\big(j(\omega_{c,i}-\omega_{vc,k})t\big)\Big\} \\ +\frac{1}{2}\Re\Big\{x_{B,i}(t)\exp\big(j(\omega_{c,i}+\omega_{vc,k})t\big)\Big\} \tag{A.11}$$

Similarly, exploiting the well known identity

$$\sin(x)=\frac{e^{jx}-e^{-jx}}{2j} \tag{A.12}$$

and using equation (A.4), the product $x_{H,i}(t)\sin(\omega_{vc,k}t)$ (that emerge from term (2) of equation (3.8)) can be rewritten as

$$x_{H,i}(t)\sin(\omega_{vc,k}t)=\frac{1}{2}\Re\Big\{x_{B,i}(t)\exp\big(j(\omega_{c,i}-\omega_{vc,k})t\big)\Big\} \\ -\frac{1}{2}\Re\Big\{x_{B,i}(t)\exp\big(j(\omega_{c,i}+\omega_{vc,k})t\big)\Big\} \tag{A.13}$$

For the same reasons, the products $x_i(t)\sin(\omega_{vc,k}t)$ and $x_{H,i}(t)\cos(\omega_{vc,k}t)$ (that emerge from term (2) of equation (3.9)) can be rewritten respectively as

$$\begin{aligned} x_i(t)\sin(\omega_{vc,k}t) = &\frac{1}{2}\Re\Big\{jx_{B,i}(t)\exp\big(j(\omega_{c,i}-\omega_{vc,k})t\big)\Big\} \\ &-\frac{1}{2}\Re\Big\{jx_{B,i}(t)\exp\big(j(\omega_{c,i}+\omega_{vc,k})t\big)\Big\} \end{aligned} \tag{A.14}$$

$$\begin{aligned} x_{H,i}(t)\cos(\omega_{vc,k}t) = &-\frac{1}{2}\Re\Big\{jx_{B,i}(t)\exp\big(j(\omega_{c,i}-\omega_{vc,k})t\big)\Big\} \\ &-\frac{1}{2}\Re\Big\{jx_{B,i}(t)\exp\big(j(\omega_{c,i}+\omega_{vc,k})t\big)\Big\} \end{aligned} \tag{A.15}$$

Notice that, summing equation (A.11) to equation (A.13), terms centred at $(\omega_{c,i}+\omega_{vc,k})$ cancel each others:

$$x_i(t)\cos(\omega_{vc,k}t) + x_{H,i}(t)\sin(\omega_{vc,k}t) = \Re\Big\{x_{B,i}(t)\exp\big(j(\omega_{c,i}-\omega_{vc,k})t\big)\Big\} \tag{A.16}$$

Notice that, summing equation (A.14) to equation (A.15), terms centred at $(\omega_{c,i}-\omega_{vc,k})$ cancel each others:

$$x_i(t)\sin(\omega_{vc,k}t) + x_{H,i}(t)\cos(\omega_{vc,k}t) = -\Re\Big\{jx_{B,i}(t)\exp\big(j(\omega_{c,i}+\omega_{vc,k})t\big)\Big\} \tag{A.17}$$

A.3.3 Mixed products between and OFDM bands

In this subsection, we rewrite some band-to-band products that emerge from terms (1) of equation (3.6), equation (3.8) and equation (3.9). Our aim is to express them as a function of the baseband signal $x_{B,i}(t)$.

Using the identity

$$\Re\{x\}\Re\{y\} = \frac{1}{2}\Re\{xy^*\} + \frac{1}{2}\Re\{xy\}, \tag{A.18}$$

and reasoning as in subsection A.3.2, the product $x_i(t)x_k(t)$ can be expressed as

$$\begin{aligned} x_i(t)x_k(t) = &\frac{1}{2}\Re\Big\{x_{B,i}(t)x^*_{B,k}(t)\exp\big(j(\omega_{c,i}-\omega_{c,k})t\big)\Big\} \\ &+\frac{1}{2}\Re\Big\{x_{B,i}(t)x_{B,k}(t)\exp\big(j(\omega_{c,i}+\omega_{c,k})t\big)\Big\} \end{aligned} \tag{A.19}$$

Similarly the products $x_{H,i}(t)x_{H,k}(t)$, $x_i(t)x_{H,k}(t)$ and $x_{H,i}(t)x_k(t)$ can be expressed respectively as

$$\begin{aligned} x_{H,i}(t)x_{H,k}(t) = &\frac{1}{2}\Re\Big\{x_{B,i}(t)x^*_{B,k}(t)\exp\big(j(\omega_{c,i}-\omega_{c,k})t\big)\Big\} \\ &-\frac{1}{2}\Re\Big\{x_{B,i}(t)x_{B,k}(t)\exp\big(j(\omega_{c,i}+\omega_{c,k})t\big)\Big\} \end{aligned} \tag{A.20}$$

$$\begin{aligned} x_i(t)x_{H,k}(t) = &\frac{1}{2}\Re\Big\{jx_{B,i}(t)x^*_{B,k}(t)\exp\big(j(\omega_{c,i}-\omega_{c,k})t\big)\Big\} \\ &-\frac{1}{2}\Re\Big\{jx_{B,i}(t)x_{B,k}(t)\exp\big(j(\omega_{c,i}+\omega_{c,k})t\big)\Big\} \end{aligned} \tag{A.21}$$

$$\begin{aligned} x_{H,i}(t)x_k(t) = &-\frac{1}{2}\Re\Big\{jx_{B,i}(t)x^*_{B,k}(t)\exp\big(j(\omega_{c,i}-\omega_{c,k})t\big)\Big\} \\ &-\frac{1}{2}\Re\Big\{jx_{B,i}(t)x_{B,k}(t)\exp\big(j(\omega_{c,i}+\omega_{c,k})t\big)\Big\} \end{aligned} \tag{A.22}$$

Notice that, summing equation (A.19) to equation (A.20), terms centred at $(\omega_{c,i}+\omega_{c,k})$ cancel each others:

$$x_i(t)x_k(t) + x_{H,i}(t)x_{H,k}(t) = \Re\Big\{x_{B,i}(t)x^*_{B,k}(t)\exp\big(j(\omega_{c,i}-\omega_{c,k})t\big)\Big\} \tag{A.23}$$

Notice that, summing equation (A.21) to equation (A.22), terms centred at $(\omega_{c,i}-\omega_{c,k})$ cancel each others:

$$x_{H,i}(t)x_k(t) + x_{H,i}(t)x_k(t) = -\Re\Big\{jx_{B,i}(t)x_{B,k}(t)\exp\big(j(\omega_{c,i}+\omega_{c,k})t\big)\Big\} \tag{A.24}$$

A.4 Fourier transforms of mixed products

In some situations, it is easier to identify cancellation between second-order products by reasoning in the frequency domain. Thus, in this subsection, we try to determine the Fourier transform (FT) of some mixed products.

Calling $X_i(f)$ the FT of $x_i(t)$ and $X_{B,i}(f)$ the FT of $x_{B,i}(t)$, it results [25]

$$X_i(f) \propto X_{B,i}(f-f_{c,i}) + X^*_{B,i}(-f-f_{c,i}) \tag{A.25}$$

Similarly, the following FTs can be proved:

$$\begin{aligned} F\Big[\Re\Big\{x_{B,i}(t)\exp\big(j(\omega_{c,i}+\omega_{vc,k})t\big)\Big\}\Big] \propto\ & X_{B,i}(f-f_{c,i}-f_{vc,k}) + \\ &+ X^*_{B,i}(-f-f_{c,i}-f_{vc,k}) \end{aligned} \tag{A.26}$$

$$\begin{aligned} F\Big[-\Re\Big\{jx_{B,i}(t)\exp\big(j(\omega_{c,i}+\omega_{vc,k})t\big)\Big\}\Big] \propto & -jX_{B,i}(f-f_{c,i}-f_{vc,k}) + \\ &+ jX^*_{B,i}(-f-f_{c,i}-f_{vc,k}) \end{aligned} \tag{A.27}$$

where $F[\cdot]$ denotes the FT, $f_{c,i} = \omega_{c,i}/(2\pi)$ and $f_{vc,k} = \omega_{vc,k}/(2\pi)$.

Equation (A.26) and equation (A.27) can be used to obtain the FT of the band-to-carrier products of subsection A.3.2.